DEVELOPMENT OF PRECISION TEM HOLDER ASSEMBLIES FOR USE IN EXTREME ENVIRONMENTS

by

Khaled Bataineh

BS, Jordan University of Science and Technology, 1999

MS, Carnegie Mellon University, 2001

Submitted to the Graduate Faculty of

School of Engineering in partial fulfillment

of the requirements for the degree of

Doctor of Philosophy

University of Pittsburgh

2005

UNIVERSITY OF PITTSBURGH

SCHOOL OF ENGINEERING

This dissertation was presented

by

Khaled Bataineh

It was defended on

December 5, 2005

and approved by

D. Marangoni, Associate Professor, Department of Mechanical Engineering, University of Pittsburgh

Sylvanus N. Wosu, Associate Professor, Department of Mechanical Engineering, University of Pittsburgh

Laura Schaefer, Assistant Professor, Department of Mechanical Engineering, University of Pittsburgh

Dissertation Director: Michael Lovell, Department of Industrial Engineering, University of Pittsburgh

DEVELOPMENT OF PRECISION TEM HOLDER ASSEMBLIES FOR USE IN EXTERME ENVIROMENTS

Khaled Bataineh, PhD

University of Pittsburgh, 2005

This dissertation focuses on the development of "in-situ" environmental – transmission electron microscope (TEM) specimen holder assemblies. To date, experimentation with TEM has essentially been two-dimensional and static. In-situ experiments are presently not possible for analyzing complex hot deformation, dynamic recovery and dynamic recrystallization processes because of limitations in the specimen holder design. By developing technology that allows in- situ TEM, it will be possible to assess phenomena such as materials microstructural changes throughout heating process rather than using traditional post mortem techniques. The ability to conduct environmental in -situ experiments is also important because many biological applications currently analyze catalyst samples under static, post-reaction conditions that do not adequately represent reaction dynamics. The lack of an ability to perform in –situ analysis has delayed the fundamental understanding of dynamic catalytic surfaces, complex structural changes, and reaction mechanisms that evolve during processes such as oxidation-reduction. In this respect, this dissertation present novel holder technology that enables in- situ experiments for dynamically capturing microstructure and texture changes in specimens. Such analyses are not capable at the present time and will lead to breakthrough technologies for evaluating mechanisms of microstructural evolution and chemical process reactions.

Environmental instability has been shown to be the limiting factor in holder design when attempting to obtain TEM atomic resolution. In this dissertation, two of the most common environmental problems associated with TEM resolution have been analyzed, air pressure and temperature fluctuations. The present approach to solving these limitations has included extensive experimental and numerical analyses. Based on these analyses, we have designed and optimized two heated TEM holders that overcome the current technical problems associated with performing in situ experiments. These novel holder designs are dynamically stable and accurate for image processing, are capable of elevating the sample temperature to 2000 K, allow the specimens to be subject to diverse environments, and have minimum drift in sample position over time.

Our initial work utilized the finite element method to dynamically and thermally analyze presently available TEM holder assemblies. From these simulations, the dynamic and thermal behavior of the holders were obtained. This information proved to be critical for establishing the limitations of the present TEM technology. It also allowed creation of optimization objectives for designing holders for in-situ TEM experiments. Utilizing the numerical results of the current TEM holders as a basis, two novel different holder technologies were designed and numerically analyzed. The first holder utilized existing resistive heating technology and was found to be significantly better than existing holders with respect to its dynamic stability, uniformity in heating, and minimization of stresses induced in the sample. The new design also had less thermal drift and significantly lower heat loss from the furnace than prior holder designs. The second holder design incorporated a localized laser diode to heat the sample to 2000 K. Such technology has never been applied to TEM technology, making it completely novel to the field.

Based on the numerical simulations performed, the laser-diode holder significantly outperformed all of the other heater specimen holder designs analyzed in this dissertation. In addition, laser heating of the sample was found to overcome important restrictions associated with small pole piece gaps that are required in resistive heating holders. Overcoming these restrictions will allow the TEM holder to be used in completely new application of tomography. Finally, in addition to the finite element simulations, Direct Simulation Monte Carlo (DSMC) analyses were performed to determine the performance of the holder in different gas environments. These analyses allowed for optimizing the holder design when specific molecular densities or molecule impingement rates were required to induce a chemical reaction. Through the DSMC and finite element analyses, the new specimen holders were demonstrated to be greatly improved over existing holder technology and will allow a new level of materials analysis. Both the new resistive heater and laser diode designs will significantly advance TEM technology by allowing atomic level and chemical reaction information to be obtained dynamically, something which is not possible today.

TABLE OF CONTENTS

LIST OF TABLES

LIST OF FIGURES

ACKNOWLEDGMENTS

This thesis would not be possible without the help, guidance and constant encouragement of my dear advisor, Dr. Michael Lovell, and my dear co-advisor Dr. Roy Marangoni. They have been a great source of inspiration for me. Without a doubt, they taught me much about identifying problems, analyzing and simplifying them by dividing them into smaller parts, and then marching into a problem all the way to obtain a complex but accurate solution.

I want to thank Dr. Laura Schaefer and Dr. Sylvanus N. Wosu for serving on my committee and their valuable suggestion and advice.

Special thanks to Mr. David Smith. He has served as my experienced engineering advisor. He has freely and generously provided me with much technical expertise that has contributed reatly to my work.

Thanks to my personal friends and colleagues David, Jim, Hasballah, Michael, Pushkar, Roxana and Sergey for their help and suggestions during several phases of my work, for some stimulating conversation and in general for being wonderful friends.

I must thank also Mr. Frank Marx, Ms. Glinda Harvey and Ms. Camillia Hick for administrative support, and for supplying me with the resources that I needed in general.

These years of study have been among the best of my life. I acknowledge my family and friends for their moral support. Thanks to all of you, now I am able to contribute much to this country, my country of origin, and the world in general.

1.0 TRANSMISSION ELECTRON MICROSCOPY

This dissertation is focused on developing novel specimen holders for use in in-situ Transmission Electron Microscopy. Transmission Electron Microscopy is an imaging technique whereby a beam of electrons is focused onto a specimen causing an enlarged version to appear on a fluorescent or layer of photographic film, or to be detected by a CCD camera. This chapter will provide an overview of TEM technology.

1.1 MOTIVATION FOR DEVELOPING TEM

The transmission electron microscope was first developed in the 1930s after it was apparent the effective role that wavelength has on the theoretical resolution. For example, green light which is used for a light microscope has a wavelength of 0.5 μm and therefore has a theoretical resolution of about 0.2μm. The shorter the wavelength, the higher the resolution. X-ray microscopes would have a vastly superior increase in resolution, but X-rays can not be easily refracted to form an image. Electron waves offered the best alternative. Being a charged particle, an electron could be easily refracted in a magnetic field and accelerated by an electrical potential. The stronger the potential the faster the electron will move, and as per the de Broglie relationship, the shorter the wavelength therefore the better the resolution. In fact a typical electron microscope which operates at an accelerating voltage of 75kV would have a wavelength less than 5 picometers. This makes the theoretical resolution about a hundred thousand times better than that of light. Unfortunately, this theoretical resolution has never come close to being attained. The basic draw back is that magnetic fields can not be manipulated, shaped and grouped the way an optical engineer does with glass lenses. As a result, electron microscopes

must use very small apertures which seriously attenuate the resolution on the order of a hundred times.

TEMs can reveal the finest details of internal structure - in some cases as small as individual atoms. Magnifications of 350,000 times can be routinely obtained for many materials, whilst in special circumstances; atoms can be imaged at magnifications greater than 15 million times.

1.2 WORKING THEORY

As shown in Figure 1.1 a TEM works much like a slide projector. A projector shines a beam of light through (transmits) the slide, and as the light passes through, it is affected by the structures and objects on the slide. These effects result in only certain parts of the light beam being transmitted through certain parts of the slide. This transmitted beam is then projected onto the viewing screen, forming an enlarged image of the slide. TEMs work the same way except that they shine a beam of electrons (like the light) through the specimen (like the slide). Whatever part is transmitted is projected onto a phosphor screen.

A more technical explanation of typical TEMs workings is as follows. The Virtual Source at the top of Figure 1.1 represents the electron gun producing a stream of monochromatic electrons. This stream is focused to a small, thin, coherent beam by the use of condenser lenses 1 and 2. The first lens, usually controlled by the spot size knob, largely determines the spot size; the general size range of the final spot that strikes the sample. The second lens, usually controlled by the intensity or brightness knob, actually changes the size of the spot on the sample; changing it from a wide dispersed spot to a pinpoint beam. The beam is restricted by the condenser aperture, knocking out high angle electrons (those far from the optic axis, the dotted line down the center). The beam strikes the specimen and parts of it are transmitted. This transmitted portion is focused by the objective lens into an image. Optional Objective and Selected Area metal apertures can restrict the beam; the Objective aperture enhances contrast by blocking out high-angle diffracted electrons, and the Selected Area aperture enables the user to examine the periodic diffraction of electrons by ordered arrangements of atoms in the sample.

The image is passed down the column through the intermediate and projector lenses, being enlarged all the way.

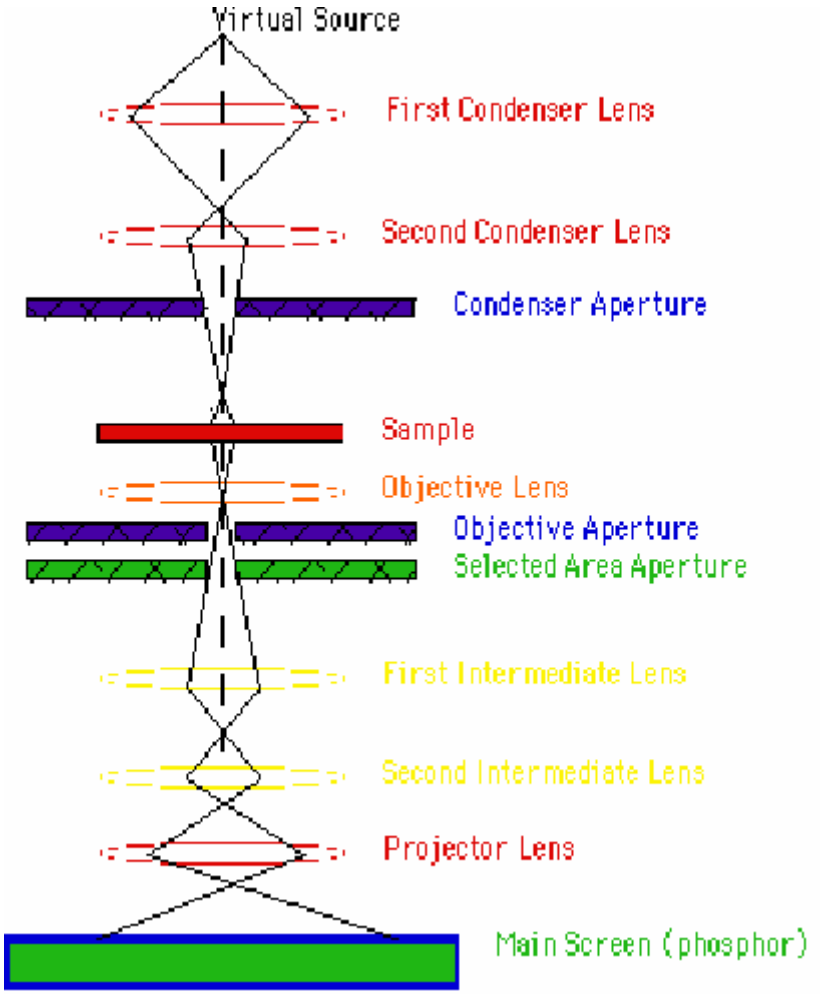

Figure 1.1. Schematic Diagram for a TEM

The image strikes the phosphor image screen and light is generated, allowing the user to see the image. The darker areas of the image represent those areas of the sample that fewer electrons were transmitted through (they are thicker or denser). The lighter areas of the image represent those areas of the sample that more electrons were transmitted through (they are thinner or less dense).

1.3 APPLICATIONS OF THE TEM

The TEM is used heavily in the material and the biological sciences. In both cases, the specimens must be very thin and able to withstand the high vacuum present inside the instrument. Typical biological applications include tomographic reconstructions of small cells or thin sections of larger cells and via Single Particle Reconstruction. In addition, cell structure and morphology is commonly determined while the localization of antigens or other specific components within cells is readily undertaken using specialized preparative techniques.

For non-biological materials, phase determination as well as defect and precipitate orientation are typical outcomes of conventional TEM experiments. Microstructural characterization of non-biological materials, including unit cell periodicities, can be readily determined using various combinations of imaging and electron diffraction techniques. Images obtained from a TEM are two-dimensional sections of the material under study, but applications which require three-dimensional reconstructions can be accommodated by these techniques. In analytical TEMs the elemental composition of the specimen can be determined by analyzing its X-ray spectrum or the energy-loss spectrum of the transmitted electrons.

1.4 SPECIMEN PREPARATION

For the TEM, it is essential to have the specimen thickness reduced to permit electron transmission.[19][24] To achieve electron transparency, it is necessary to reduce the specimen thickness to less than 5000 Angstroms. For equal resolution, the thickness of the specimen is dependent on the accelerating voltage of the TEM. For a 120kV TEM, it is required that the specimen thickness be on the order of 100 to 800 Angstroms. A 1,000kV TEM can tolerate a specimen thickness up to 5000 Angstroms.[20][23]

Specimens are prepared by various, material dependent methods. They are typically a 3mm diameter disk. For most electronic materials, a common sequence of specimen preparation techniques is ultrasonic disk cutting, dimpling, and ion-milling.[2] A critical aspect of preparing a specimen from the bulk state to a 3 mm disk is the ability to rapidly capture the specific area of interest and to preserve it in an unaltered state. When analyzing a failed device in an electronic circuit, it is important to position the specific area of interest in the center of the 3 mm diameter TEM specimen disk. In addition, for composite materials, when the analysis of an interface is required, it is beneficial to obtain a disk whereby an interface is situated near the disk's center.

Ultrasonic disk cutting is an extremely important technique used to obtain the initial 3 mm disk from many types of electronic materials. Dimpling is a preparation technique that produces a specimen with a thinned central area and an outer rim of sufficient thickness to permit ease of handling.[3] This specimen configuration is achieved by the simultaneous rotation of both the specimen and a grinding wheel containing abrasive slurry (typically diamond) whose axes are orthogonal and intersecting. Advancements in process control have greatly increased the capabilities and performance of the dimpling process. Ion milling is traditionally the final form of specimen preparation. In this process, charged argon ions are accelerated to the specimen surface by the application of high voltage. The ion impingement upon the specimen surface removes material as a result of momentum transfer.

1.5 LIMITATIONS

There are a number of drawbacks of TEM material analysis. Many materials require extensive sample preparation to produce a sample thin enough to be electron transparent, and changes in the structure may be caused during this process. Also the field of view is relatively small, raising the possibility that the region analysed may not be characteristic of the whole sample. In addition, there is the potential that the sample may be damaged by the electron beam, particularly in the case of biological materials. Finally, it is presently very diffcult to perform TEM measurments in –situ. This is due to the fact that many TEM measurments examine

specimen that are heat –treated, and this heating causses thermal expansion & vibrations that make it diffcult to focus on areas at the atomic level.

1.6 TEM VERSUS SEM

The transmission electron microscope produces images by detecting electrons that are transmitted through the sample, while the scanning electron microscope (SEM) produces images by detecting secondary electrons which are emitted from a material surface due to excitation by the primary electron beam.

Generally, the TEM resolution is about an order of magnitude better than the SEM resolution. However, because the SEM image relies on surface processes rather than transmission, it is able to image bulk samples and has a much greater depth of view. For this reason SEM produces images that are a good representation of the 3D structure of the sample.

In the TEM, the transmitted beam is magnified by a series of magnetic lenses until they hit a flourescent screen, photographic plate, or light sensitive sensor to produce an image on a monitor or computer. In the SEM, the electron beam is rastered across the sample, with detectors building up an image by mapping the detected signals with the beam position.

2.0 MOTIVATION

2.1 BACKGROUND INFORMATION

For many years, a practical limitation has existed in TEM that precludes the ability to conduct in-situ experimentation. This is related to the physical gap between the microscope pole pieces. The pole pieces are individual components within the TEM's lens system that define the three dimensional space for the specimen. In a TEM, the specimen is placed into this pole piece gap. For ultra-high resolution TEMs, the pole piece gap is on the order of 2.2mm. It should be noted that smaller gaps yield higher resolution. In the case of lower resolution TEMs, mainly used in the life sciences, the gap can be greater than 5mm. The gap is typically on the order of 10mm as required to address the high contrast needs associated with life science imaging. However, these large pole piece gap systems are not capable of conducting atomic scale imaging. Within the space between the pole pieces, a typical 3mm diameter specimen needs to be translated in X, Y, and Z, and tilted along a primary axis (α) and often times a secondary axis (β). In addition, the need for continuous in-plane rotation is often considered important so that the specimen can be properly oriented with respect to the electron optical axis. For electron tomography that yields three-dimensional information, it is important that the specimen is tilted to +/-70 degrees.[16] Images are taken in increments of a few degrees and are subsequently re-constructed to generate the 3D information. The 3D reconstruction can also be enhanced by in-plane specimen rotation.

As one can determine from the size of the specimen and the geometry of the pole piece gap in high resolution TEMs, minimal space exists to achieve even the most simple specimen manipulation, let alone any type of experimentation.

2.2 IDENTIFICATION OF THE PROBLEM

The goal of this research is to develop a completely novel specimen holder technology that is capable of elevating the temperature of a material research specimen from ambient to +2,000K while simultaneously subjecting it to varying gas environments.[18][19] It is designed to control specimen temperature within 10^{o}C. Various environments will be created by injecting one or more gases into the volume surrounding the specimen. Gas pressure and flow must be accurately controlled. It is planned that specimen positioning within the TEM will be accurately controlled by the combination of the TEM's goniometer and the in-situ holder mechanism. The holder must position the specimen will be positioned in 5 degree of freedom (DOF) space. These degrees of freedom include three translations (X,Y, Z) and two tilt axes (α,β) with a targeted accuracy of +/-0.005^{o}.

The main challenge in developing the new holder technology relates to the small physical gap between the microscope pole pieces. In a TEM, the specimen is placed into this pole piece gap; the pole piece gap is on the order of 2.2mm. Such a small gap makes it very difficult to introduce mechanisms for heating and positioning the specimen, as well as loading and unloading the specimens**.** The second challenge is the extremely high demand on thermal and mechanical stability of the system when elevating the temperature. The final challenge is the workability of the material under high vacuum and high temperature. Methods for overcoming these challenges form the motivation for this dissertation and will be discussed throughout the next chapters.

2.3 COMMON ENVIROMENTAL EFFECTS ON TEM STABILTY

Improvements in TEM technology have provided the ability to capture atomic scale features; however, atomic scale stability is required for these measurments. These improvements have led to an increase in the sensitivity of the TEM to enviromental distrubances. Enviromental effects include, but not limited to, electromagntic field, temperature changes, airflow across the

column and air pressure changes. One of the major challenges of creating a new holder design is to ensure that the sensetivity of the TEM is maintamed while increasing the functionality.

Electromagnetic interference can cause beam deflections in both the scanning systems and the spectrometer.[10] The Electromagnetic fields should be less than .1 mG r.m.s for .2 nm resolution. Quasi-DC fields can be generated from elevators and nearby trains and buses. Major sources of AC electromagnetic interference are unbalanced electrical loads. A straight conductor carrying current *I* will generate magnetic field *B* according to Amperes law as

$$B = 2I / d$$

where d is the distance from the conductor.

If as much current leaves through the neutral wire as enters through the live wire in a conduit, the magnetic field from the two wires will cancel, and there will be no net effect field. Only the current leaks to the ground will generate a magnetic field. Figure 2.1 illustrates the difficulty that arises when the neutral wires are accidentally bonded to the ground. The net AC generated by the conductors will be proportional to the current (δ), lost to the ground.

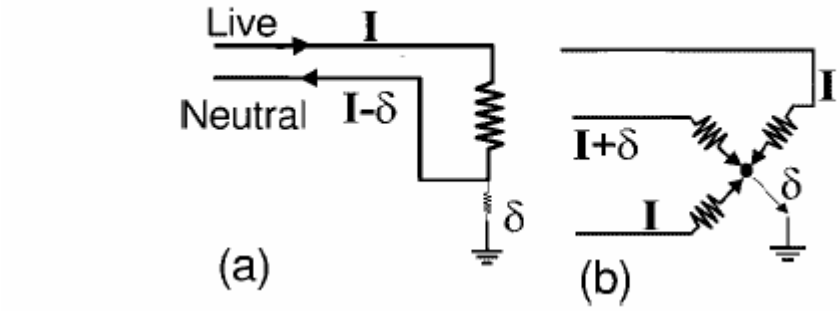

Figure 2.1. The Origin of Ground Currents in (a) a Single Phase Circuit and (b) a Three-Phase Circuit.[34]

Any material with a high magnetic permeability moving through earth's magnetic field will cause magnetic field lines to deflect in the spectrometer. A Pen –Knife waved in front of a spectrometer causes shifts of an eV. The Iron wheels or axles of a typical office chair will cause similar shifts when moved.[34] Figure 2.2 shows the deflection of the zero- loss peak on the post –column energy loss spectrometer as a truck pulls to the loading dock outside the microscope room. The signal is dipped at 2 eV. The truck is first detected at about 50 feet away (t ~ 55s). It

pulls up to the loading dock, and then backs up to come in straight. The spikes at (a) and (b) correlate well with driver opening his door (a) and dropping the tailgate of the truck (b).

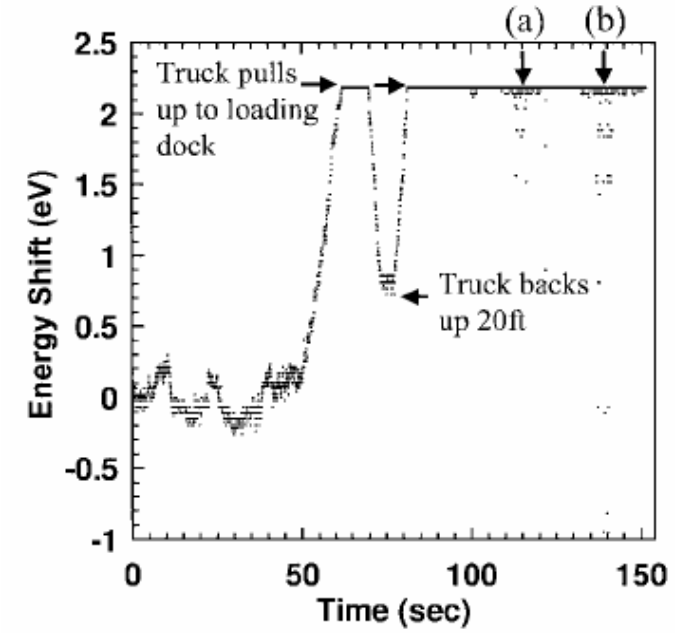

Figure 2.2 Deflection of the Zero- Loss Peak on the Post –Column Energy Loss Spectrometer as a Truck Pulls to the Loading Dock Outside the Microscope Room.[34]

Pressure fluctuation from air flow across the microscope column can lead to random displacements in the image (especially over 1-30 s). Airflow across the column must be 15 feet min^{-1} or less for .2 –nm resolution.[34] Figure 2.3 shows some common sources of air movement.

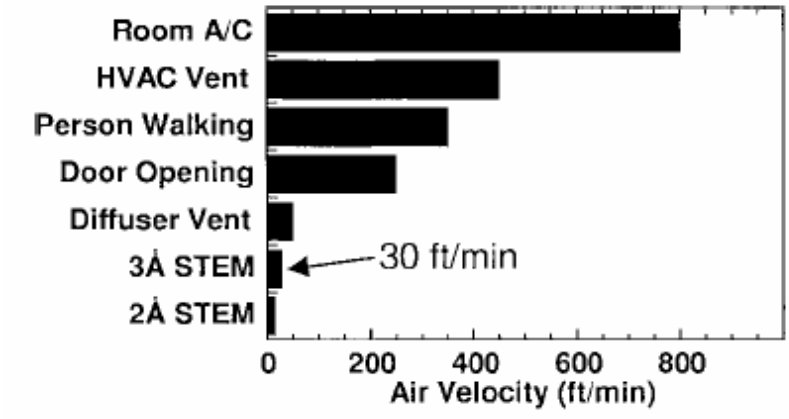

Figure 2.3. Maximum Airflow Across the Microscope Column That can be Tolerated for sub .3 and .2 nm STEM Compared with Common Causes of Drafts.[34]

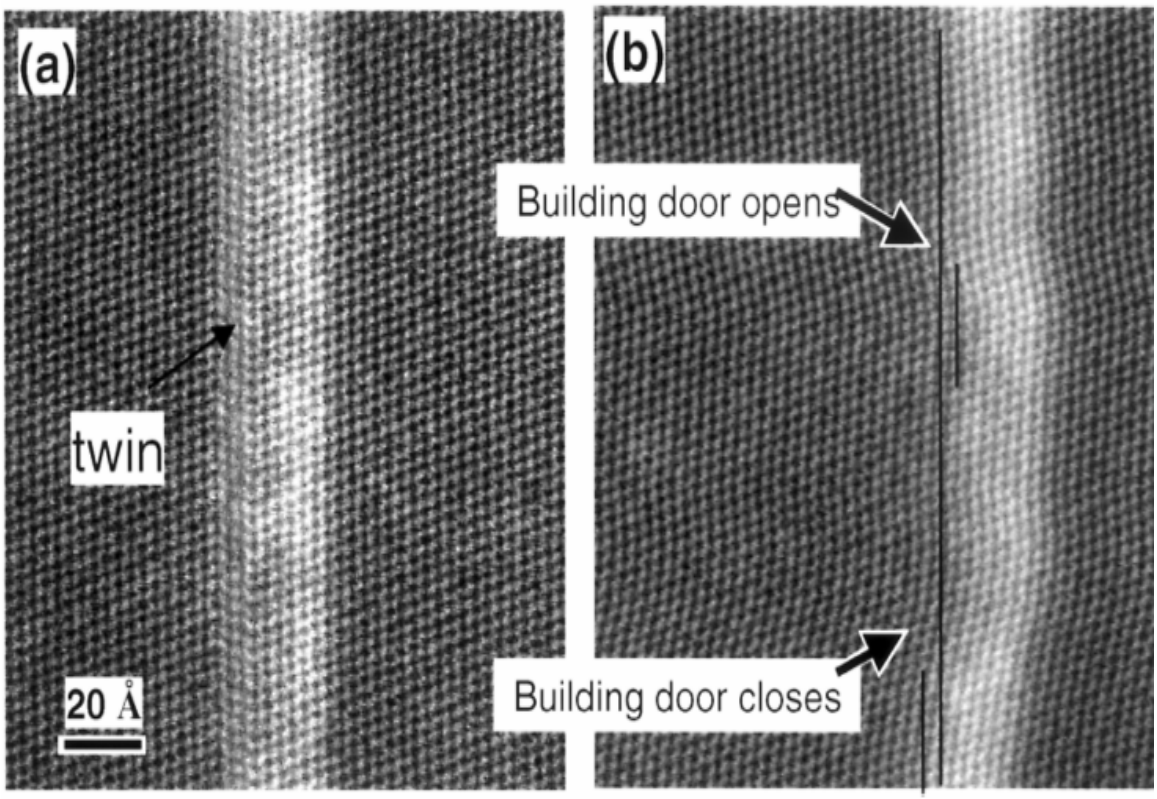

Figure 2.4. Annual Dark Field Images of Arsenic-Delta Doped Layer Grown on (111) Si. (a) Recorded at 10 PM. When there is No Traffic in the Building. (b) Recorded at 11a.m.

Figure 2.4 shows an image recorded while somebody opened the outside door of the building (the room door was closed throughout). The image is undistorted until the main door to the building opened, and the image settles down again when the door is closed. The air pressure change of a few Pascals is felt throughout the building and deflects the specimen stage by a few angstroms.[34]

The sample is usually under a high vacuum of 3×10^{-6} Pa, while the outside of the sample holder is at atmosphere pressure (~ 10^5 Pa). David A Muller and John Grazul [34] used a high precision barometer to calibrate the deflection of the sample rod to 0.1 nm Pa^{-1}.[34]

J. Adeler & S. N. Pagkis (2003), studied distortions in confocal 3D image data sets. They concluded that the distortions were related to movements of the microscope stage that matched fluctuations in laboratory temperature. Figure 2.5 shows the Z axis distortions seen in XZ

confocal images of propidium iodidestained nuclei of the cells forming the wall of a rat mesenteric artery. The three nominally homologous XZ sections were extracted from Z series of XY images acquired with extensive frame averaging. Reasonable interpretation of the images shown in Figure 2.5, based on prior knowledge of the shape of the nuclei found in this tissue. Figure 2.5 (a) shows the longitudinal nucleus and the transversely section have undergone elongation in the Z axis due to fluctuations in laboratory temperature. Figure 2.5 (b) shows the transversely section has undergone elongation in the Z axis, while the longitudinal nucleus is undistorted. Figure 2.5 (c) shows transversely section is undistorted while the longitudinal nucleus has undergone elongation in the Z axis.[1]

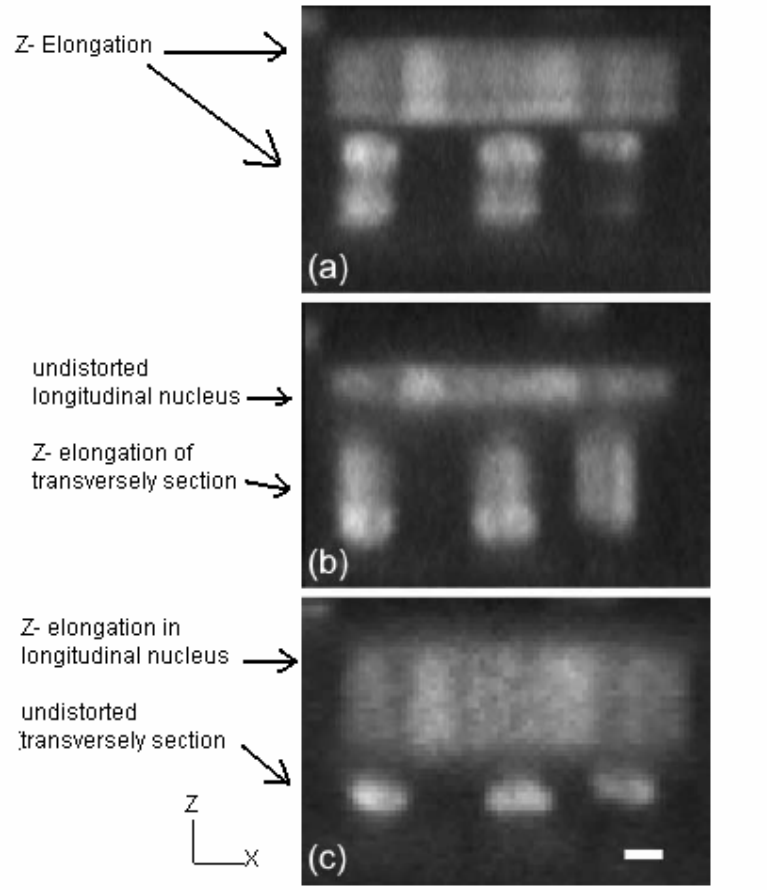

Figure 2.5. Z Axis Distortions Seen in XZ Confocal Images of Propidium Iodidestained Nuclei of the Cells Forming the Wall of a Rat Mesenteric Artery. Scale bar =1 μm.[1]

J. Adler & S. N. Pagakis also performed more rigorous tests which demonstrated that the distortion was related to the length of image acquisition time as shown in Figure 2.6. This Figure shows the relationship between image distortions and acquisition time. Each panel shows

four images of the same microsphere acquired with progressively increasing acquisition times (a–e: 1.5, 3, 6, 12 and 24 min). In the left panels (a1–e1) the microscope was uncovered and in the right panels (a2–e2) the thermal protective enclosure was in place. A 5-min cyclical variation in laboratory temperature (amplitude: a1–e1 of 1.2 °C and a2–e2 of 1.9 °C) occurred during image acquisition. Within the enclosure the temperature remained stable but with an underlying increase of 0.6 °C over 160 min.

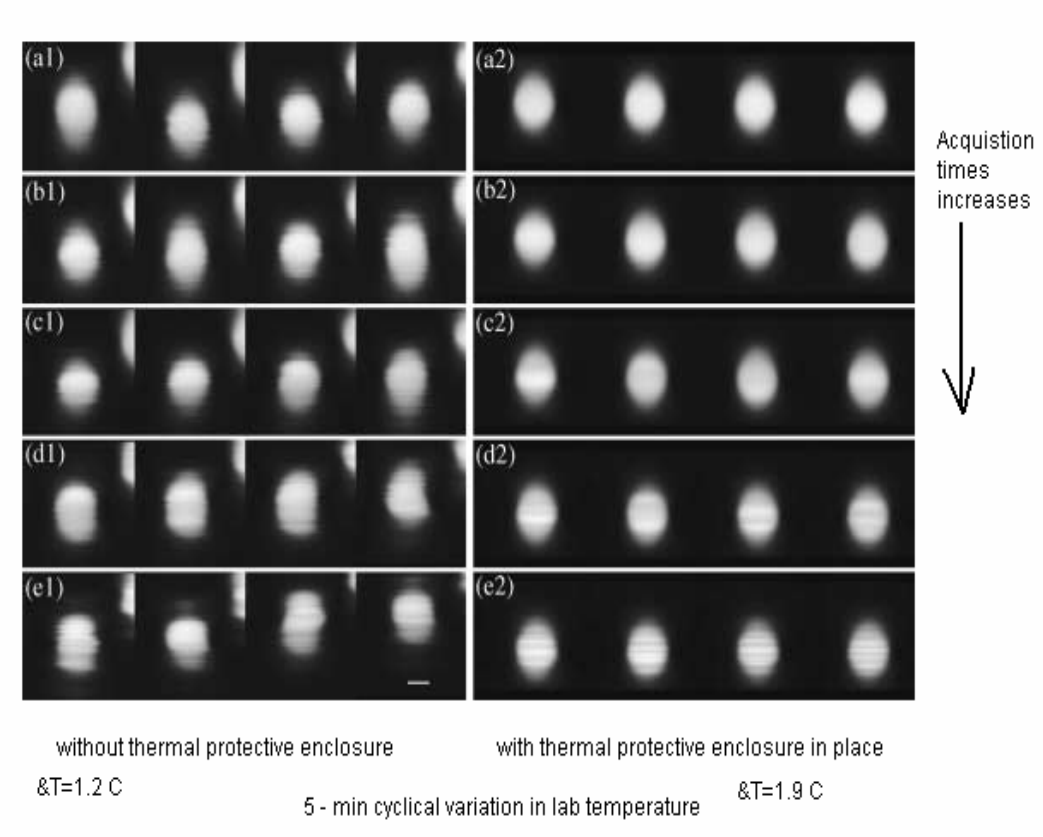

Figure 2.6. The Relationship Between Image Distortions and Acquisition Time.[1]

They found that the distortions in the image data sets are of a similar magnitude to the measured movements of the microscope stage. Figure 2.7 shows the microscope stability for X and Y axis movement. Figure 2.7 (a) shows the case when the thermal protective enclosure was mounted and fully sealed. The front access port opened (b) and finally the back ports also opened (c).

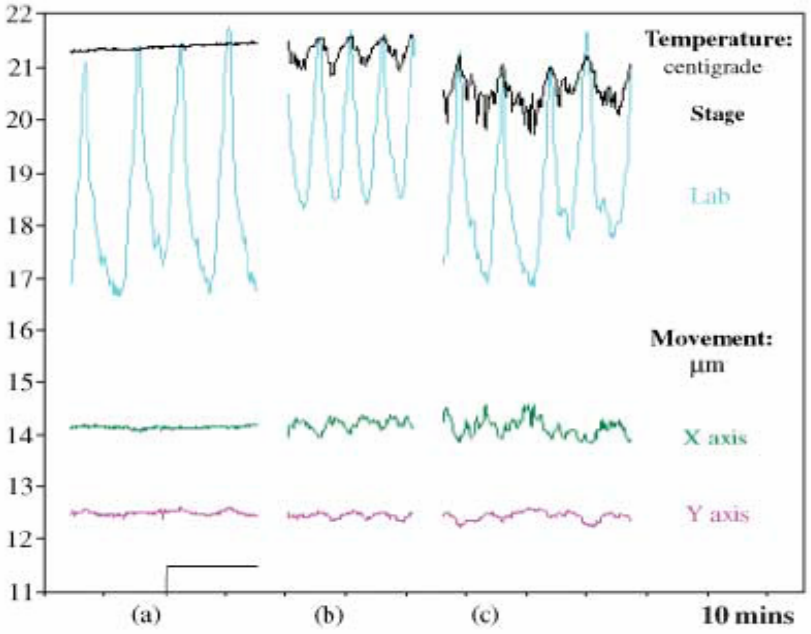

Figure 2.7. Microscope Stability *X* and *Y* Axis Movement.[1]

Suggestions have been developed to reduce the sensitivity of the TEM to environmental disturbances and reduce these disturbances. First, it is much easier to fix the problem before the microscope is installed than after installing it. It is also easier to fix the problem at its source rather than shielding at the instrument. Shielding attenuates, rather than removes disturbance. In many cases a new building might be cheaper than a new microscope. Active cancellation systems can be effective up to a point. For example, active compensation systems work best at low frequencies (10 Hz and below). The most common vibrations at industrial sites are at 30, 60 and 120 Hz from AC motors, and active systems provide little over passive systems at frequencies above 30 Hz. However, in many cases, the microscope will be a more sensitive monitor of the disturbance than the sensor used in the feedback loop.

All the examples presented in this section demonstrated the significant task that designing new specimen holder technology entails. Not only does the design need to meet all of the nternal requirements within the TEM, but it must also address any of the potential disturbances external to the TEM.

2.4 EXPERIMENTAL WORK

In order to fully understand the problems associated with TEM design and control, experiments were performed in the present research. These experiments investigated the pressure fluctuations on the stability and resolution of TEM experiments. To conduct these experiments, a specialized experimental system was designed as shown on Figure 2.8. Qualitative data was obtained that demonstrated the sensitivity of the TEM experiment to air pressure fluctuations. This experiment was not meant to verify our finite element simulations of a proposed holder design that will be presented later in this work. Rather, it was conducted to allow our research team to gain experience on TEM analysis when external disturbances are present. The experiments allowed our team gain valuable knowledge that was used in our innovative holder design.

In the experiments sound was generated from a speaker at known frequencies to induce air pressure fluctuations were of 73 Bd. A CCD camera was used to display the images on a computer screen. The holder was excited in two directions: the longitudinal X- axis and lateral Y- axis, as shown in Figure 2.8.

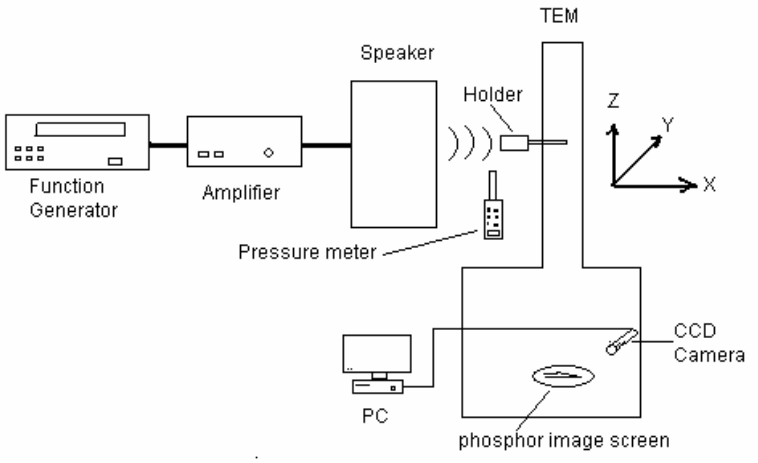

Figure 2.8. Schematic Diagram of Experimental Set Up

Figure 2.9 shows a snap shot of the sample (needle) under X330,000 magnification. In Figure 2.9, note that the image is clear and stable which make it useful for image interpretation.

Figures 2.10 to 2.14 show the sample experiencing vibrations when the speaker is turned on. In our proposed holder design, these vibrations will be eliminated.

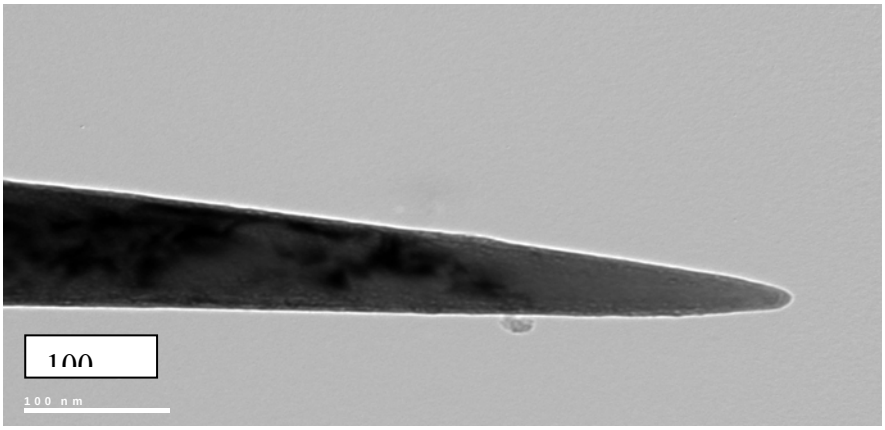

Figure 2.9. TEM image when the speaker is off

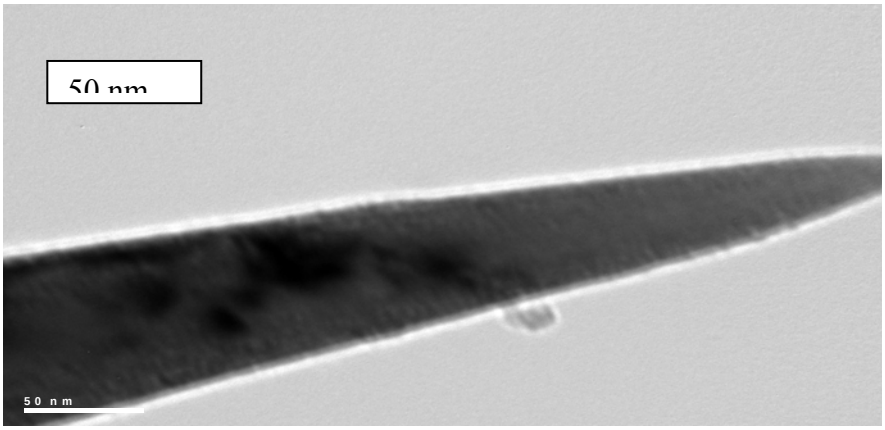

Figure 2.10. TEM Image at Excitation Frequency = 776 Hz Y-direction

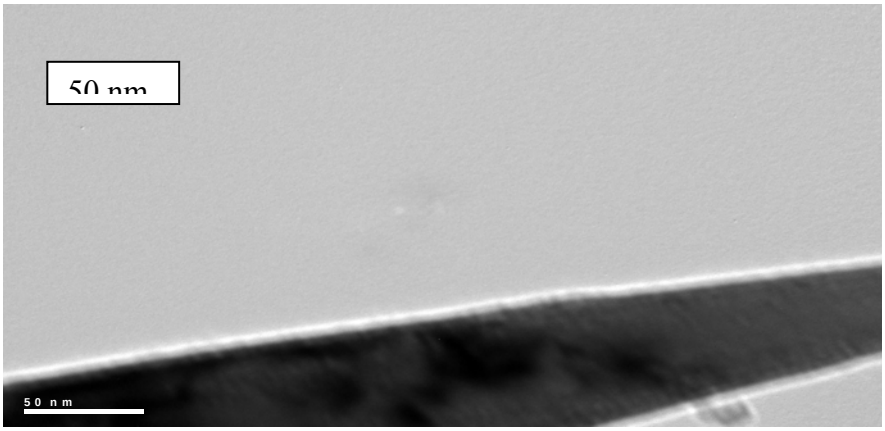

Figure 2.11. TEM Image at Excitation Frequency = 786 Hz in X-Direction

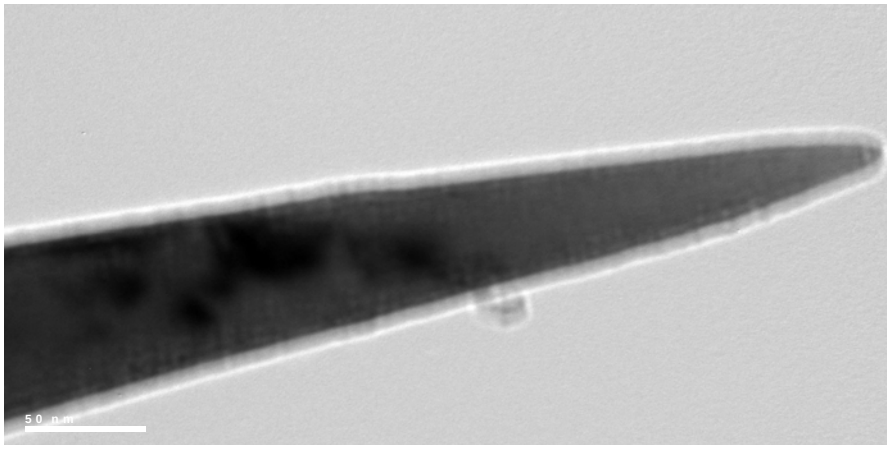

Figure 2.12. TEM Image at Excitation Frequency = 3430 Hz in Y-Direction

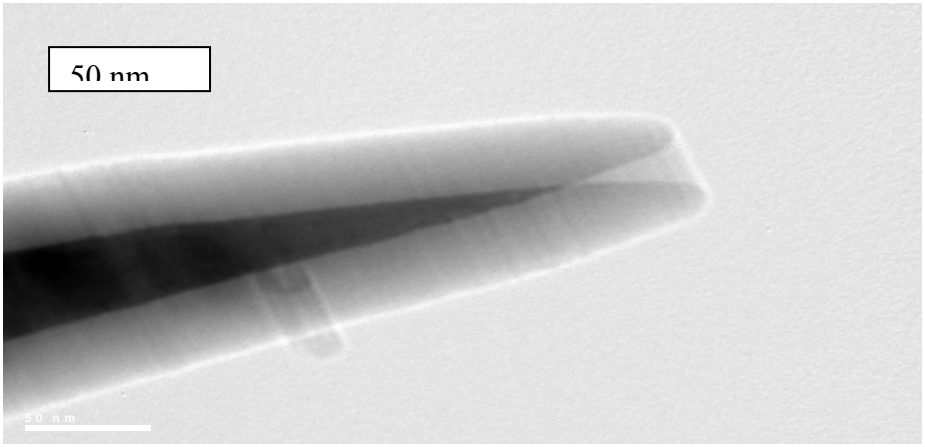

Figure 2.13. TEM Image at Excitation Frequency = 3436 Hz in X-Direction

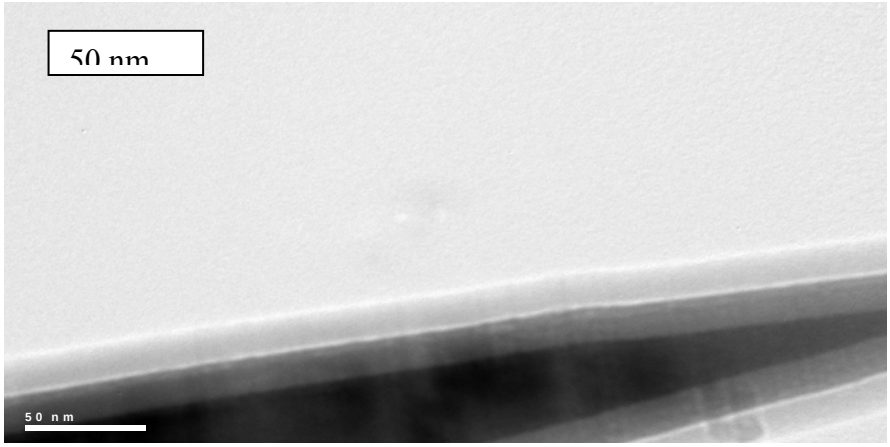

Figure 2.14. TEM Image at Excitation Frequency = 5576 Hz in X-Direction

2.5 SIGNIFICANCE OF THE PROBLEM

Transmission Electron Microscopy (TEM) has become an invaluable characterization technique in both the life and physical sciences. TEM allows high resolution imaging of the specimen as well as the spectroscopic acquisition of data relating to the material's elemental composition, and electronic structure. In the rapidly expanding field of nanotechnology, TEM has become the preferred technique for imaging nanoscale structures.[14] Electron microscopy enables materials analysis to be conducted at atomic resolution. Data resulting from this analysis yields the material's microstructure, crystalline orientation, elemental composition, and electronic structure.[29] This data can then be fed back into the material's manufacturing process to optimize its properties on the nanometer and sub-nanometer scale.

To date, experimentation in TEM has largely been two-dimensional and static. There is a current desire to move from the traditional imaging of atomic columns to individual atoms, from generation of two-dimensional information to three-dimensional information, and from static experimentation to dynamic experimentation.[16] It is the static to dynamic aspect that is defined by the term "in-situ" and will be significantly enhanced by the technology development described in this dissertation.

Hot deformation, dynamic recovery and dynamic recrystallization are important processes responsible for the evolution of microstructure and texture during deformation at high temperatures these processes are part of the scientifically and industrially important subject of thermomechanical processing.[35] However, many of the dynamic processes are not well understood, principally because it is very difficult to assess the nature of the high temperature microstructural processes solely from the traditional post mortem study of samples which have been deformed and subsequently cooled and examined. In contrast, *in situ* deformation experiments enable changes of microstructure and texture to be followed in a single region and, within the limits of such experiments, enable information to be obtained about the mechanisms of microstructural evolution.

Environmental TEM is a very effective instrument to understand the structural and chemical changes during gas–solid chemical reactions. It is particularly useful for nanomaterials that cannot be observed using other methods, e.g., catalytic reaction, corrosion, interface reactivity.[37] In situ experiments offer valuable insight into the chemical reaction processes. The early stages of nucleation and growth can be followed, and the morphology and the crystallography of the reactants and the products could be easily established. Many of the traditional techniques analyze catalyst samples under static, post-reaction conditions (reacted ex situ and cooled to room temperature) with samples held under high vacuum. These technologies are often not representative of the true dynamic state of a reacting catalyst, and in these techniques catalyst interactions are not observed directly. This has delayed a better fundamental understanding of dynamic catalytic surfaces, complex structural changes, and reaction mechanisms that evolve during oxidation-reduction processes.

The development of *in situ* specimen holder technology should greatly enhance the quantity of information generated by TEM. Substantial benefits would accrue to both life and physical science research by furthering the characterization of structures while undergoing various changes. This technology can also be used for a variety of applications, including the study of dynamic processes that need to be investigated in situ. Examples of such processes are the reactions involving the solid state, phase transitions, crystallite growth, thermal expansion, etc. thus effectively providing phase identification, texture analysis, and crystallite size measurement.

Three features were to be taken into account for the design of a new in situ specimen holder technology: the temperature homogeneity and stability of the sample, the correct measurement of the sample temperature, and minimum wattage usage and material outgasing characteristics.

One of the objectives of this research is the ability to accurately control and predict the sample temperature. Presently, the sample temperature can not be measured accurately, since a thermocouple can not be placed into contact with the sample. The thermocouple might also

interfere with X-rays. Typically, the temperature is measured by a type S thermocouple located as close as possible to the surface of the sample, where it does not interfere with X-rays. As the thermocouple can not be in direct contact with the sample, as in most heating systems, it is essential to carry out a temperature calibration, commonly performed using phase transitions with known Tc, which provides the temperature correction curve. However, it has been reported the problem with the uncertainty of the sample temperature. Through numerical analysis, this dissertation will demonstrate that the temperature variation within the sample can be modeled and accurately measured.

Design considerations will include ease of loading the specimen into the holder, the positioning of the holder in relation to the electron optics, the physical integration of the system with the TEM, methodology for applying the heat load, development of alternate heating methods, isolation of the specimen area from the TEM components, the possible adaptation of active compensation to adjust for changes in temperature and dimension as the specimen is heated, and technology for the presentation of varying environments and control technology relating to flow and pressure. Ideally, the device will be configured in such a manner so as to allow tomographic analysis. All of these issues will be considered in terms of the relationship to the physical characteristics of the TEM and the corresponding effects on imaging and acquisition of analytical data.

2.6 TECHNICAL APPROACH

2.6.1 Solid Models

Solid modeling is a powerful design technique. It will be the first step in developing our proposed new specimen technology. Prior to the fabrication of any component, a complete design will be simulated in a computer-generated design space. Each component of a design is simulated to scale in a three-dimensional "solid" form. All of the components will then be assembled in the design space. Upon assembly, the model will be assessed for proper fits and clearances between parts. Kinematic motion will be simulated and checked for proper clearance

between moving parts. Force vectors will be established in order to generate the desired motion. The model of the in-situ hardware will be combined with a model of the applicable TEM components (goniometer, vacuum port, pole piece, apertures, etc.) and a similar analysis will be performed. Finally, the models will be transferred directly into ANSYS software for the execution of Finite Element Analysis (FEA).

2.6.2 Finite Element Analysis

FEA is a powerful design tool. When attempting to assess a design characteristic of a part (such as mechanical stress, or thermal loading), conventional calculations are impeded by complex geometries. FEA is a method of breaking down a complex geometry into manageable "elements" or simpler geometries whose boundary conditions are known. Solid models are used as a basis for FEA analysis. Initially, the overall geometry is divided into elements of known size and shape so as to nearly approximate the initial geometry. The design characteristics of the various elements are calculated based on initial boundary conditions. This type of analysis will be used to qualify the components and assemblies in terms of mechanical stress, thermal loading and dynamic mechanical behavior.

2.6.3 Direct Simulation Monte Carlo

Direct Simulation Monte Carlo (DSMC) is a well-established approach that has been widely and successfully used to simulate high Knudsen Number (Kn) gas flow problems. DSMC will be used to optimize the design of E-Cell TEM holder and to specifically model inlet and exhaust gasses, map pressures, and assess specimen impingement rates in a vacuum chamber.

2.7 OUTLINE OF THE THESIS

The objective of this thesis is to develop a novel in situ environmental specimen holder technology that is capable of elevating the temperature of a material research specimen from ambient to +2,000 K while simultaneously subjecting it to varying environments. It is apparent from our previous discussion that no prior quantitative analyses have been performed. Up to this date, design on specimen holders has performed using trail and error techniques and experiments which lacked high accuracy. Experiments which lacked with TEM have been largely two dimensional and static. Hence, our objective is to develop an in situ holder using more rigorous design tools. Specifically, this dissertation will use the following approaches to develop state of the art specimen holders that can be used in in -situ TEM experiments:

1. Performing in depth vibration analyses using FEA tools for the current holder assemblies developed by Fischione Instruments. (Chapter 3)
2. Performing thermal analysis (radiation) for the current straining holder developed by Fischione Instruments. (Chapter 4)
3. Designing optimum heating holders that overcome the technical problems associated with the current assemblies. These holders must be dynamically stable for accuracy and image processes, capable of elevating the sample temperature up to 2000 K with minimum controllable drift of the sample position. (Chapter 5)
4. Investigating alternative heating techniques, more specifically utilizing a localized laser diode for heating a specimen. (Chapter 5)
5. Designing and optimizing an environmental TEM holder technology using DSMC methods. (Chapter 6)

3.0 TOMOGRAPHY HOLDER VIBRATION ANALYSIS

The specimen holder is typically a cylindrical rod approximately 10 mm in diameter and 250 mm in length that is inserted into the TEM's goniometer stage (Figure 3.1). Such a holder affords high tilt and extended fields of view in high resolution TEMs with narrow gap pole pieces. This model is ideal for life and physical sciences electron tomography as well as any other application requiring high-specimen tilt. It uses two diametrically opposed clamps and minimizes the specimen holder material in the area immediately adjacent to the specimen. This geometry allows for a relatively large viewable area at angles in excess of 70^{o}. The primary material used for holder assembles is beryllium copper because of its desirable X-ray characteristics.

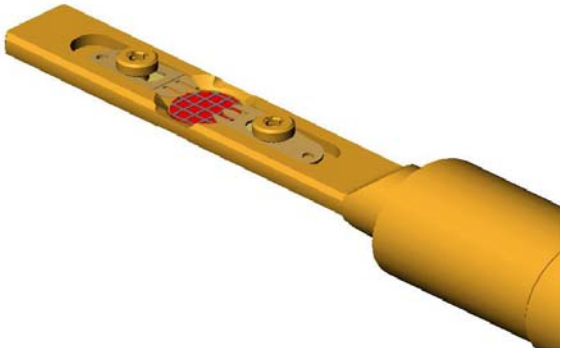

Figure 3.1 Tomography Holder

3.1 DYNAMIC ANALYSES

On high precision instruments, stringent demands must be imposed on the dynamic stability of the system. Distortion of the image or positioning accuracy of critical parts can

originate from both inside and outside of the microscope. Internal sources include the vacuum pump and coolant circulating inside the microscope. External sources include mechanical vibration, electrical disturbances, magnetic fields, electromagnetic interference (EMI), air flow, thermal fluctuations and acoustic vibrations.

As discussed in chapter 2, the acoustic vibrations may originate from external sources such as planes, trains, automobiles, machinery facility noise and other laboratory equipment. Internal acoustic sources are caused by fans, electronic noise and human noise. Typical methods of minimizing the effect of vibration modes are maximizing the natural frequencies of the system and increasing the structural damping of the modes. These two methods will lead to increases in the accuracy of the system.

This study presents dynamic analyses of a TEM holder assembly designed by Fischione Instruments. The analyses were performed with the finite element package ANSYS. The disturbance in this study was confined to vibrations caused by human being's voice inside the microscope room. The human voice is a series of harmonically related sine waves which cause a periodic variation in air pressure about atmospheric mean. Frequencies typically range between 100 -10000 Hz. Sound pressure levels are measured on a logarithmic scale. For normal human conversation these range between 40 and 60 db, where 60 db corresponds to 1 Pa. Although this study is limited to the particular disturbance caused by a human voice, many other disturbances take the same forms.

3.2 MODAL ANALYSIS

Modal analysis is used to determine the vibration characteristics (natural frequencies and mode shapes) of a structure. The natural frequencies and mode shapes are important parameters in the design of a structure for dynamic loading conditions. It also can be a starting point for another, more detailed, dynamic analysis, such as a transient dynamic analysis, a harmonic response analysis, or a spectrum analysis.

Modal analysis in the ANSYS family of products is a linear analysis. There are several mode-extraction methods: Block Lanczos (default), subspace, PowerDynamics, reduced, unsymmetric, damped, and QR damped. The damped and QR damped methods can be used to include damping in the structure.[12]

The equation of motion for an undamped system is

$$[M]\{\ddot{U}\} + [K]\{U\} = \{0\} \tag{3-1}$$

where [K] is the structure stiffness matrix,

[M] is the structure mass matrix, and

{U} is the displacement vectors.

For a linear system, free vibrations will be harmonic of the form:

$$\{U\} = \{\Phi\}_i \cos \omega_i t \tag{3-2}$$

where, $\{\varphi\}_i$ is eigenvector representing the mode shape of the ith natural frequency,

ω_i = ith natural circular frequency (radians per unit time), and

t = time.

Substituting the harmonic form (3-2) into equation (3-1), yields:

$$(-w_i^2[M] + [K])\{\Phi\}_i = \{0\} \tag{3-3}$$

This equality is satisfied if either $\{\varphi\}_i = \{0\}$ or if the determinant of ([K] - ω^2 [M]) is zero. The first option is the trivial one and, therefore, is not of interest. Thus, the second one gives the solution:

$$\left|[K] - \omega^2[M]\right| = 0 \tag{3-4}$$

This is an eigenvalue problem which may be solved for up to n values of ω^2 and n eigenvectors $\{\varphi\}_i$ which satisfy Equation 3-1, where n is the number of DOFs. The equations of elastic structural systems without external excitation can be written in the following form:

$$[M]\{\ddot{U}\} + C\{\dot{U}\} + [K]\{U\} = \{0\} \tag{3-5}$$

The dynamic response of the system is given by

$$\{u\}_i = \{\Phi\}_i e^{(\sigma_i + j\omega_i)t} \tag{3-6}$$

where [C] is the structure damping matrix

Let, $\lambda_i = \sigma_i + j\omega_i$ (3-7)

where, λ_i is the complex eigenvalue, σ_i is the real part of the eigenvalue and ω_i is the imaginary part of the eigenvalue.

3.3 HARMONIC RESPONSE ANALYSIS

Harmonic response analysis provides the ability to predict the sustained dynamic behavior of a structure, thus enabling a designer to verify whether or not their designs will successfully overcome resonance, fatigue, and other harmful effects of forced vibrations. It is a technique used to determine the steady-state response of a linear structure to loads that vary sinusoidally (harmonically) with time. The idea is to calculate the structure's response at several frequencies and obtain a graph of some response quantity (usually displacements) versus frequency. "Peak" responses are then identified on the graph and stresses are reviewed at those peak frequencies. The transient vibrations, which occur at the beginning of the excitation, are not accounted for in a harmonic response analysis.

The transient dynamic equilibrium equations of interest are as follows for a linear structure:

$$[M]\{\ddot{U}\} + C\{\dot{U}\} + [K]\{U\} = \{F^a\} \tag{3-8}$$

where $\{\ddot{U}\}$ is a nodal acceleration vector,

$\{\dot{U}\}$ is a nodal velocity vector.

{U} is a nodal displacement vector, and

$\{F^a\}$ is a load vector.

The harmonic response analysis solves the time-dependent equations of motion (equation 3-8) for linear structures undergoing steady-state vibration.

All points in the structure are moving at the same known frequency, however, not necessarily in phase. Also, it is known that the presence of damping causes phase shifts. Therefore, the displacements may be defined as:

$$\{u\} = \{u_{\max} e^{j\varphi}\} e^{j\Omega t} \tag{3-9}$$

where: u_{max} = maximum displacement,

Ω= imposed circular frequency (radians/time) = $2\pi f$, and

φ= displacement phase shift (radians).

Note that u_{max} and φ may be different at each DOF. The use of complex notation allows a compact and efficient description and solution of the problem. Equation 3-9 can be rewritten as:

$$\{u\} = \{u_{\max} (\cos\varphi + j \sin\varphi)\} e^{j\Omega t} \tag{3-10}$$

$$\{u\} = (\{u_1\} + j\{u_2\}) e^{j\Omega t} \tag{3-11}$$

$$\{F^a\} = \{F_{\max} e^{j\varphi}\} e^{j\Omega t} \tag{3-12}$$

$$\{F^a\} = (\{F_1\} + j\{F_2\}) e^{j\Omega t} \tag{3-13}$$

Substitution of equation 3-11 and equation 3-13 into equation 3-8 gives:

$$([K] - \Omega^2[M] + j\Omega[C])(\{u_1\} + j\{u_2\}) = \{F_1\} + j\{F_2\} \tag{3-14}$$

3.4 FINITE ELEMENT MODEL

The ANSYS CAE (Computer-Aided Engineering) software program was used in conjunction with 3D CAD (Computer-Aided Design) solid geometry to simulate the behavior of mechanical bodies under dynamic loading conditions. Each simulation includes known factors about a design such as material properties, contact behavior between bodies (in an assembly), and types and magnitudes of loading conditions. The results of a simulation provide insight into how the bodies may perform and how the holder design can be improved for in-situ

experimentations. The bounding box for all positioned bodies in the present model (see Figure 3.2) measures .24 by 1.4×10^{-2} by 1.4×10^{-2} m along the global X, Y and Z axes, respectively. The model has total mass of .14 Kg.

The actual assembly 'solid model' created by Fischione Instruments was imported into ANSYS. No geometry simplifications were required. ANSYS is very powerful package that has the capability to communicate with many CAD software packages. Material properties such as density, modulus of elasticity and Poisson's ratio were required for dynamic analysis for each body. A modal analysis is the starting point for a harmonic response analysis. Modal analysis was used to determine the vibration characteristics (natural frequencies and mode shapes) of the model. The model consisted of approximately 88,000 elements. All elements for the assembly components were of type SOLID187 and SOLID186 chosen from the standard ANSYS element library. These elements are a higher order 3-D, 10-node element and 20 – node, respectively. SOLID187 and SoOLID186 have a quadratic displacement behavior and are well suited to modeling irregular meshes such as those produced from various CAD/CAM systems. Conta174, Targe170 and Conta174 were used between contacting bodies. A very fine mesh was generated at critical parts of the assembly, especially in the parts of the holder tip that were very near or in contact with the sample. Among other locations where a fine mesh was used were locations at the TEM's goniometer stage (spherical support).

The TEM goniometer stage was modeled as three 3mm silver spheres 120^0 apart at two locations along the holder as shown in Figure 3.2. The X-axis lies along the length of the holder. The Y-axis is perpendicular to the sample face. Of the three spheres at each support location, the sphere that was located along the Y- axis was assumed to be attached to a spring damper. The loading condition for free vibration analysis requires only a constraint from rigid body motion. This loading condition for free vibration analysis (modal) is a fixed support at the six spheres. We assumed that the clamping mechanism between the sample and the sample grid fully constrained the sample. A contact bond was used to satisfy this condition. We also assumed that the clamping mechanism between the sample grid and the holder tip were bonded. Standard contact conditions were used between the spheres and the holder body.

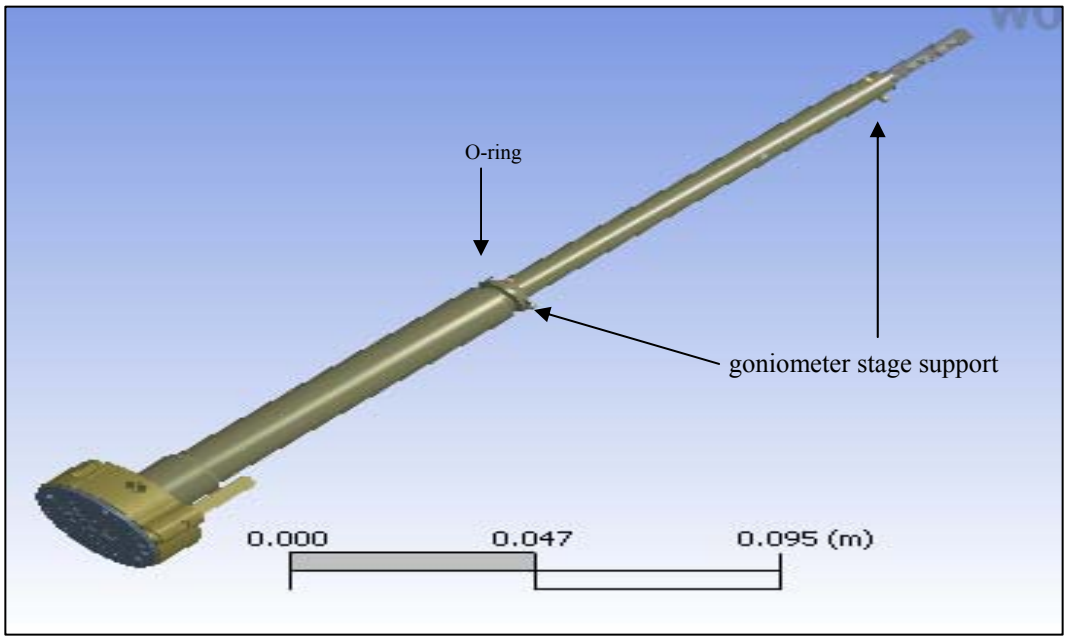

Figure 3.2. Tomography Holder Model

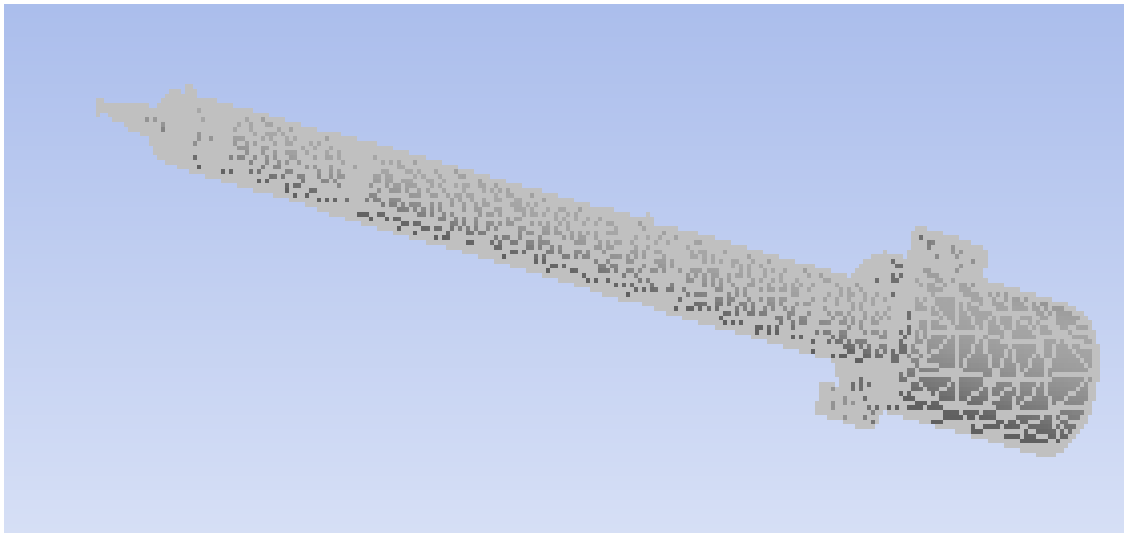

Figure 3.3. Finite Elements Mesh

3.5 RESULTS AND DISCUSSION

3.5.1 Modal Analysis

From the finite element model, natural frequencies of vibration were obtained for the original holder design. Table 3-1 lists the first 10 frequencies, Figure 3.4 shows the mode shapes corresponding to the first and fourth natural frequencies.

Table 3-1 Natural Frequencies

SET	FREQ(Hz)
1	112.93
2	165.36
3	1270.8
4	1403.5
5	1599.8
6	1674.1
7	1864.6
8	2726.4
9	3048.2

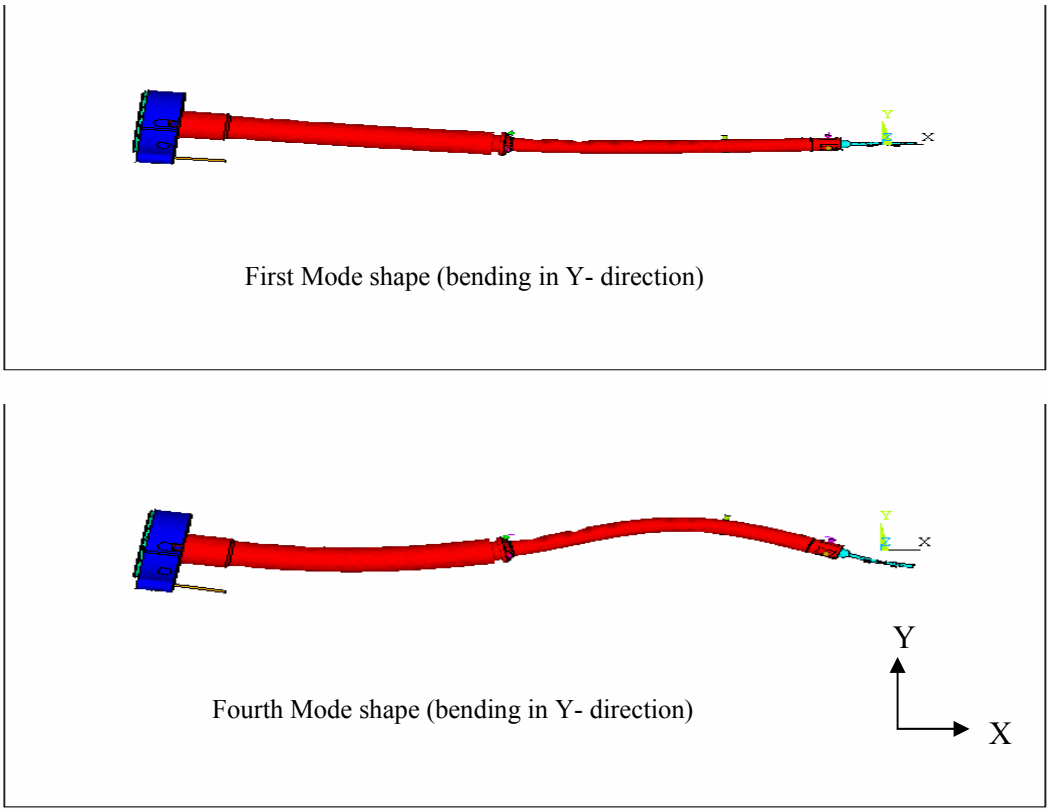

Figure 3.4. Mode Shapes

The values for the natural frequencies fall within range of the audio exciting frequencies, which obviously posses a significant limitation within attempting to perform accurate experiments. Dynamics response will be studied in the vicinity of those frequencies where the resonant phenomena might occur.

3.5.2 Harmonic Analysis

Harmonic response analysis was used to predict the dynamic behavior of the model a under sustained dynamic load. This technique was used to determine the steady-state response of a linear structure to loads that vary sinusoidally with time. In addition to the previous assumptions, we assumed there are no thermal strains due to irradiation from the electron beam. We chose a value of 1 Pa to be the dynamic load. This value was a very conservative value which represents a loud human conversation. We used a structural damping constant of 5% for

the entire simulation. This value is very conservative due to the fact that screws and bolts are used to connect many parts. These types of connections would provide higher damping values compared to more rigid connections such as welds.

Figure 3.5 shows the sample displacements in three directions. SI units were used throughout all simulations (m, s, kg). These simulations were focused to obtain the response in the vicinity of the first natural frequency obtained from the previous analysis. The modal analysis predicted a value of 100 Hz for the first natural frequency and found that the Uy displacement would be significantly larger than the other two degrees of freedom as shown in Figure 3.5. The damped resonance frequency is less than the undamped natural frequency due to included internal damping. The peak amplitude of displacement in the y-direction is on the order of 10 nm when the damping coefficient of the goniometer stage was set to zero (left plot). When damping was added, the magnitude was on the order of 1nm as shown in the plot on the right. The lateral displacement is on the order of .8nm at this excitation frequency. The lateral displacement (Uz) when the system was exited around the second natural frequency was near 1nm.

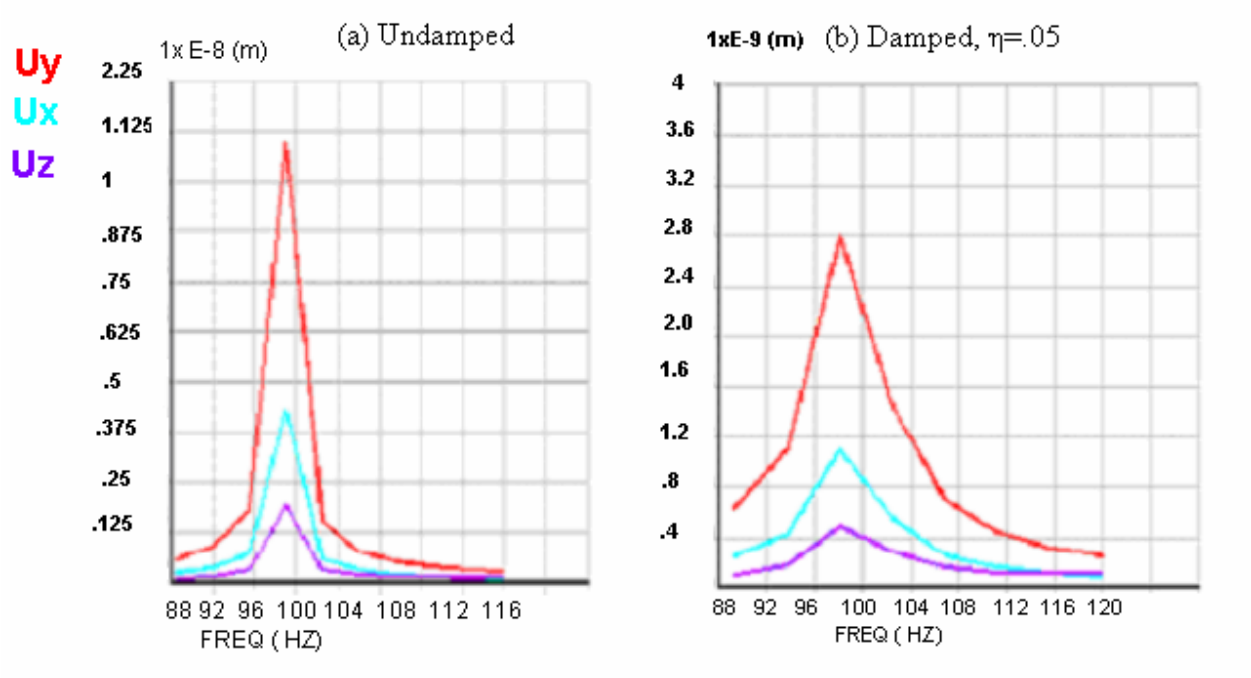

Figure 3.5. Ux, Uy, Uz Displacement (m) at Sample Location

Since damping plays a significant role in minimizing the amplitude of the displacement around the natural frequencies, simulations were run to obtain the response at different damping values. Figure 3.6 shows the maximum displacement response as a function of damping magnitude at the resonance frequency. The magnitude of the displacement has been reduced by an order of approximately 10 as a result of damping.

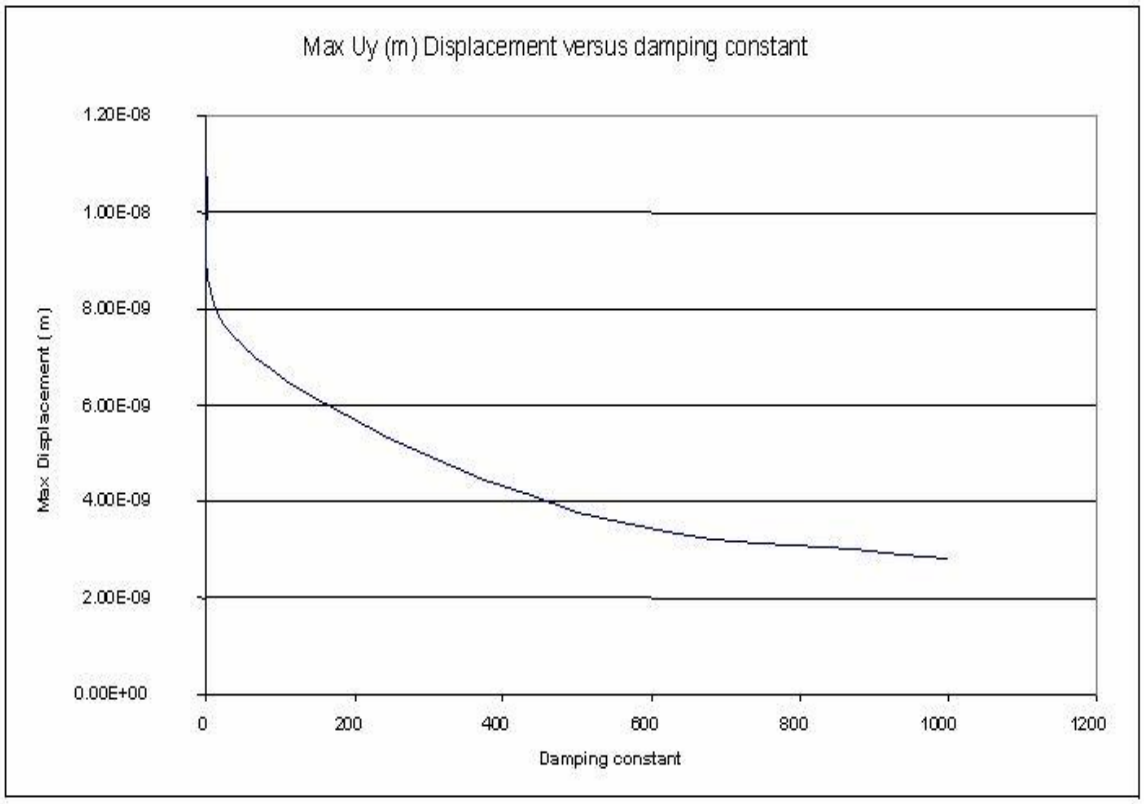

Figure 3.6. Uy Displacement at Sample Location versus Damping Constant

3.6 DISCUSSION

Dynamic analyses using ANSYS were carried out on the tomography holder designed by Fischione Instruments. FEA predicted a displacement on the order of 1nm in response to a harmonic pressure of 1 Pa. Since the driving frequency has a wide range of 100 -10000 HZ, changing the natural frequency will not be effective. Two methods can therefore be used to

reduce the vibration at resonance, increasing internal damping and vibration isolation. Internal damping can be achieved by using very stiff material that has a high loss factor or by using concentric laminated shells that allow internal sliding instead of solid-body. A vibration isolator can be used to reduce the transmitted force to the specimen area.

3.7 VACUUM TRANSFER MECHANISM ANALYSIS

Figure 3.7 and 3.8 show the solid model layout of a vacuum transfer design with TEM pole pieces for reference. The main risk identified is effectively decoupling the specimen cartridge from the holder body. This technology has a very thin tip that ultimately allows viewing the specimens at $\pm 80^0$. It also incorporates a driving mechanism for protecting the specimens during transferring it through different stages. FEA analyses were used to assess the effect on specimen stability due to decoupling. Also, the distance from the leading surface to the central axis of the specimen will vary from one microscope to the next. This distance effects specimen stability, and was analyzed through FEA. The vacuum seal door is suppressed in the FEA models as a simplifying assumption.

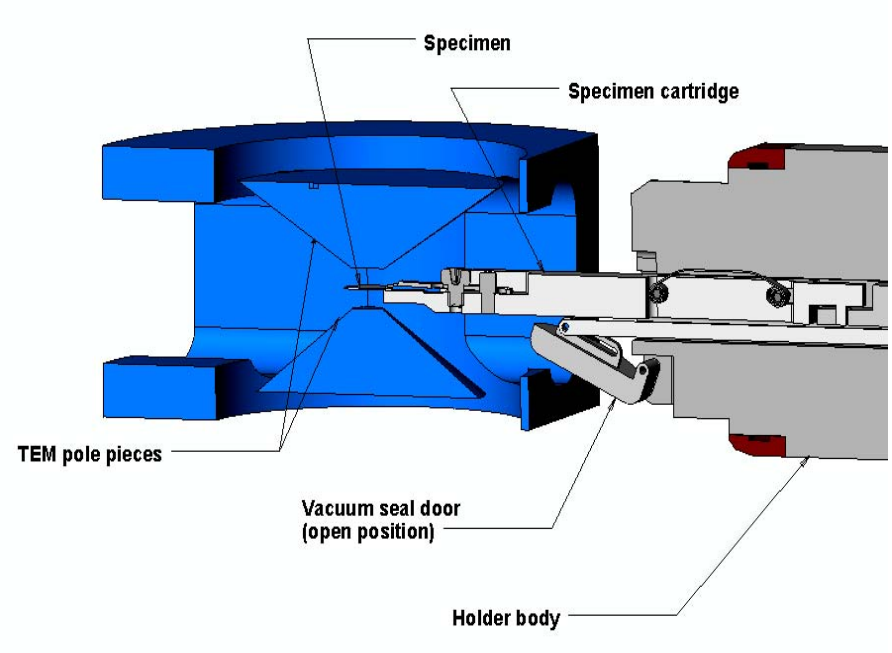

Figure 3.7. Vacuum Transfer Holder Technology

Procedures that were carried out to develop the finite element model on the tomography holder were repeated for this holder. Identical boundary conditions, loading conditions and computational parameters were applied. The X-axis lies along the length of the holder. The Y-axis is perpendicular to the sample face.

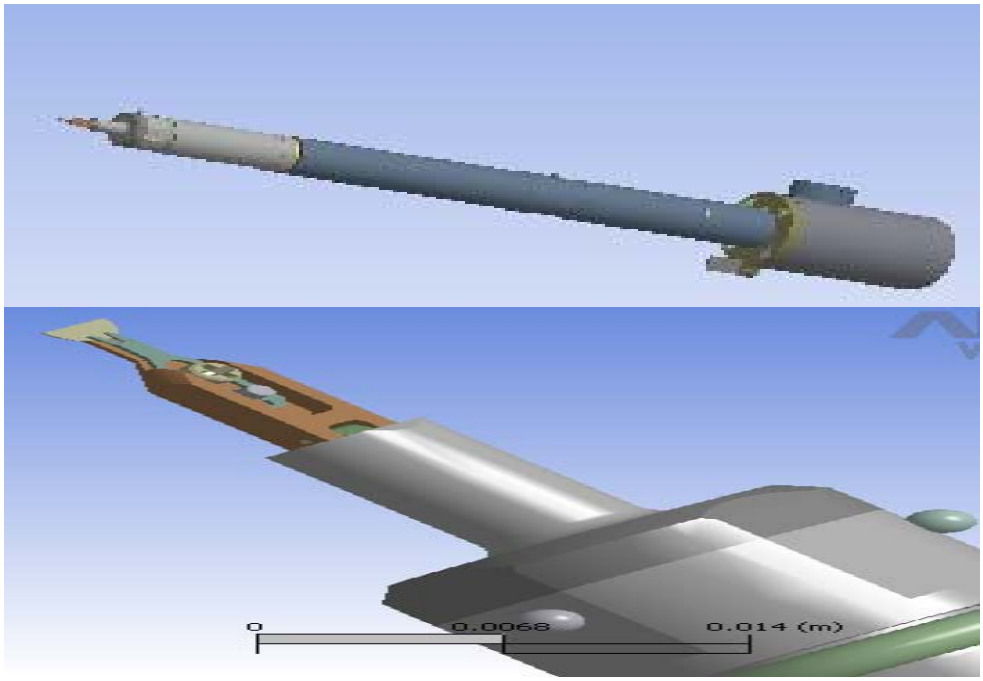

Figure 3.8. Vacuum Transfer Holder Technology

Natural frequencies were obtained from the modal analysis. Figures 3.9, 3.10 and 3.11 show the displacements in three directions at the sample location obtained from the harmonic analysis. The magnitude of the displacement in the Z- direction for this holder is lower than the standard tomography holder. The reason is that the retracting mechanism provides both damping and isolation to the specimen cartridge. The displacement in the X- direction is higher for this technology. The reason is that the retracting mechanism does not provide a rigid connection in this direction. This may be overcome with a stronger spring load on the cartridge, or a more rigid connection to the retraction mechanism. Both of these alternatives will be considered as part of the future study.

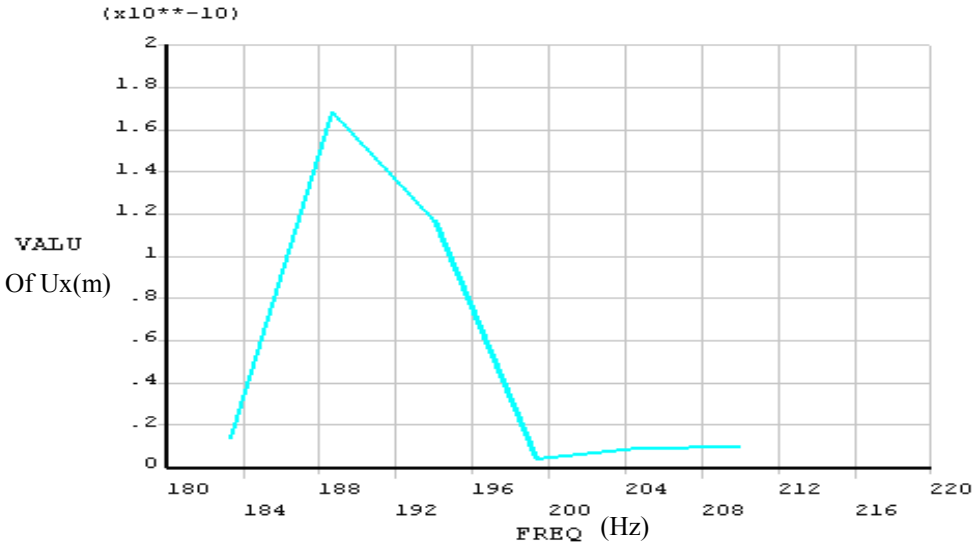

Figure 3.9. Ux (m) Displacement at Sample Location

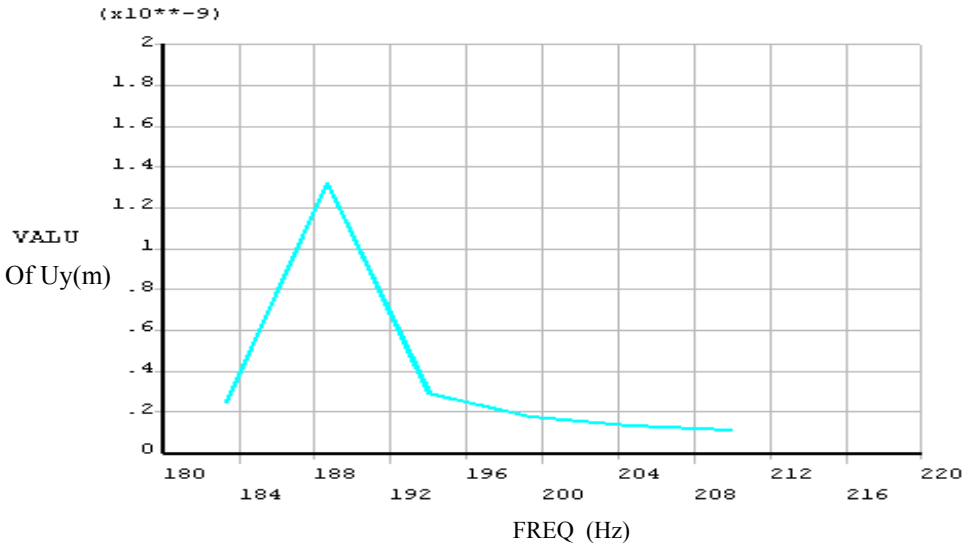

Figure 3.10. Uy (m) Displacement at Sample Location

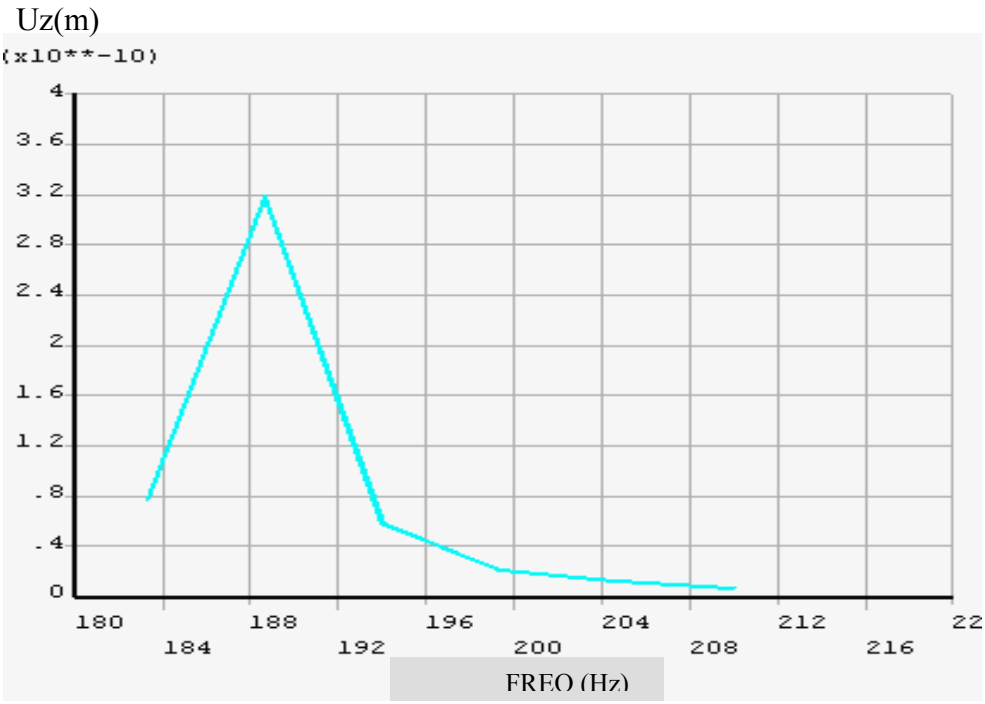

Figure 3.11 Uz(m) Displacement at Sample Location

Further simulations were carried out to investigate the effect of extending the tip holder 3 mm to be incorporated into different TEM technology. Simulations were made using the same boundary and load conditions. Figure 3.12 shows the effect of incrementing the tip holder on Uy displacement. As is expected, extending the length of the tip holder will increase the displacement at the sample area.

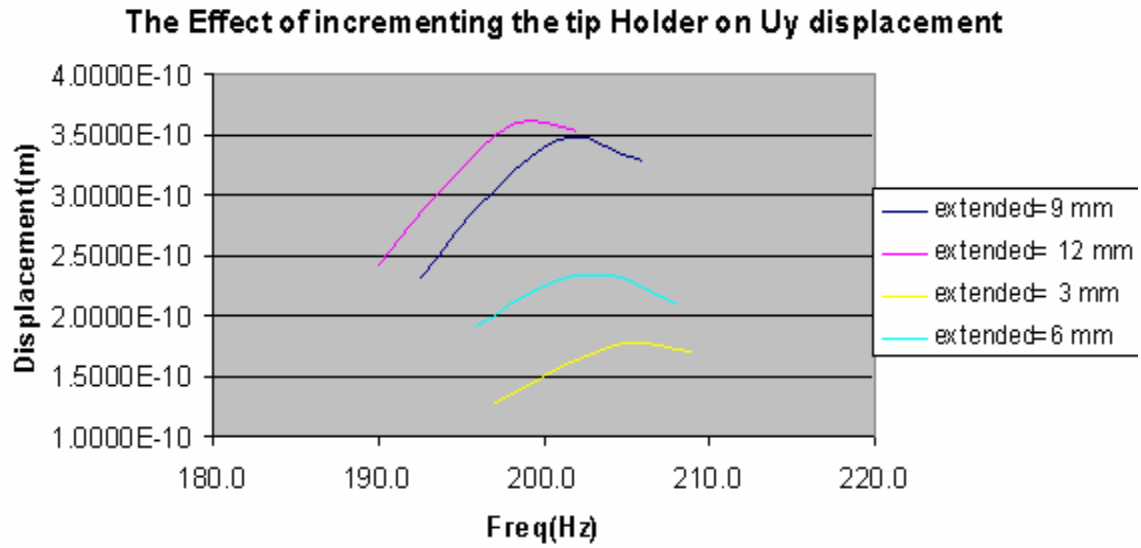

Figure 3.12. Uy (m) Displacement at Sample Location

Based on vibration simulations presented in this chapter, it is clear that a redesigned holder can significantly improve the dynamic behavior of the system so that more reliable experiments can be performed.

4.0 HEATING/STRAINING HOLDER

Hot deformation, dynamic recovery and dynamic re-crystallization are important processes responsible for the evolution of microstructures and textures during deformation at high temperatures and are part of the scientifically and industrially important subject of thermomechanical processing.[35] Many of the dynamic processes of heating, however, are not well understood, principally because it is very difficult to assess the nature of the high temperature microstructural processes solely from the traditional post study of samples which have been deformed and subsequently cooled and examined. In contrast, in situ deformation experiments enable changes of microstructure and texture to be followed in a single region, thus enabling information to be obtained about the mechanisms of microstructural evolution. Fig 4.1 shows a heating straining holder designed by Fischione Instruments. This holder is capable of heating the specimen up to 1,200 ^{o}C, while simultaneously applying a one-pound tensile load in a constant force mode. This type of holder is mainly used for conducting creep experiments on Ni-based superalloys.

4.1 OBJECTIVE

The objective of this chapter is to develop a comprehensive simulation model of the present holder assembly using FEM for conducting transient heat transfer analysis. Simulation will be used to predict the temperature distribution in the holder and to investigate ways of improving the current designs based on the predicted results.

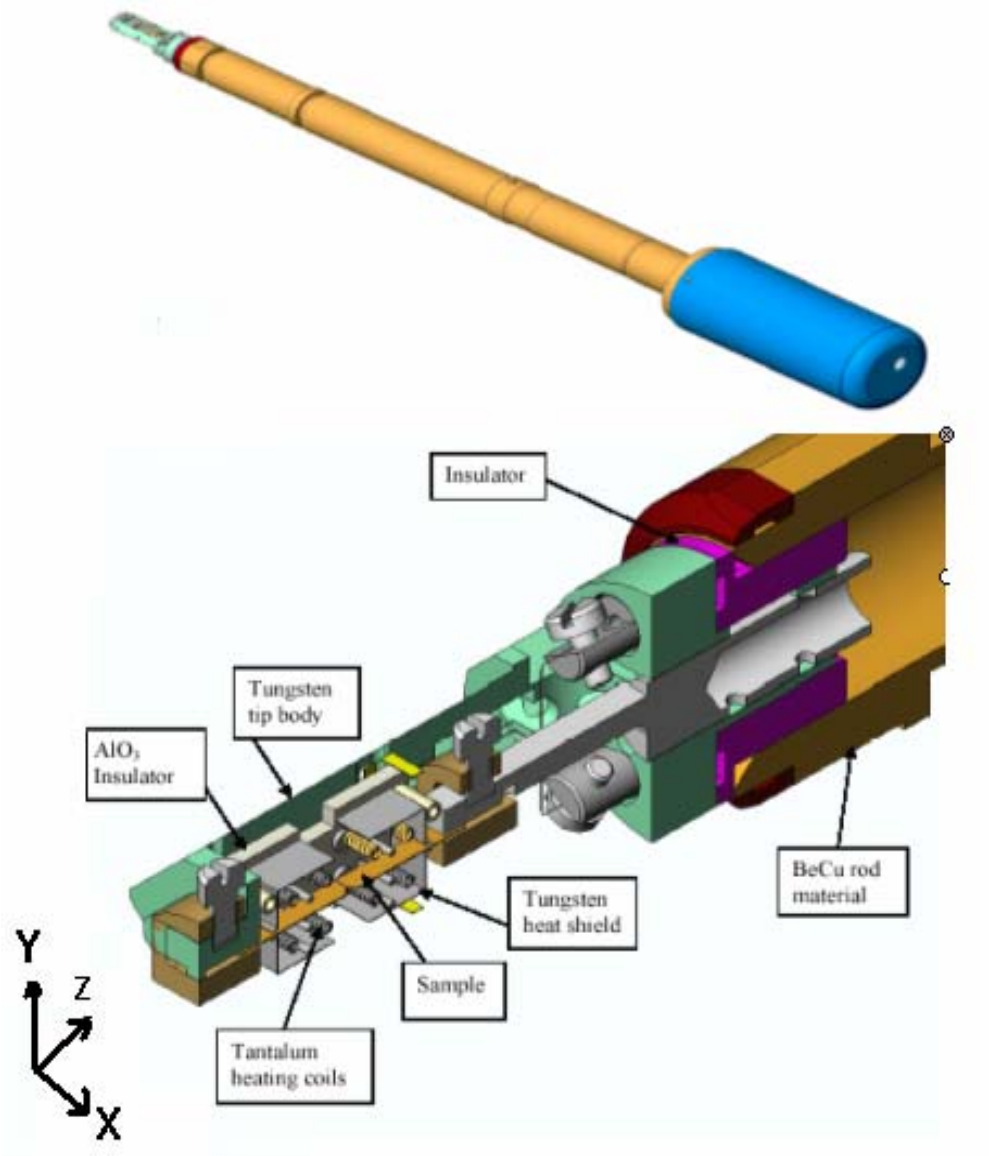

Figure 4.1. Heating Straining Holder

4.2 HEAT TRANSFER FUNDAMENTALS

The first law of thermodynamics states that thermal energy is conserved. The differential equation governing the heat flow on a differential volume is:

$$\rho c(\frac{\partial T}{\partial t} + \{V\}^T [L]T) + [L]^T \{q\} = \ddot{q} \qquad (4\text{-}1)$$

where ρ = density

c = specific heat

T = temperature (=T(x, y, z, t))

[L] is a vector operator, $[L] = \{\frac{\partial}{\partial x}, \frac{\partial}{\partial y}, \frac{\partial}{\partial z}\}$ (4-2)

{V} is the velocity vector for mass transport of heat

{q} is heat flux vector

$\{\ddot{q}\}$ is the heat generation rate per unit volume

Fourier's law is used to relate the heat flux vector to the thermal gradients:

$$\{q\} = -[D]\{L\}T \quad (4\text{-}3)$$

where [D] is conductivity matrix

$$[D] = \begin{bmatrix} K_{xx} & 0 & 0 \\ 0 & K_{yy} & 0 \\ 0 & 0 & K_{zz} \end{bmatrix} \quad (4\text{-}4)$$

There are three types of boundary conditions encountered in solving thermal problems: specified temperatures acting over a surface, specified heat flows acting over a surface and specified convection acting over surface (Newton's law of cooling).

4.2.1 Radiation

Radiation is the transfer of energy via electromagnetic waves. The waves travel at the speed of light, and energy transfer requires no medium. Thermal radiation is just a small band on the electromagnetic spectrum (i.e. wavelength λ ranges between 0.1 and 100 μm). Because the heat flow that radiation causes varies with the fourth power of the body's absolute temperature, radiation analyses are highly nonlinear. ANSYS introduces radiation effects only through the boundary conditions; the coupling is especially strong due to nonlinear dependence of radiation on surface temperature.

The heat transfer rate between surfaces i and j radiating to each other is:

$$Q_i = \sigma \varepsilon_j F_{ij} A_j (T_i^4 - T_j^4) \quad (4\text{-}5)$$

where:

T_i, T_j are the absolute temperature at surface i and j, respectively

Q_i is energy loss of surface i

σ is Stefan-Boltzmann constant

ε_i is effective emissivity of surface i

F_{ij} is radiation view factors

A_i = area of surface i

The view factor, F_{ij}, is defined as the fraction of total radiant energy that leaves surface i which arrives directly on surface j

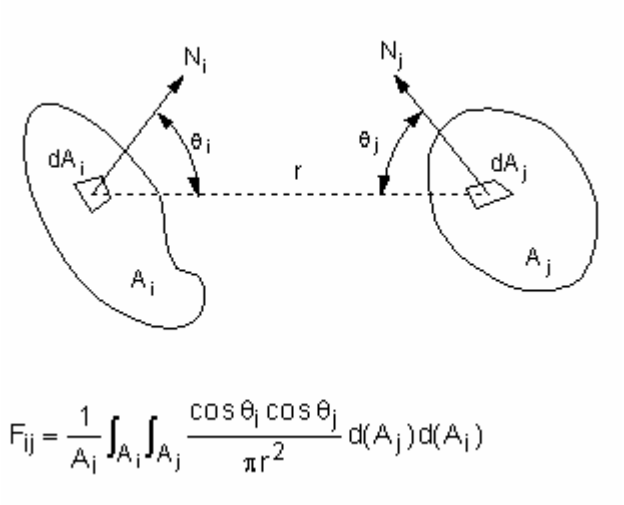

Figure 4.2. View Factor Calculation Terms

Emissivity is a surface radiative property defined as the ratio of the radiation emitted by the surface to the radiation emitted by a black body at the same temperature. ANSYS restricts radiation exchange between surfaces to gray-diffuse surfaces. The word grey signifies that the emissivity and absorptivity of the surface do not depend on wavelength. The word diffuse signifies that emissivity and absorptivity do not depend on direction. For a gray diffuse surface, emissivity = absorptivity; emissivity + reflectivity = 1. A black body surface has a unit emissivity.

4.3 FINITE ELEMENT MODEL

A comprehensive simulation model using FEM for the analysis of transient heat transfer in the current holder assembly was developed. The simulations were carried using the ANSYS Package. The objective of this work was to predict the temperature distribution in the holder and to investigate ways of improving the current designs based on the predicted results.

The actual Solid Model provided by Fischione was imported into ANSYS. The material properties which were input to the finite element model were obtained from a combination of various sources.[8][36] The model consisted of about 113,000 elements. All solid elements were of type SOLID87 and SOLID90 which are well suited to model irregular meshes (such as those produced from various CAD/CAM systems). These elements are a 3-D 10-Node tetrahedral thermal solid and a 3-D 20-Node thermal solid, respectively. These elements have one degree of freedom, temperature, at each node. Three modes of heat transfer (conduction, convection and radiation) were included in all simulations. Convection heat transfer was applied as a surface load on the part of the model that is not under vacuum condition. We chose a value of 15 ($W/m^2.C$) for the heat convection coefficient at the very end of the holder. A lower value was chosen on the part of the holder that is inside the microscope up to the vacuum seal. Under vacuum conditions there are only two modes of heat transfer (radiation and conduction). Because the heat flow that radiation causes varies with the fourth power of the body's absolute temperature, radiation analyses are highly nonlinear and become more dominant at high temperatures. For this reason, we chose to ignore the heat radiation (heat losses) in the part of the models that are known to operate under relatively low temperatures ($<100\ C^0$). We chose to use the Radiosity Solver Method for the radiation analysis, simply because it can be used for more generalized radiation problems in 3-D/2-D involving two or more surfaces.

Figure 4.3 shows the boundary conditions that have been applied through all the simulations. Radiation heat transfer was applied between all tip surfaces. The emissivities of the tip material were set constant with temperature. ANSYS assumes heat transfer by radiation as a surface property and not volumetric. That assumption is valid since in most solids, radiating from interior molecules is strongly absorbed by adjoining molecules.

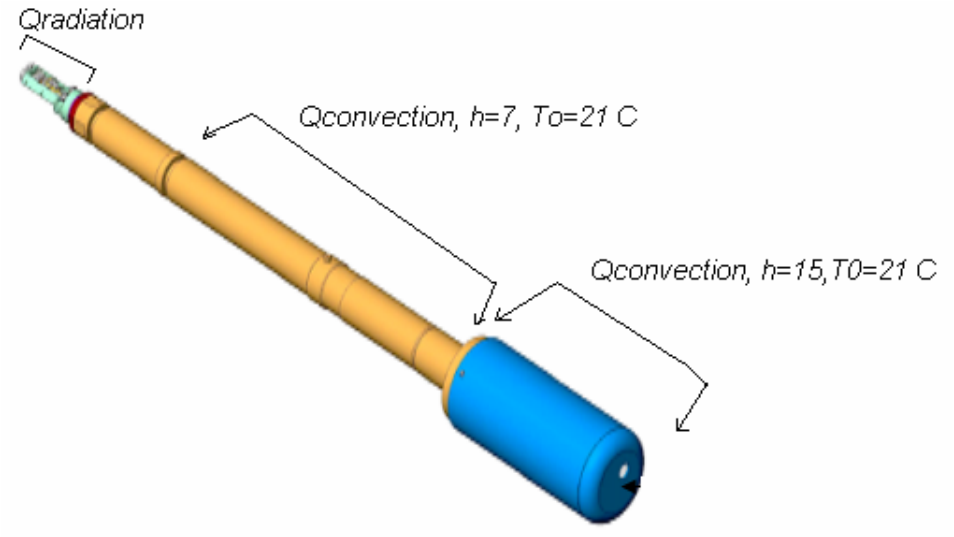

Figure 4.3. Boundary Conditions

Since the tip area has an open enclosure, ANSYS requires specification of a space temperature for energy balance to the ambient. We chose the space temperature to be 50 C^o. The heat generation due to current passing through resistance was modeled as a body force on the heater coils. The value of this body force was computed by dividing the input power by the total volume of the heater coils. The total volume of the heaters was 6.4E-9 m^3, and the heat generation was Q = 3.0E 9W/m^3.

4.4 RESULTS AND DISCUSSION:

Figure 4.4 shows the coils and sample temperature variation with time obtianed from the transient analysis. 19.2 Watts of power was applied to the heater coils as heat generation. The steady state temperaure of the coils was 1500 ^oC and the sample temperature was 1010 ^oC. The difference between the temperature of the sample and the heater coils is on the order of 500 ^oC. This large difference was the reason for short life of the heater coils when this technology was used at elevated temperature. The heater coils have to operate at much higher temperatures (on the order of 1900 ^oC) to elevate the sample temperature to 1200 ^oC. Design optimization was carried out to reduce temperature difference between the heater coils and the sample. Since the radiation is the dominant heat transfer mode, focus is on optimizing radiation factors. Radiation

depends on: the temperature difference between the load and the source, viewing factor, emissivity of radiating surfaces, and surface area of radiating surfaces. Viewing factor can be increased by reducing the distance between the sample and the heater coils (viewing factor is inversely proportional to the square of the distance). Further optimization could be achieved if the emissivity of the heat coils was increased by applying a special coating.

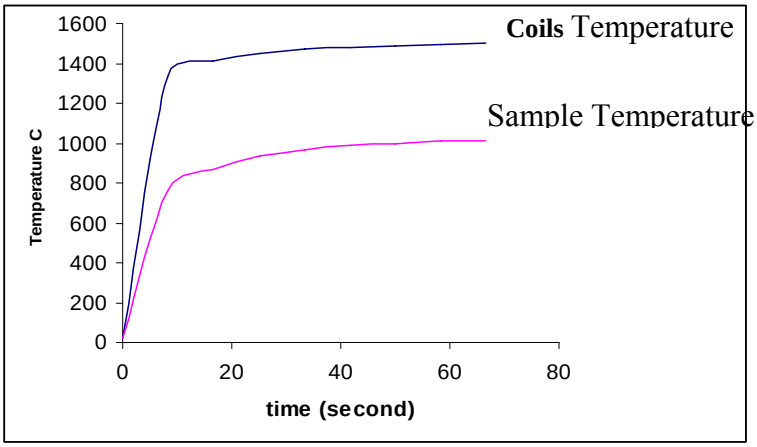

Figure 4.4. Transient Coils and Sample Temperature

Figure 4.5 shows the temperature distribution of the sample after it has reached steady state. In Figure 4.5, it is notable that the distribution is not unifrom. The parts that were very close to the heater coils reach a higher temperature than the rest of the specimen. At locations where the specimen is very thin for electron transparency (close to the hole), the simulation predicted a uniform temperature distribution.

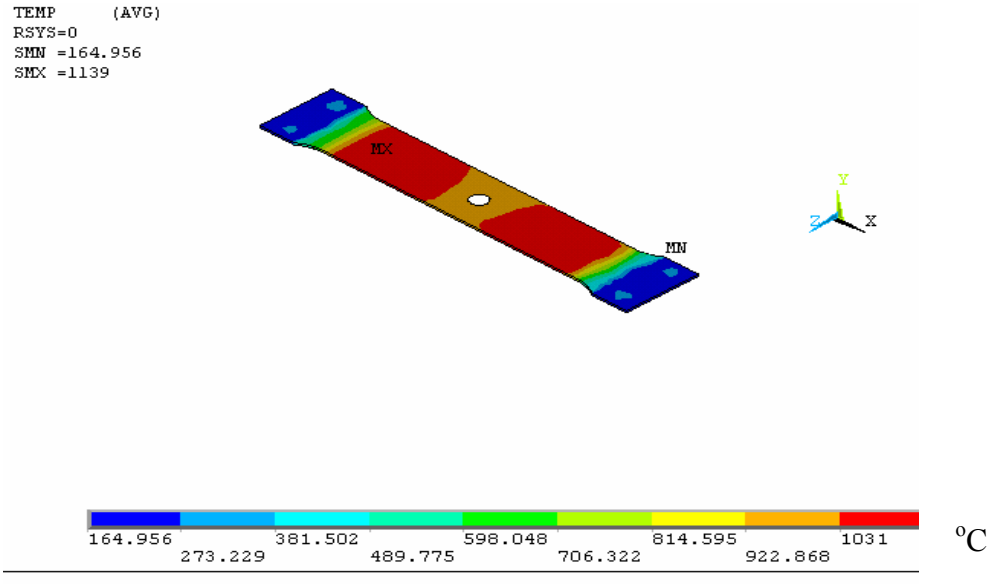

Figure 4.5. Steady State Temperature Distribution of the Sample

A parametric study was then conducted to analyze the variations of the sample temperature as a function of the emissivity of the tungsten shield. The energy (19.2 Watt) was kept constant through all these simulations. The reflectivity of materials is 1 – emissivity. It is clear from Figure 4.6 that to obtain an optimum high sample temperature at minimum power supply, highly reflective material should be used.

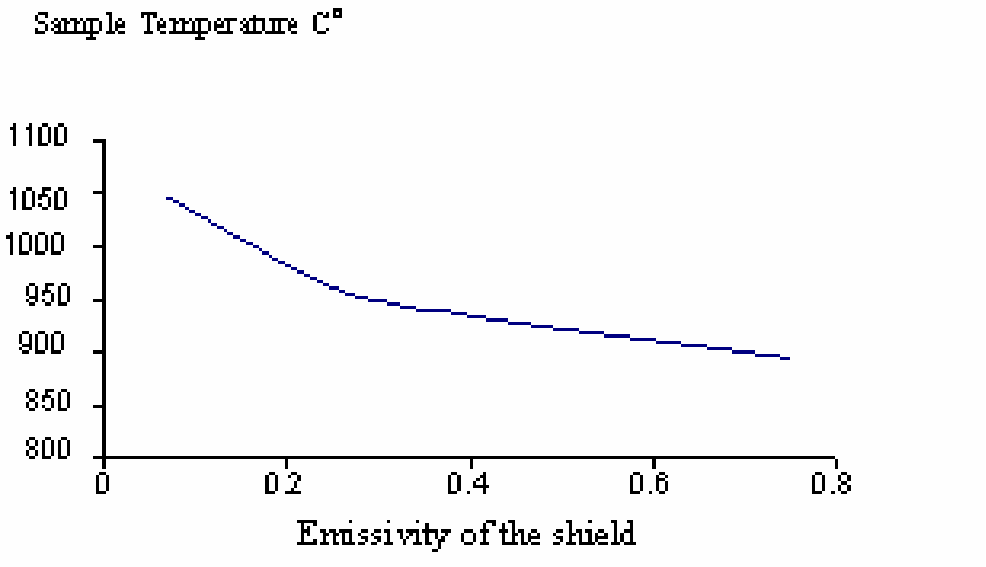

Figure 4.6. Sample Temperature vs. the Emissivity of the Shield

5.0 HEATING HOLDER (PROPOSED DESIGN)

In this chapter, two proposed new design for in–situ specimen holder technology are presented that are capable of elevating the temperature of a materials from ambient to 1770 ^{o}C while simultaneously subjecting it to varying environments.[18][19] The differences in each design are based on their heat source. One uses a resistive heating while the other utilizes laser heating. The specimen temperature will be controlled to within 10 ^{o}C. Various environments will be created by injecting one or more gases into the volume surrounding the specimen. Gas pressure and flow will be accurately controlled. The specimen positioning within the TEM will be accurately controlled by the combination of the TEM's goniometer and the in-situ holder mechanism. The specimen will be positioned in 5 degree of freedom (DOF) space. These will include three translations (X, Y, Z) and two tilt axes (α,β) with a targeted accuracy of +/-0.005^{o}.

5.1 RESISTIVE HEATER DESIGN

The proposed design incorporates heating technology that has been used in past TEM heating holder designs. Heating elements have historically been encased in a ceramic insulator to prevent electrical shorts in the heating coils. Typically, supporting mechanisms for the heating elements are designed to minimize the contact area (thus conductive heat transfer). The attached analysis also includes a radiation shield surrounding the heater assembly to protect the TEM pole pieces. In the attached model, the specimen loading and retention mechanisms are not shown for clarity.

5.1.1 Solid Model and Design Consideration

Figure 5.1 shows a solid model for first proposed specimen holder design. Restrictions on the dimensions of the holder tip as a function of a 6mm pole piece gap were satisfied. Since this proposed design will ultimately be compatible with different microscope stages, generic dimensions were applied to the holder barrel. Tungsten was chosen for the heater coils, the heat shield, sample rings, and the enclosure that covers the electrical insulator. Four 1mm diameter spheres made of Al_2O_3 provide symmetrical support for the specimen containing the furnace assembly. Those spheres are attached to a spring like outer support structure to allow expansion without inducing significant stresses. 34 AWG wire was chosen for the heater coils. This geometry allows 26.4cm of tungsten wires to be used for the heater.

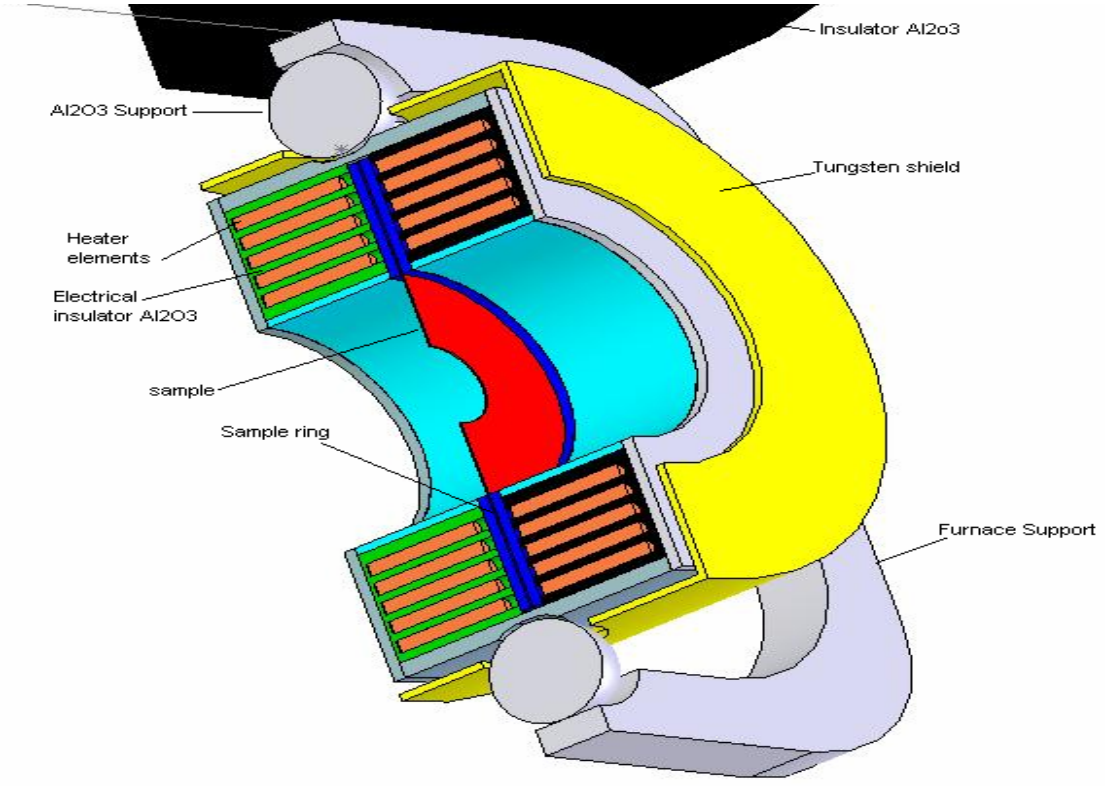

Figure 5.1. Solid Model for the Proposed Design

Increasing the resistance of the coils is one of the critical design parameters. This will allow large wattage with minimum amperage, and hence increase the heater life. The contact area between the spheres and outer shell need to be minimized to increase the thermal resistance

and keep the heat in a very localized area. The proposed design has a contact area of 9×10^{-8} m^2 at four locations. The function of the shield theoretically is to maintain the heat inside. Since the reflected radiation does not change the internal energy of the reflective material, using high reflective material will have the advantages of minimizing the heat loss by increasing the resistance of heat flux out of the furnace. This will also serve to protect of the microscope components.

5.1.2 Finite Element Analyses

Finite element analyses were carried out to quantify the performance of the new design. Thermal-stress analysis was used to take into account the interaction (coupling) between thermal and stresses due to thermal expansion or contraction. Heat transfer analysis was used to obtain the temperature distribution of model, the heat power requirements to obtain the desired temperature, the temperature distribution on the sample, and finally the temperature varying with time especially at the goniometer stage. After obtaining thermal results, structural analyses were carried out to obtain the thermal stresses and displacements of the model parts.

5.1.3 Finite element model

The actual Solid Model shown in Figure 5.1 was imported into ANSYS. The material properties which were input to the finite element model were obtained from a combination of two sources.[36][8] The model consisted of about 200,000 elements. All solid elements were of type SOLID87 and SOLID90. SOLID90 is a 3-D thermal element that has 20 nodes with a single degree of freedom, temperature, at each node. The 20-node elements have compatible temperature shapes and are well suited to model curved boundaries. SOLID87 is a 3-D 10 node element that is well suited to model irregular meshes (such as produced from various CAD/CAM systems). The element has one degree of freedom (temperature) at each node. These elements are applicable to a 3-D, steady-state or transient thermal analysis.

Three modes of heat transfer (conduction, convection and radiation) were included in all simulations. The Radiosity Solver Method was used to solve the radiation thermal analysis.

This method works for generalized radiation problems involving two or more surfaces receiving and emitting radiation. The method is supported by all 3-D/2-D elements having a temperature degree of freedom. The heating elements were modeled as solid cylinders with diameters comparable the 34AWG. The total length of those cylinders was set equal to the total length of the resistors. Heat generated was applied as a body force on the heating elements. All thermal contact resistances were set to constant values 0.0001.[8] Boundary conditions were the same as in the previous analyses. Table 5-1 lists the material properties that were input to the finite element model.

Table 5-1 Material Properties

Material	Density kg/m³	Thermal conductivity W/m·°C	Modulus of elasticity Pa	Heat capacity J/kg·°C	Yield Strength Pa	Emissivity
Tungsten	19,300.0	163.0 at 25 C 100 at 1800C	4.0×1011	134.0 (25)157 at 2000k	7.5×108	.15
Al2O3	3960	30 at 25 C 5 at 1800 C	3.7×1011	850 at 21 C 1300 at 1800 C	2.8×106	.85
Copper	8300	60.5	2.0×1011	434.0 J/kg·°C	2.5×108	.25

5.1.4 Results and Discussions

In the FEA simulations a power level of 9.6 Watts was applied to the heating elements. Figure 5.2 shows the transient temperature of the heater, sample, spheres, and at location of 1 cm from the tip area. The heater's temperature reached a steady state value of 1770 ^{o}C after 70 seconds. The sample temperature was 40 ^{o}C lower than the heater. This is one of the advantages of the proposed heaters compared to the straining heaters. Figure 4.4 showed that the difference in temperature between the heaters and the sample was of order ~ 500 ^{o}C). It is interesting to note that at a location 1 cm from the tip, the temperature was still increasing. Further simulations were run for longer time periods to obtain the variation in temperature with time. It is very important to keep the temperature near the stage area within ± 1 ^{o}C. This is due to the fact that many investigators reported distortions in image data sets due to movements of the microscope stages that resulted in fluctuation in room temperature. The same analogy can be used here.

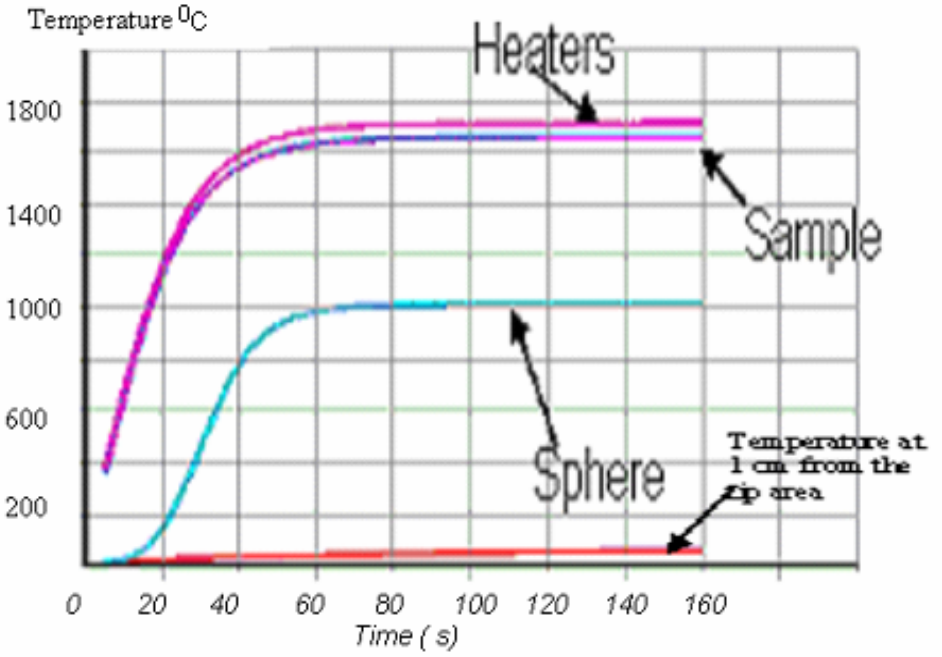

Figure 5.2. Transient Temperature, °C

Figure 5.3 shows the temperature variation with time at a position 5cm removed from the specimen area. This location was investigated since it is the position where the microscope goniometer mates with the holder. Note that the temperature at that position reached steady state after 80 minutes, which is very important for performing precision measurements.

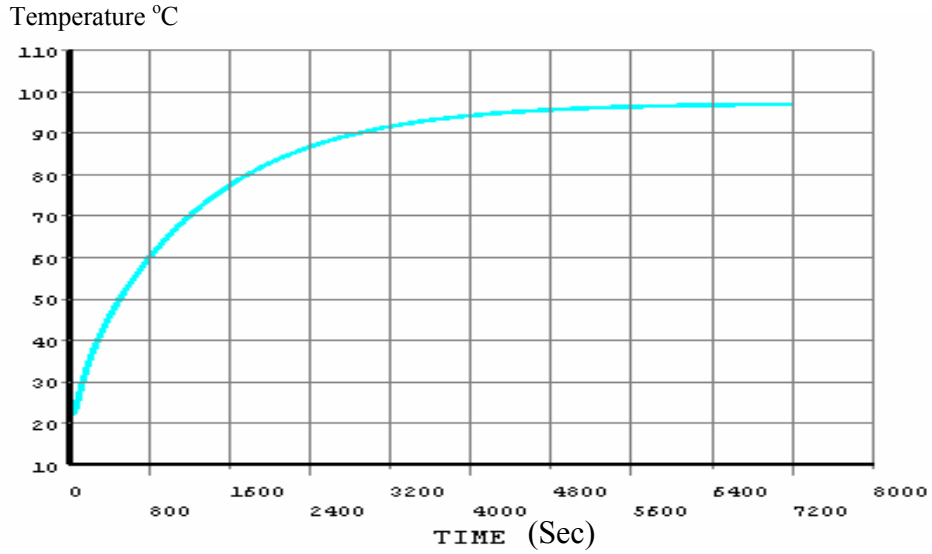

Figure 5.3. Transient Temperature at the 5 cm Removed From the Tip Area.

Figure 5.4 shows the temperature contour at time=70 seconds. It is noteworthy to mention that a symmetric temperature distribution existed for all tip components. This distribution symmetry results in a symmetric expansion that can easily be compensated. Under these conditions, the specimen achieved a temperature of 1,727 ºC (2000 K); however, the shield temperature reached a steady state value of 896 ºC. The contour legend shown below varies form a minimum value of 21.9 to 1779, with a step increment of 219. The thermal gradient in the ring is below 219 ^{o}C and hence appears uniform in Figure 5.4. At this temperature, the shield will radiate a significant amount of heat to the microscope parts. Future investigations will consider the possibilities of incorporating either a double shield or partial second shield that will simultaneously retain the heat and protect the microscope components.

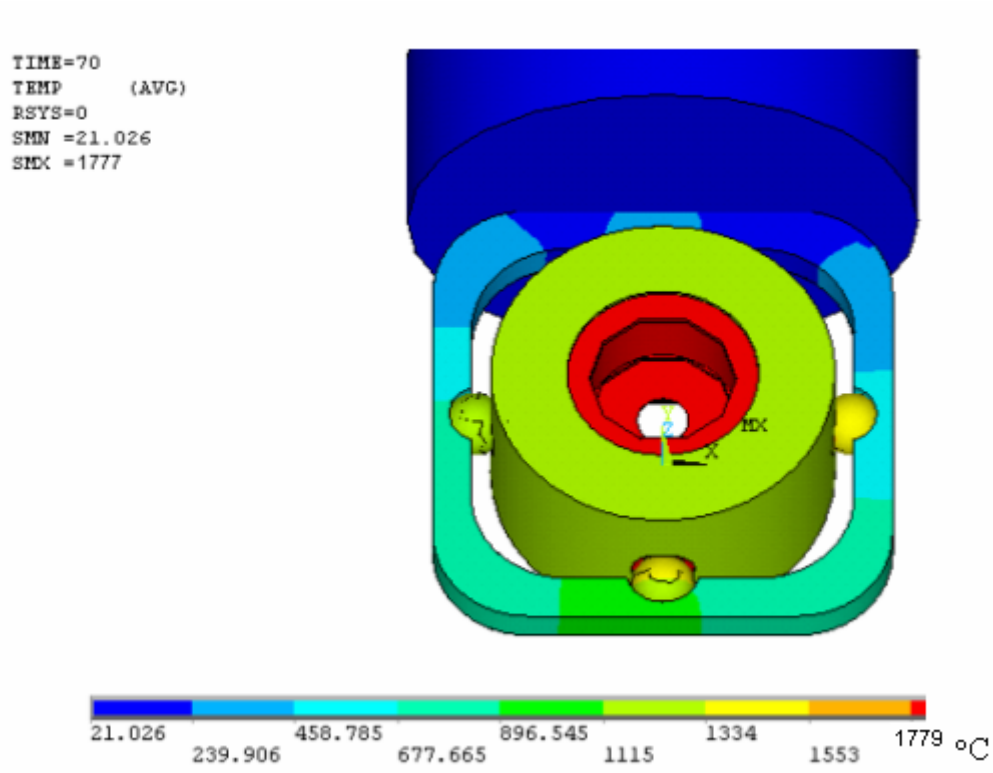

Figure 5.4 Temperature Contour at Time =70 Seconds

Figure 5.5 shows the thermally-induced radial stresses developed in the specimen. The sample rings provide frictional support to the sample. The frictional coefficient of 0.4 was used. The magnitude is on the order of 3 MPa. Those stresses arise due to friction between the sample

and the sample ring. As a design consideration, it will be necessary to capture the specimen in such a manner that takes into consideration this amount of stresses. Rigidly mounting the sample will decrease the amount of expansion; however, it will produce significant stress. The corresponding friction between the specimen and capturing mechanism will be investigated and optimized.

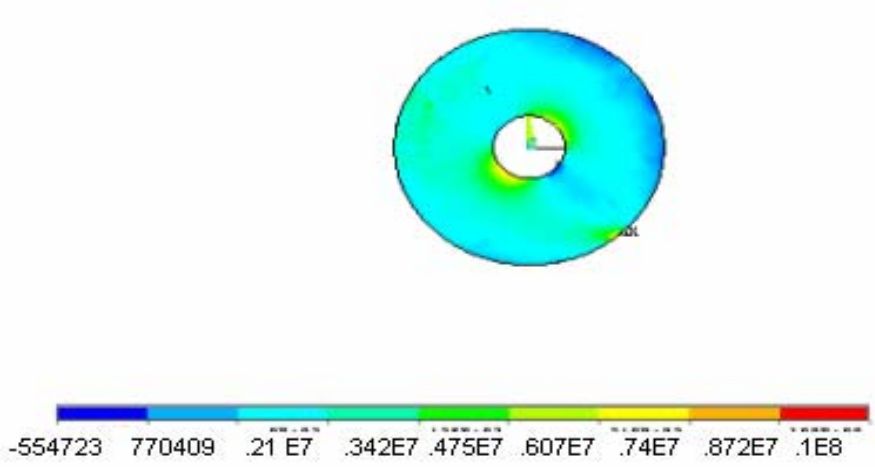

Figure 5.5. Radial Stresses (Pa)

The bracket which supports the furnace is a critical part of the design since it establishes the connection between the specimen/furnace assembly and the holder barrel. Figures 5.7 and 5.8 show the tangential and radial stresses of the support bracket, respectively. These values are on the order of 4 MPa, which is well below the yield strength of Al_2O_3.

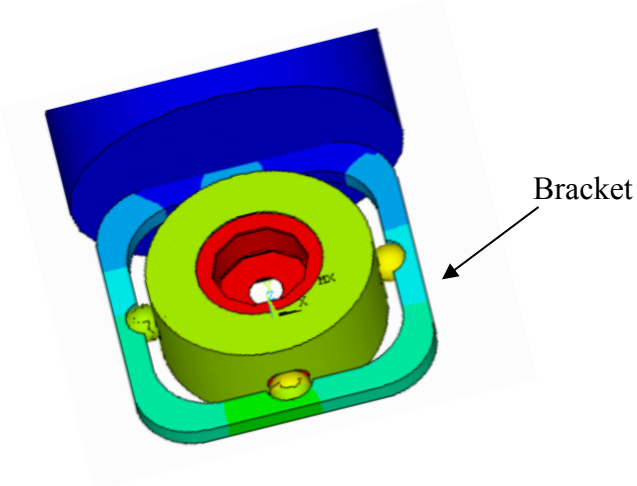

Figure 5.6. Holder Tip

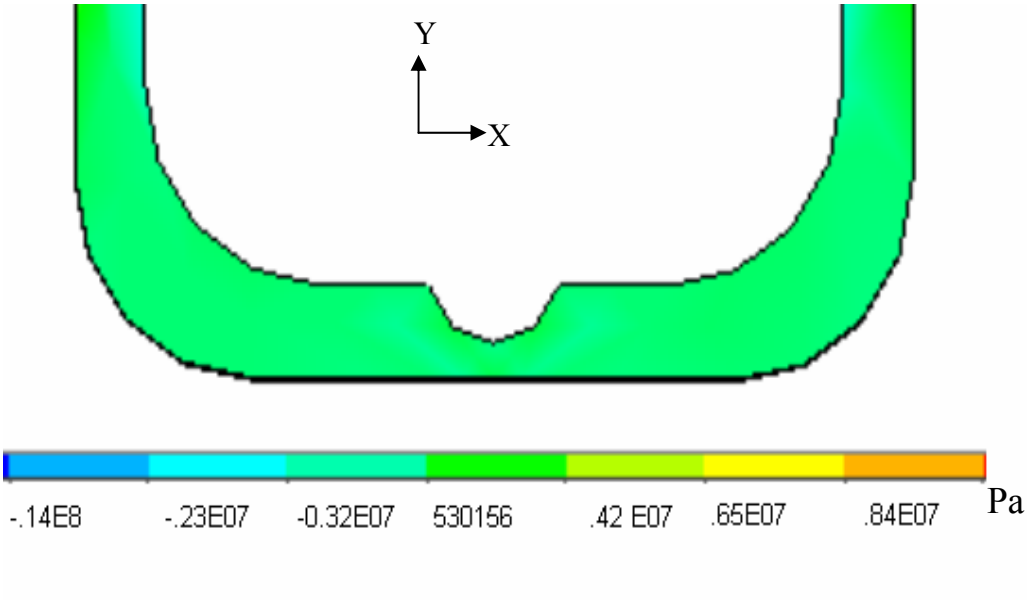

Figure 5.7. Y-Direction Stresses (Pa) in the Bracket

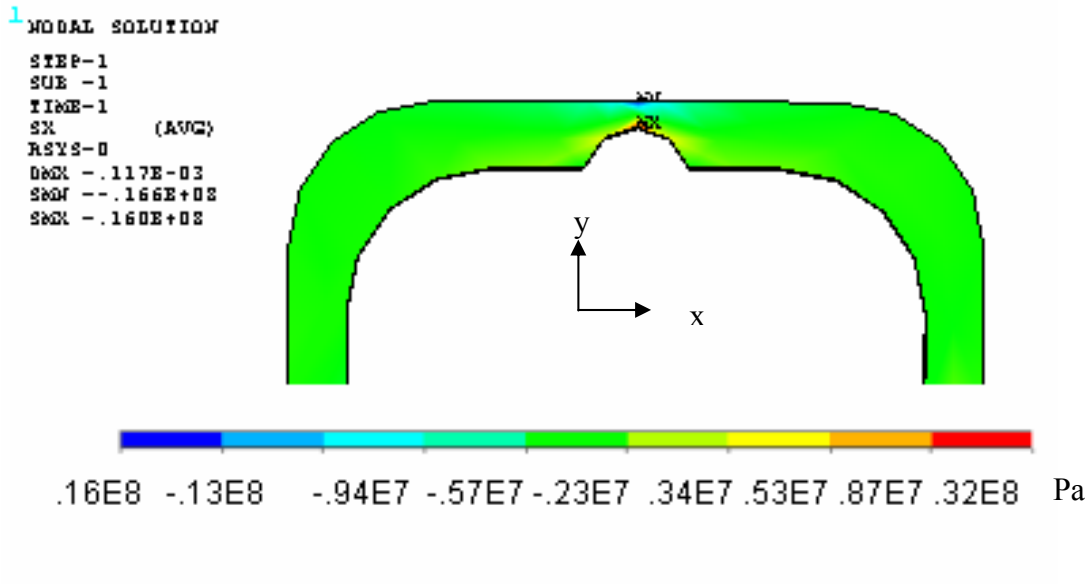

Figure 5.8. X-Direction stresses (Pa) in the bracket

Figure 5.9 shows the transient sample radial deformation when the sample is heated to the desired temperature of 2000 K. It is easy to see from Figure 5.9 that the sample experiences continuous deformation while it is being heated. This amount of deformation can be easily reduced by modifying the design to allow higher values of friction coefficient between the sample and the sample ring. However, as mentioned previously, redesigning this technology

with higher friction will increase the amount of stresses within sample which is undesirable. A successful design will utilize a compensation mechanism to account for the sample movements.

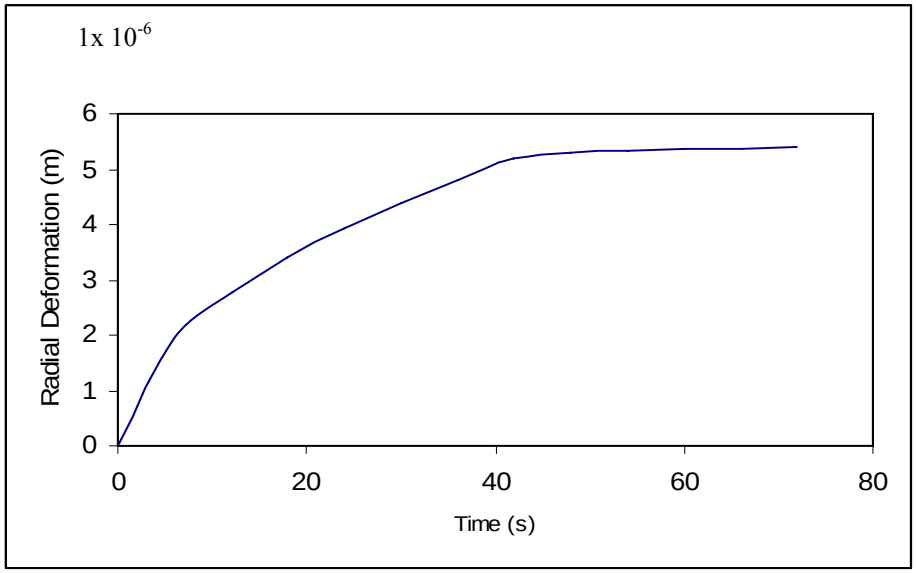

Figure 5.9. Sample Radial Deformation during Transient Heating

Figure 5.10 shows radial displacements in the sample. This technology has been carefully designed to allow uniform symmetric expansion. From Figure 5.10, note the uniformity of the expansion due to the temperature load.

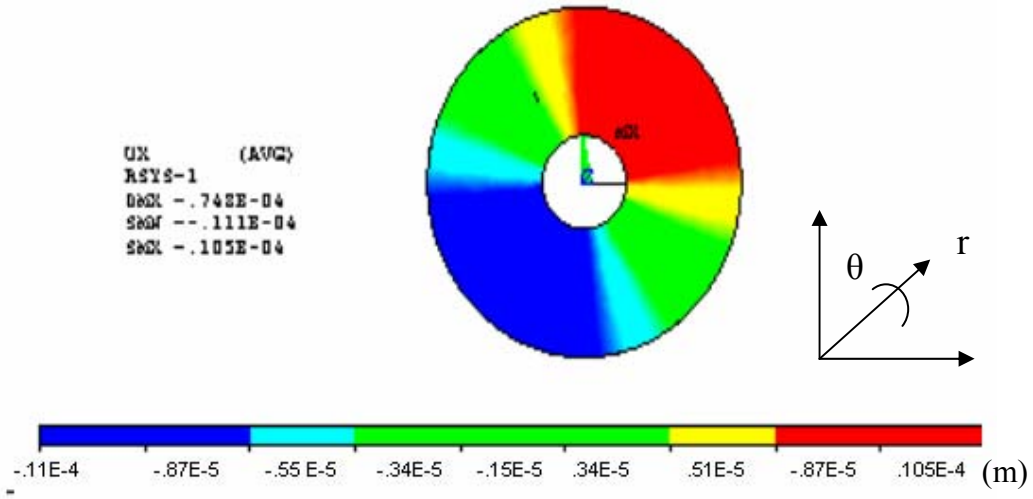

Figure 5.10. Radial Displacement Contour

5.2 DYNAMIC ANALYSES

The ultimate goal of this dissertation was to develop specimen holders that were not only capable of operating at extremely high temperatures, but they were also capable of attaining high mechanical stability. Dynamics analysis was carried out to predict the dynamic behavior of holders under harmonic loading conditions. Procedures that were used to perform dynamics analysis on the topography holder were used in the present analysis for the dynamic stability of the new proposed holders. The first step was to perform a modal analysis. After obtaining the natural frequencies, harmonic analyses were carried out using 1 Pa of pressure.

5.2.1 Results and discussion

Table 5-2 lists the natural frequencies obtained from modal analysis.

Table 5-2 Natural Frequencies

set	Freq (Hz)	Mode shape
1	248.58	Bending in Y direction
2	552.11	Bending in lateral direction (-Z)
3	868.42	Bending in Y direction
4	900.59	Bending in lateral direction (-Z)
5	1023.6	Bending in y direction
6	1109.7	Bending in lateral direction (-Z)

Figure 5.11 shows the Uy displacement at the specimen location obtained after performing a harmonic analysis. Focus was placed on the first natural frequency. Uy displacement was provided, since modal analysis predicted that the Uy displacements were going to be the largest in the displacement of the sample in the y- direction. These values were lower than those values predicted for the tomography holder. This is due to the fact that a standard tomography holder possessing a relatively long, thin tip. This design takes this into consideration. The other simulations were carried out to obtain the displacement around the second natural frequency.

Results for Z- direction displacements are on the order of .08 nm. This amount of deflection is less than that found on the present holder technology. The proposed design has better dynamic stability one order of magnitude than present holder technologies. These stabilities improvements will permit obtain atomic resolution.

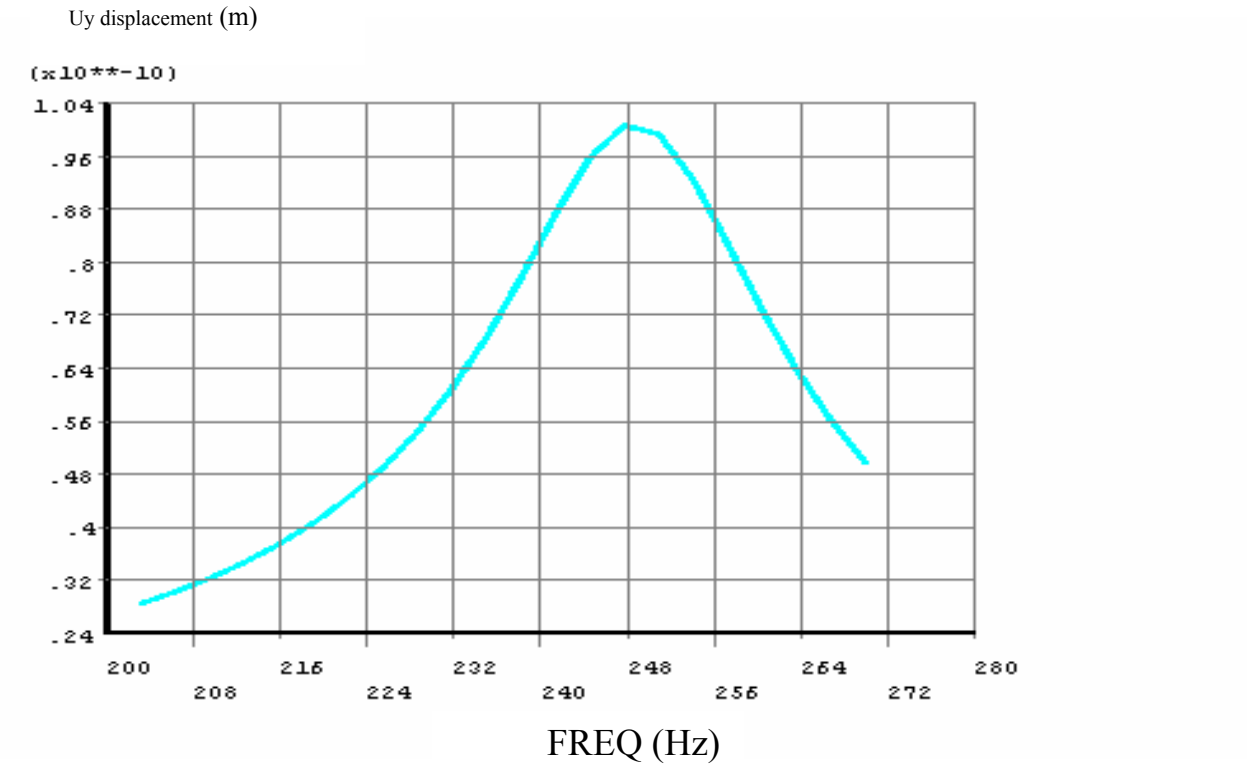

Figure 5.11. Uy Displacement at Sample Locations

5.3 LASER HEATING (TOMOGRAPHY)

As an innovative alternative design, this section of the dissertation investigates the utilization of a localized laser diode for heating a specimen to 2000K. This technology has not been considered previously in TEM applications and would be considered state-of-the-art if constructed. Since resistive heating requires space to insert the resistors into the holder tip, the overall depth will restrict the possibilities of using this technology for tomography. A CO_2 laser is distinguished by its much higher efficiency and extremely high power output. The CO_2 laser wavelength is 10.6 μm and falls within the range of infrared radiation, which is also referred to as thermal radiation. The interaction of this radiation with matter is thermal. The coherence of the laser beam permits it to be focused on a diameter of 10μm. This design style will include a laser source which is separate from the holder assembly. The laser will be transmitted to the specimen cup via a fiber optic bundle. A fiber optic cable may be mounted through the body of the holder or through an alternate port.

5.4 FINITE ELEMENT MODEL:

Figure 5.12 shows a solid model of the proposed design. The overall depth of the specimen cup is 1.5 mm, which allows the tip to be tilted up to ±70 degrees. The irradiating heat from a CO_2 laser was modeled as heat generation on a very small element on the specimen cup. Transient heat transfer analyses were carried out, similar to the above simulations. The irradiating heat from the CO_2 laser was modeled as a heat generation on a very small element of volume on the order of 1 E-13 m^3.

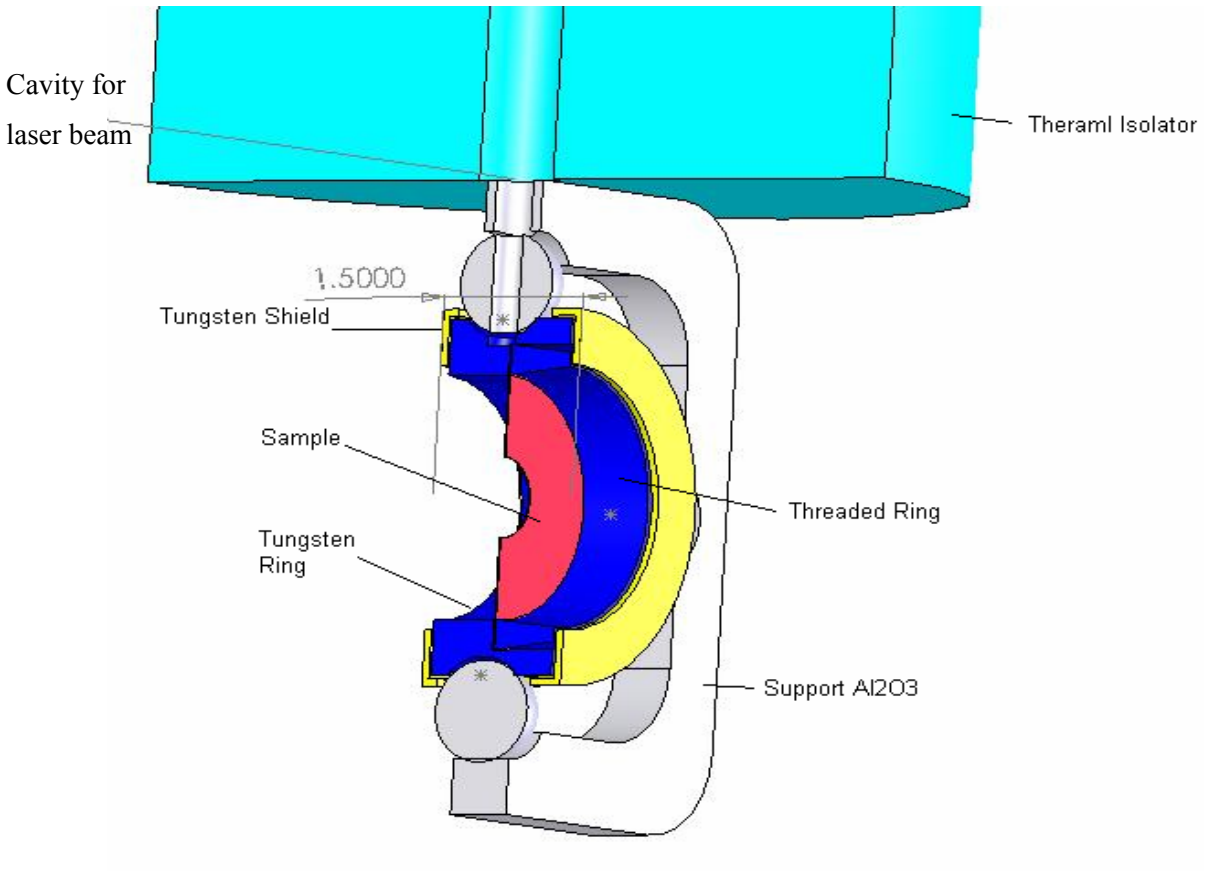

Figure 5.12. Tomography Holder Utilizing Laser Heating

5.4.1 Results and Discussions

Simulations were carried out to predict the temperature distribution of the holder due to localized intensive heat generation where the CO_2 laser is striking only one area. Results obtained will be used to check the design performance. The uniformity of the temperature distribution among the sample and the highest temperature of the target will be used as design criteria. 4.6 Watts of power were supplied to an element of volume ~ 4.8 E-13 m^3. Figure 5.13 shows the temperature contour at a time of 500 seconds. The overall picture shows a symmetric distribution. This symmetric distribution of the temperature will enforce a uniform expansion of the tip body which is highly desirable.

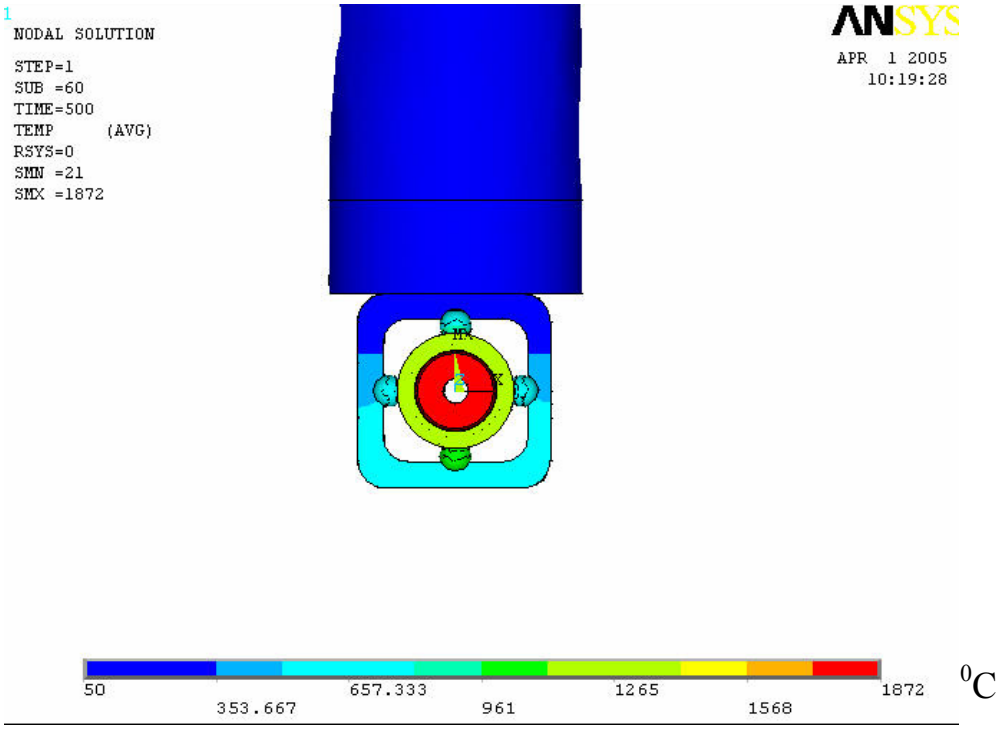

Figure 5.13. Temperature Contour

Figure 5.14 shows a closer look at the temperature distribution in the targeted part (ring). The difference in temperature between highest and lowest is on the order of 100 ^{o}C. Figure 5.15 shows the temperature contour of the sample. The difference in temperature is on order of 80 ^{o}C. As discussed in the next section, the targeted part was redesigned to reduce the temperature gradient within the sample.

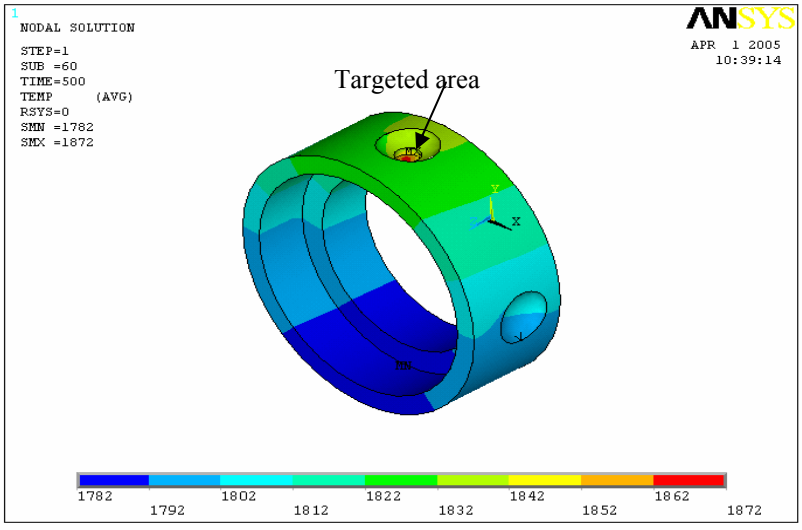

Figure 5.14. Temperature Contour on the Targeted Part (^{o}C)

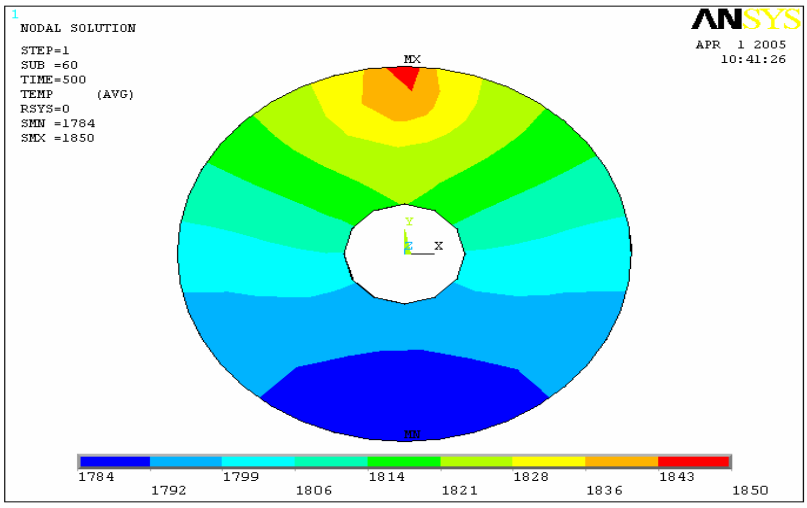

Figure 5.15. Temperature Contour of the Sample (^{o}C)

5.4.2 Revised Model

To obtain a more uniform temperature distribution, we modified the design so that the laser beam strikes two opposite areas. For the same amount of energy, Figure 5.16 shows the temperature contour for the sample area. Figure 5.17 shows the temperature contours for the ring. Using the modified design results in a more uniform distribution compared to the original design. For example, in the area where is the sample is very thin, the temperature can range between 1753 and 1757 ^{o}C with the double target area design which is much better than any specimen holder heating mechanism available on the market.

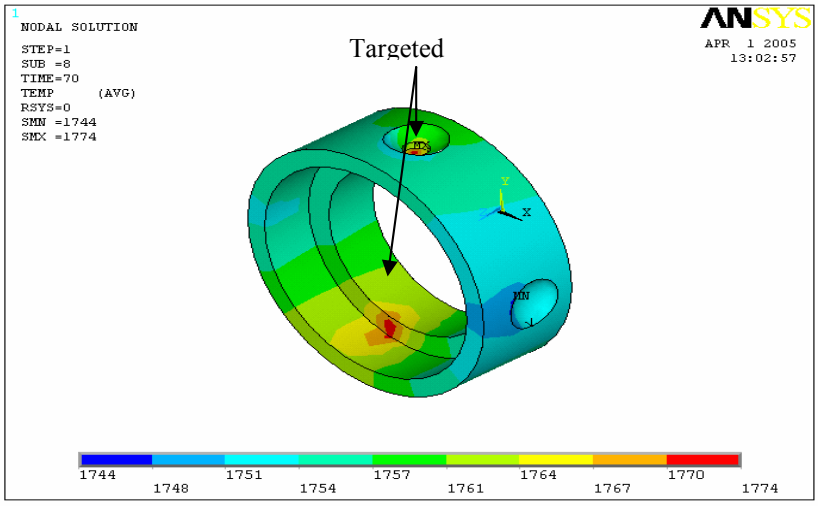

Figure 5.16. Temperature Contour for the Ring (^{o}C)

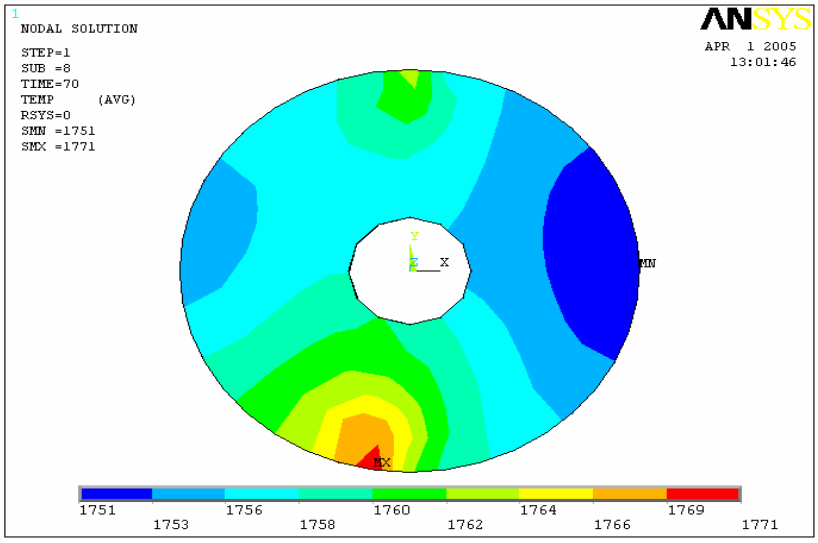

Figure 5.17. Temperature Contour for the Sample (^{o}C)

Figure 5.18 shows the temperature contour of the holder at (t= 70 Sec). A uniform temperature distribution among the holder tip is one design objective. In Figure 5.18, the temperature distribution within the holder is extremely uniform.

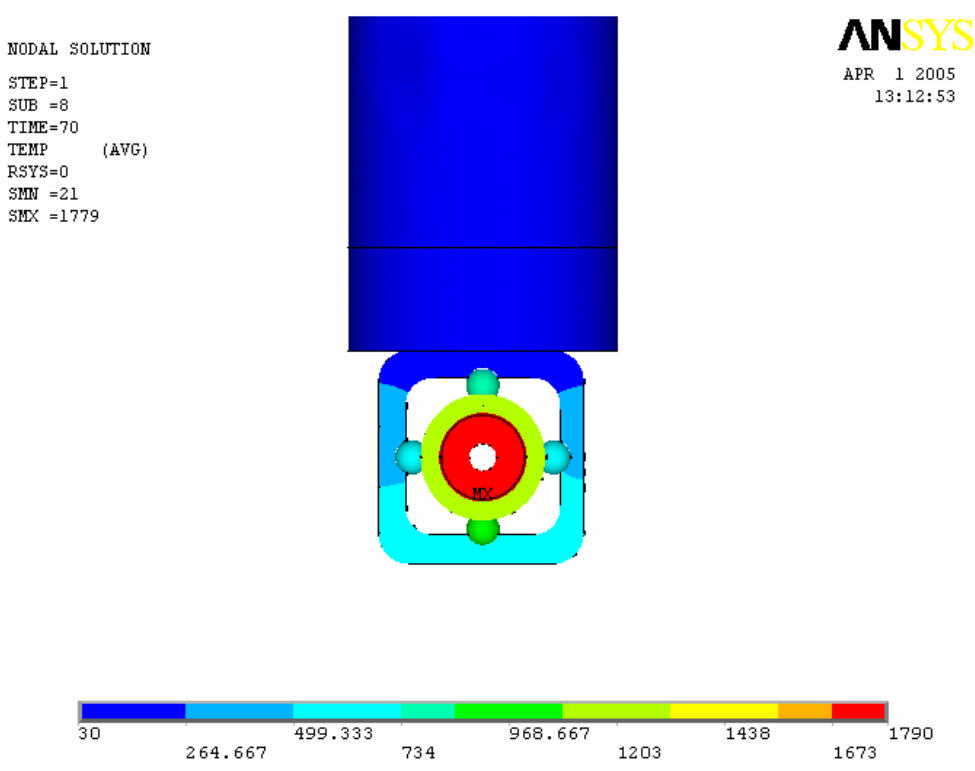

Figure 5.18. Temperature Contours for the Whole Holder at Time =70 Seconds

Figure 5.19 shows the temperature contour for the whole holder assembly at t= 500 seconds. The locations where the holder mates the goniometer stages are very critical for the holder stabilty and hence image stabilty. Any expansion due to the temperature increase in the part will lead to undesirable movements of the holder and hence the sample. To restrict this undesirable temperture increase, the new design uses a large mass of thermal resistance material between the holder tip and the rest of the holder body. In addition, the new design utilizes a very small area of contact between the bracket support and the sample ring to further increase the thermal resistance and hence reduce the heat flux to the rest of the holder body.

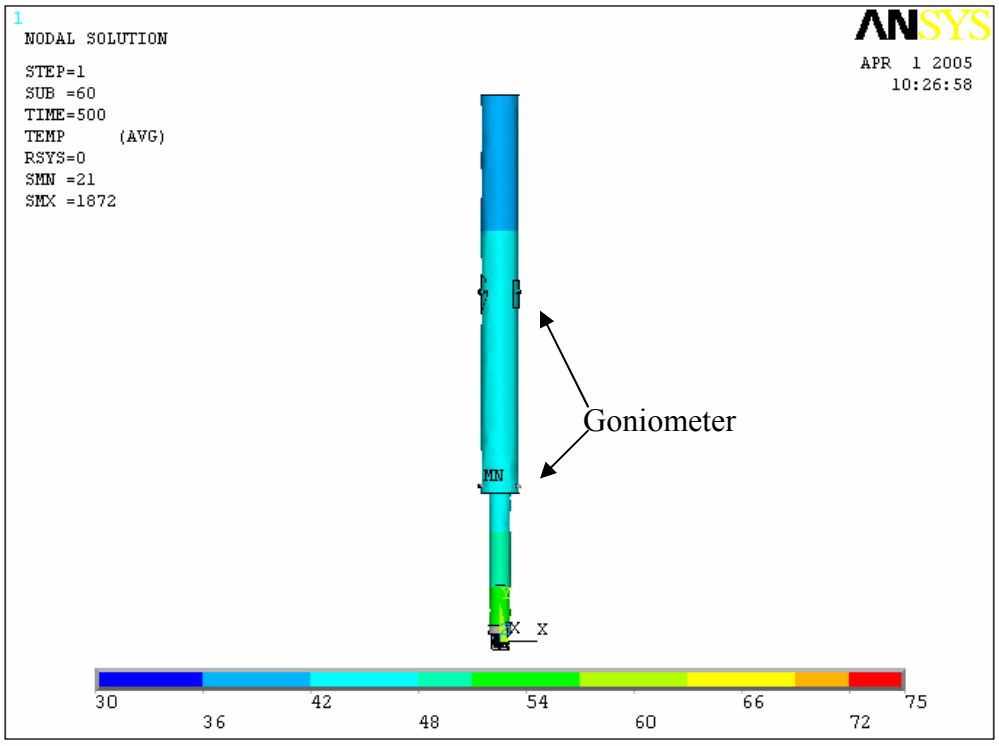

Figure 5.19. Temperature Contour for the Whole Holder at Time =500 Second

5.5 SUMMARY OF DESIGN IMPORVEMENTS

Transient heat transfer analyses using FEA were carried out for two holder assembly designs. Results were obtained for the temperature distributions in both holder models. The mass of the specimen furnace in both the resistive heating and laser technology heating models made as small as possible to ensure rapid response to changes in heater current and minimum wattage usage. The rate of increase of specimen temperature can be controlled as required, to a maximum of 3600°C per minute, or held at any selected temperature for long periods for the study of diffusion processes and precipitation kinetics. The new technology has been designed to have minimum thermal drift. To achieve minimum thermal drift, heat loss from the furnace to the specimen tip has been minimized by careful design of the ceramic furnace supports. Such careful design results in the specimen rod temperature held as closely as possible to the temperature of the specimen stage. This has advantages over the current commercial holders that use cooling water to maintain the holder rod temperature close to the stage temperature. We believe that using circulating cooling water will induce vibration and hence reduce the stability and the resolution that can be obtained otherwise. A modified design that utilizes two point laser heating was found to result in a more uniform temperature distribution and minimize the temperature gradient of the target area. Utilizing laser heating will permit the design of a heating holder that is thin enough for tomography (compared to resistive heat that requires a minimum depth on the order of 3 mm). It is believed this technology will have a longer life compared to resistive heating. Future studies need to be conducted to accurately model the heat transfer (radiation) from the CO_2 laser. These analyses will take into consideration parameters like emissivity, reflectivity and geometry shape factor. Also, a parametric study will be needed to optimize the target area, and will include the size, surface finish, and cone like shape area. To increase the stability due to temperature variations, a material with a near zero coefficient of expansion should be used for the holder part that mates the goniometer stage.

6.0 ENVIRONMENTAL HOLDER TECHNOLOGY

This chapter of dissertation focuses on the development of an in situ environmental holder technology. The term environment refers to the sample being continuously subject to impingent by gases opposed to conventional TEM where the sample is under high vacuum. Rarefied gas dynamics were performed to optimize and characterize the design. The objective of this analysis was focused on determining the molecular distribution inside the vacuum chamber and calculating the impingement rate on the target surface of the specimen. Calculations were performed to predict the molecular interaction with the specimen at given pressures to determine the proper position of a specimen within a vacuum chamber to optimize and predict reaction characteristics. This information is important for designing specimen holders that require specific impingent rates to perform experiments

6.1 SIGNIFICANT OF THE PROBLEM

The sample is under a high vacuum in conventional TEMs, while in environmental TEM, the sample is exposed to different environmental conditions such as gases or liquid. Environmental transmission electron microscopy (E-TEM) is a promising technique for in situ study of gas–solid chemical reactions with numerous applications. Successful design will make it possible not only to obtain atomic level information but also the chemical information during the reaction. The applications include, but are not limited to, oxidation, reduction, polymerization, nitridation, dehydroxylation, hydroxylation, and chemical vapor deposition.[37]

E-TEM is a very effective instrument to understand the structural and chemical changes during the gas–solid chemical reactions. It is particularly useful for nanomaterials that cannot be

observed using other methods, e.g., catalytic reaction, corrosion, and interface reactivity.[37] In situ experiments offer valuable insight into the chemical reaction processes. The early stages of nucleation and growth can be followed, and the morphology and the crystallography of the reactants and the products could be easily established. For example, Baker and colleagues have followed the filamentous growth of carbon over α-iron and γ-iron particles at different temperatures in acetylene and have been able to measure the activation energies of the reaction.[44][45]

Many of the traditional TEM techniques analyze catalyst samples under static, post-reaction conditions (reacted ex situ and cooled to room temperature) where samples are held under high vacuum. These conditions are often not representative of the true dynamic state of a reacting catalyst, and in these techniques, catalyst interactions are not observed directly. This has delayed a better fundamental understanding of dynamic catalytic surfaces, complex structural changes, and reaction mechanisms that evolve during oxidation-reduction processes.

The concept of in situ studies of gas–solid interactions using the transmission electron microscope (TEM) is nearly as old as the development of the instrument itself. The electronoptical conditions for TEM are not suitable for gaseous environments because a high vacuum is required. The purpose of a high vacuum level inside a TEM is not only to reduce scattering of the electron beam by gas molecules but also to minimize corrosion of the electron source. An alternative design is required to achieve this goal. There are two basic designs for environmental cell (EC-TEM) systems which utilize either the principles of differential pumping or window-sealed chambers. The first design requires extensive modification of the column of the transmission electron microscope. Typically, small, differentially pumped apertures can be located just above and below the sample to restrict gas flow into the rest of the microscope column.[39][40] However, the extensive modifications necessary for this design render the instrument a dedicated EC microscope.

In the second design, the pressurized environment is confined entirely within a closed cell within the specimen holder. Typically, specimen holders have been built with the sample enclosed within thin electron transparent membranes (windowed cell).[41][42] This can be achieved with essentially no modification to the transmission electron microscope. Since the EC

is self-contained within the specimen holder, the transmission electron microscope can still be used for conventional TEM using conventional specimen holders without compromising its resolution and analytical capabilities.

Typically, manufactures and researchers have built environmental TEMs without conducting any gas dynamics analysis. They assume a uniform molecular distribution inside the cell. They also used approximated formulas to calculate the number of molecules striking the surfaces based only on the value of the working pressure. Lack of such investigations might lead to running experiments under a higher pressure than is required may develop reaction models based on inaccurate values. The objective of this chapter is two-fold: 1) to determine the number of molecules striking the surface. 2) to determine the minimum value of pressure required (the density of the gas). Obtaining these objectives will serve to optimize the thickness of the electron transparent membranes (windowed seal). This thickness increases the effective thickness of the sample, which ultimately limits the resolution and contributes to the formation of the final images. In addition, using a minimum pressure will increase the life- time of such a membrane. Having a higher value of working pressure means more gas thickness, which increases the scattering of the electron beam by gas molecules, which ultimately interfere with the diffractions that occur when the beam passes the sample. Studying the diffraction of electron beams is a method used to gain information about crystalline materials.

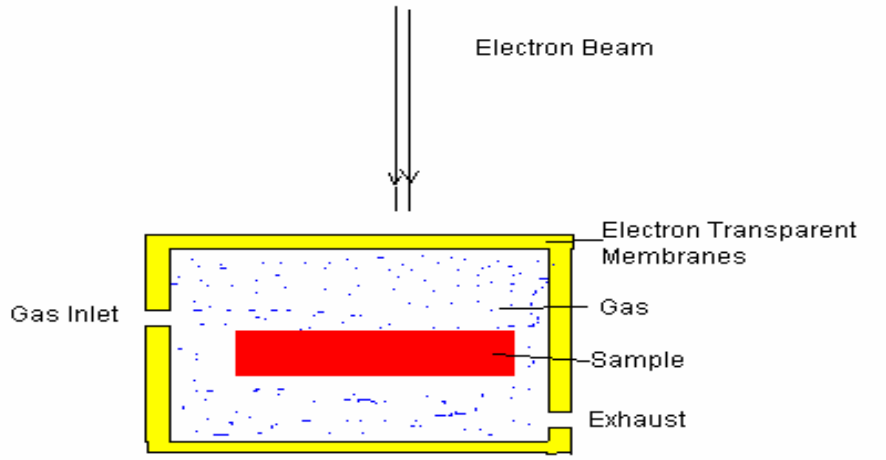

Figure 6.1. Schematic Diagram of E-C TEM

6.2 MOLECULAR MODEL FUNDAMENTALS

A gas flow may be modeled at either the macroscopic or the microscopic level. A macroscopic analysis assumes the gas to be a continuous medium that is described in terms of the spatial and temporal variations of flow properties such as velocity, density, pressure, and temperature. The Navier–Stokes equations provide the mathematical model of the gas as a continuum. The microscopic or molecular model recognizes the particulate structure of the gas as a myriad of discrete molecules and ideally provides information on the position, velocity and the state of every molecule at all time. The mathematical model at this level is the Boltzmann equation.

6.3 THE REQUIREMENT FOR A MOLECULAR MODEL

The macroscopic properties may be identified with average values of the appropriate molecular quantities at any location in a flow. They may be defined as long as there are a sufficient number of molecules within the smallest significant volume of a flow. This condition is almost always satisfied and the results from the molecular models can be expressed in terms of common continuum properties.

The degree of rarefaction of a gas is generally expressed through the Knudsen number (Kn) which is the ratio of the mean free path, λ, to the characteristic dimension, L. The traditional requirement for the Navier- Stokes equation to be valid is that Kn should be less than 0.1. The Kn limits on the conventional formulations are shown schematically in Figure 6.2. When the Knudsen number (Kn) limits approach zero, the Navier - Stokes equations reduce to the inviscid Euler equations. The opposite limit of infinite Knudsen Number (Kn) is the collisionless or free-molecule flow regime.

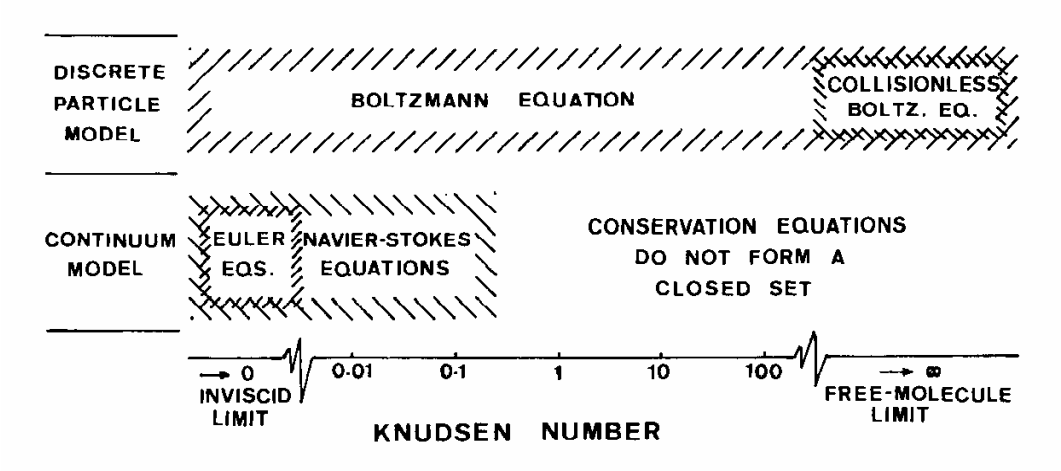

Figure 6.2. The Knudsen Number Limits on the Mathematical Models

6.4 THE SIMPLE DILUTE GAS

The basic quantities associated with the molecular model are the number of molecules per unit volume and the mass, size, velocity, and internal state of each molecule. These quantities must be related to the mean free path and collision frequency in order to establish the distance and time scales of the effects due to the collisional interactions among molecules. Let n be the number density, M be the molecular weight, and $\mathcal{N}$ is Avogadro's number, then the mass m of a single molecule is

$$m = \mathcal{M}/\mathcal{N} \tag{6-1}$$

The average volume available to a molecule is $1/n$, so the mean molecular spacing δ is given by

$$\delta = n^{-1/3} \tag{6-2}$$

A hard elastic sphere of diameter d provides an over-simplified but useful model of a molecule. Two molecules collide if their trajectories are such that distance between their centers decrease to d. The total collision cross section for these molecules is

$$\sigma = \pi d^2 \tag{6-3}$$

When the molecular spacing δ is large compared to the effective molecular diameter d, i.e. $\delta >>$ d, this situation defines a dilute gas. Moreover, when a collision occurs, it is most likely to be

binary involving only two molecules. The mean collision time is, by definition, the mean time between the successive collisions suffered by any particular molecule. The reciprocal of this quantity is called the mean collision rate or collision frequency υ per molecule.

The total number of collisions per unit time per unit volume of gas is given by

$$N_c = \tfrac{1}{2} n\nu = \tfrac{1}{2} n^2 \overline{\sigma c_r} \tag{6-4}$$

where c_r is the relative velocity between two molecules.

The mean free path λ is the average distance traveled by a molecule between collisions.

$$\lambda = c'/\nu \tag{6-5}$$

where c' is the mean thermal speed

6.5 BINARY ELASTIC COLLISION

The intermolecular collisions in dilute gases are most likely to be binary collisions involving only two molecules. An elastic collision is defined as one in which there is no interchange of translational and internal energy. Linear momentum and energy must be conserved in the collision. These equations are used to calculate the post –velocities of the two molecules. Figure 6.3 summarizes equations (6-6) and (6-7).

$$\begin{aligned} &m_1 c_1 + m_2 c_2 = m_1 c_1^{\,*} + m_2 c_2^{\,*} = (m_1 + m_2) c_m \\ &m_1 c_1^{\,2} + m_2 c_2^{\,2} = m_1 c_1^{\,*2} + m_2 c_2^{\,*2} \\ &c_r = c_1 - c_2 \end{aligned} \tag{6-6}$$

$$\begin{aligned} &c_1^{\,*} = c_m + \frac{m_2}{m_1 + m_2} c_r^{\,*} \\ &c_2^{\,*} = c_m - \frac{m_1}{m_1 + m_2} c_r^{\,*} \\ &m_1 c_1^{\,2} + m_2 c_2^{\,2} = (m_1 + m_2) c_m^{\,2} + m_r c_r^{\,2} \\ &m_1 c_1^{\,*2} + m_2 c_2^{\,*2} = (m_1 + m_2) c_m^{\,2} + m_r c_r^{\,*2} \\ &m_r = \frac{m_1 m_2}{m_1 + m_2} \end{aligned} \tag{6-7}$$

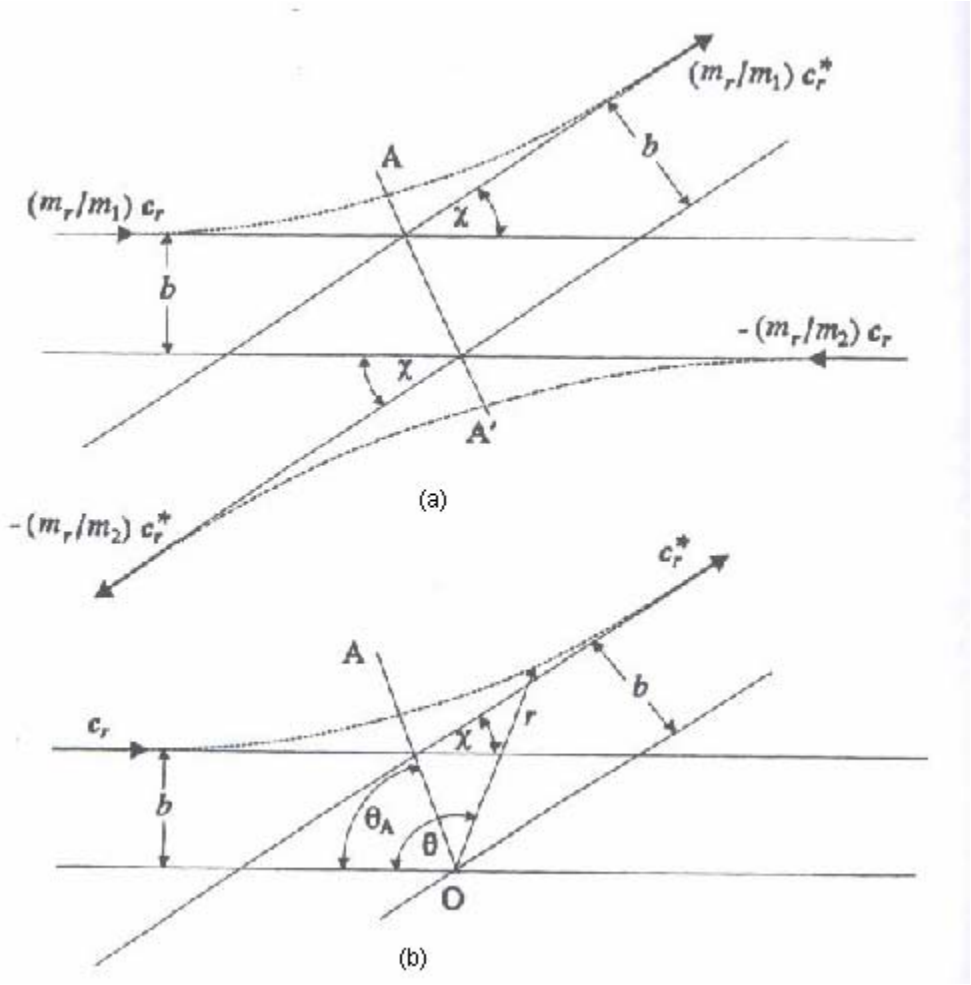

Figure 6.3. Frames of Reference for the Analysis of Binary Collision

(a) Binary Collision in the Center of Mass Frame of Reference

(b) Interaction of the Reduced Mass Particle with a Fixed Scattering Center

6.6 DIRECT SIMULATION MONTE CARLO

The Direct Simulation Monte Carlo (DSMC) method is a well-established approach that has been used widely and successfully used to simulate high Kn number gas flow problems that are similar to that encountered in a TEM chamber.[9] The DSMC method retains its validity at high Kn because no continuum assumptions are made. Conservation of mass, momentum, and energy are enforced. In the DSMC method, a real gas is simulated as a large number of

simulated particles. The positions, velocities and initial states of these simulated particles are stored and modified in time in the process of particles moving, colliding among themselves, and interacting with boundaries in the simulated physical space. Each simulated particle represents a very large number of physical molecules. In this fashion, the number of molecular trajectories and molecular collisions that must be calculated is substantially reduced, while the physical velocities, molecular size and internal energies are preserved in the simulation. Furthermore, the DSMC method uncouples the analysis of the molecular motion from that of the molecular collisions by use of a time step smaller than the real physical collision time. The computational task associated with the direct physical simulation becomes feasible when the gas density is sufficiently low. It also becomes necessary under these conditions because the Navier-Stokes equations do not provide a valid model for rarefied gases, and conventional CFD methods are unable to cope with the large number of independent variables that are involved in applications of the Boltzmann equation to realistic multi-dimensional problems.

Particle motions are modeled deterministically, while the collisions are treated statistically. Symmetries in physical space can be used to reduce the number of grid dimensions and to reduce the storage requirements for molecular spatial information. However, modeling collisions is always a three-dimensional calculation. The limitations of DSMC are the same as those of classical kinetic theory: the assumption of molecular chaos and the restriction to dilute gases. In addition, many computational studies have shown that the DSMC solutions approach Navier-Stokes solutions in the limit of very low Kn. [47][48]

There are two main reasons for using DSMC. First, there is no iterative procedure for convergence to the final solution. Most importantly, there are no numerical instabilities. The time step is set such that a typical molecule moves about one third of the cell dimension at each time step. The DSMC method uses the cell system only for the sampling of the macroscopic properties and for the selection of possible collision partners. This means that the cell geometry should be chosen to minimize the changes in the macroscopic properties across an individual cell.

6.7 COMPUTATIONAL APPROXIMATION

Using each simulated molecule to represent a large number of actual molecules introduces statistical error. The statistical error of a DSMC solution is inversely proportional to the square root of the total number N of simulated particles (or sample size). The computational work is directly proportional to N. The simplicity of the algorithm allows for straightforward application to complex geometries. The primary drawback of DSMC is its cost. However, this drawback has been mitigated by the fact that the method is capable of giving quantitative results in the high-Kn flow regime and that large-scale computer resources are more generally available.

6.8 DSMC PROCEDURES

Figure 6.4 shows the procedures involved in applying DSMC to an unsteady or steady flow problem. Execution of the method requires using a cell, or spatial element, network in physical space. The cell network provides geometric areas and volumes required to evaluate macroscopic flow properties. It is also used by the collision process model, in which only particles located within the same cell, at a given time, are allowed to interact. A DSMC simulation, like a continuum computational fluid dynamics (CFD) calculation, proceeds from a set of prescribed initial conditions. The particle positions, velocities, collision cross sections, and boundary conditions determine the subsequent evolution of the system. As in a continuum solution or an experiment, the solution that evolves may be very sensitive to the particular choice of initial, boundary, and input conditions.

The core of the DSMC algorithm consists of four primary processes: move the particles, index and cross-reference the particles, simulate collisions, and sample the flow field. These procedures are uncoupled during each timestep. Of primary importance is the selection of a timestep that is less than the mean collision time. Simulation results are independent of the timestep increment as long as this requirement and the cell-size requirement on the gradient resolution are satisfied.

The first process, moving simulated molecules, enforces the boundary conditions and samples macroscopic properties along solid surfaces. Modeling molecule-surface interactions requires applying the conservation laws to individual molecules instead of using the velocity distribution function. The second DSMC process involves indexing and tracking particles. A scheme for molecular referencing is the prerequisite for the next two steps: modeling collisions and sampling the flow field. Accurate and fast indexing and tracking are key to practical DSMC applications for large-scale processing.

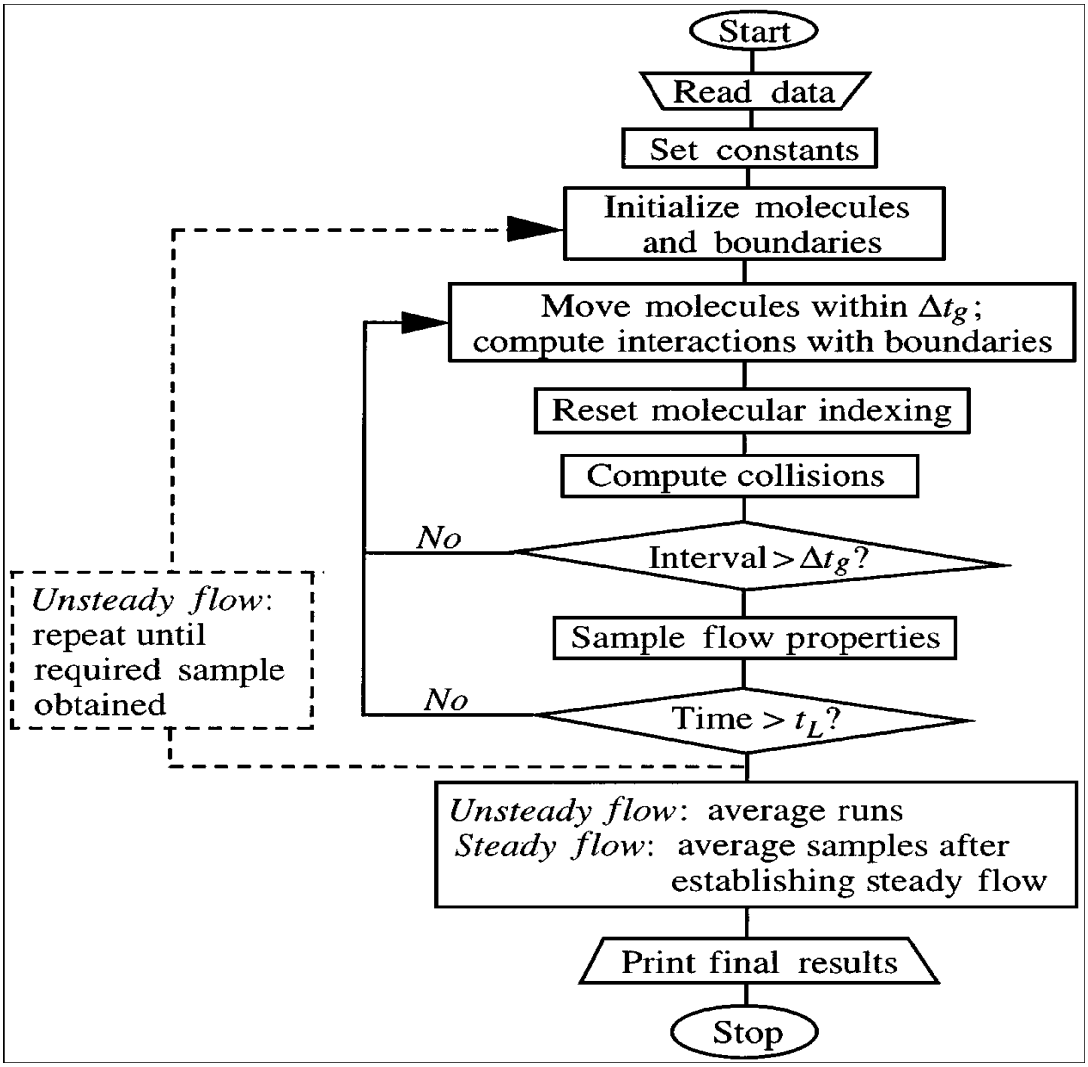

Figure 6.4 Schematic Procedures of DSMC

The next step, simulating collisions, is a probabilistic process that sets DSMC apart from deterministic simulation methods such as molecular dynamics. Several collisional modeling

techniques have been applied successfully within the framework of DSMC. All simulate an appropriate number of representative collisions between randomly selected pairs of molecules within each cell but with various degrees of computational efficiency. The currently preferred model is the no-time-counter technique [9], used in conjunction with the subcell technique.[49] The subcell method calculates local collision rates based on the individual cells but restricts possible collision pairs to subcells. This procedure improves accuracy by ensuring that collisions occur only between near neighbors. The final process is sampling the macroscopic flow properties. The spatial coordinates and velocity components of molecules in a particular cell are used to calculate macroscopic quantities at the geometric center of the cell.

The DSMC technique is explicit and time-marching, so that it always produces a flow simulation that is unsteady. For an unsteady flow application, an ensemble of many independent computations may be assembled and averaged to obtain final results with an acceptable statistical accuracy. An ensemble average (the instantaneous average over area or volume elements of an arbitrarily large group of similar systems) is commonly used to present unsteady DSMC results. To simulate a steady problem, each independent computation proceeds until a steady flow is established at a sufficiently large time, and the desired steady result is a time average of all values calculated after reaching the steady state.

Two distinct types of errors can affect the accuracy of a DSMC simulation. The first type is the result of computational approximations inherent in the method. These include errors due to the finite cell sizes in physical space; the finite size of the timestep; the ratio of actual to simulated particles; and various aspects of how boundary conditions are implemented. The second type of error is the result of uncertainties or inadequacies in the physical model input parameters. These include uncertainty about the types of species modeled, their interaction cross sections, and other aspects of boundary conditions and interactions.

6.9 COLLISION SAMPLING TECHNIQUES

The probability of a collision between two molecules in a homogenous gas is proportional to the product of their relative speed and total collision cross section. To achieve computational time proportional to the number of molecules, the NTC method was introduced by Bird in 1989.[9] Consider a DSMC cell of volume Vc in which each simulated molecule represents by Fn real molecules as shown in Figure 6.5. The probability P of the collision between two simulated molecules over the interval Δt is equal to the ratio of the volume swept out by their cross –section moving at the relative speed between them to the volume of the cell.

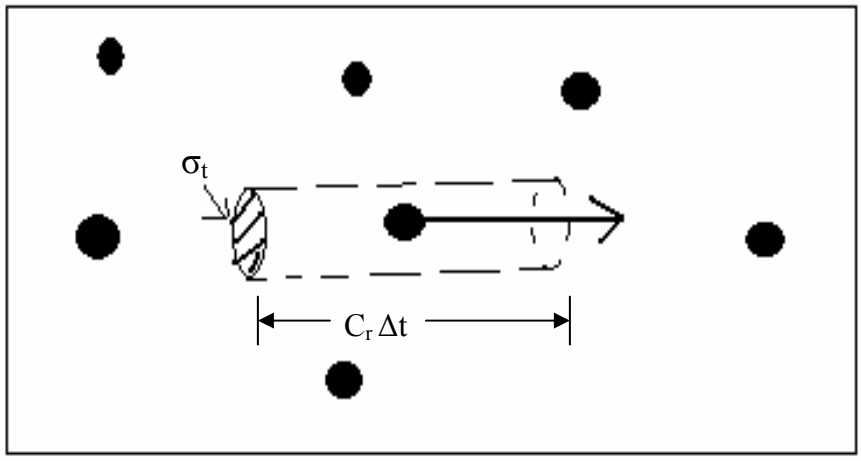

Figure 6.5. Effective Volume Swept out by Two Molecules Moving at Relative Speed c_r

$$P = F_N \sigma_T c_r \Delta t / V_c \qquad (6\text{-}8)$$

where F_N is the number of real molecules represented by simulated molecules,

σ_T is collision cross section, and

c_r is the relative velocity.

σ_t depends on the molecular model. For a hard elastic sphere model of diameter d, the total cross –section is given by

$$\sigma_t = \pi d^2 \qquad (6\text{-}9)$$

More realistic molecules models are the variable hard sphere (VHS) and variable soft sphere (VSS) models. VHS is a hard sphere molecule with diameter *d* that is a function of c_r.

The full set of collisions can be calculated by selecting all N (N-1)/2 pairs in the cell, where N is the number of simulated molecules in the cell. This method is inefficient because *P* usually will be a small quantity and the number of choices is proportional to the square of the number of molecules N. Bird developed a more efficient method. This method includes only a fraction of pairs for the collision calculation. The resultant probability is increased by dividing equation (6-8) by this fraction. This fraction is given by:

$$P_{\max} = F_N (\sigma_T c_r)_{\max} \Delta t / V_c \tag{6-10}$$

The number of pair selections per time step is obtained by multiplying equation (6-10) by $1/2N\overline{N}$, where $\overline{N}$ the average value of molecules in the cell, and N is the instantaneous value. Hence the collision is computed with probability

$$p = \frac{\sigma_T c_r}{(\sigma_T c_r)_{\max}} \tag{6-11}$$

The acceptance- rejection method was used to determine whether to accept collision between two randomly selected pair. The *p* value is compared with a random fraction R_f that is generated from a uniform distribution between 0 and 1. The collision is accepted if *p* greater than R_f and rejected otherwise.

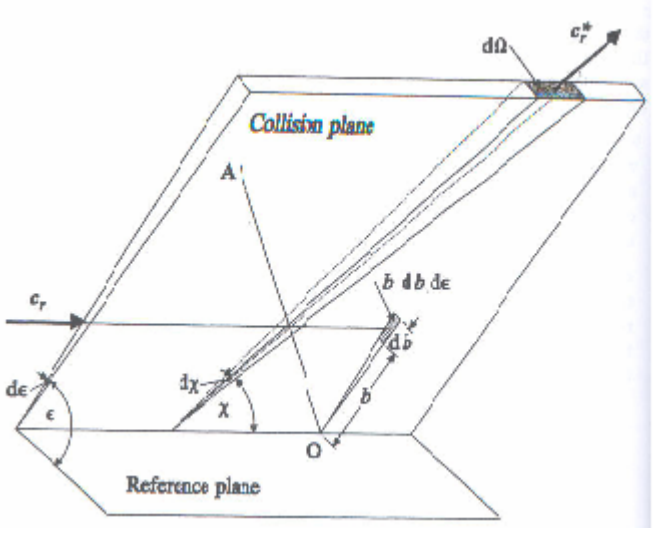

Figure 6.6. Illustration of Impact Parameters

Two impact parameters are required to completely specify a binary collision between spherically symmetric molecules. The first is b, defined as the distance of the closest approach in the center of the mass frame reference. The second is the angle ε between the collision plan and some reference plane. Let the azimuth angle ε be chosen from a uniform distribution between [0, 2π].

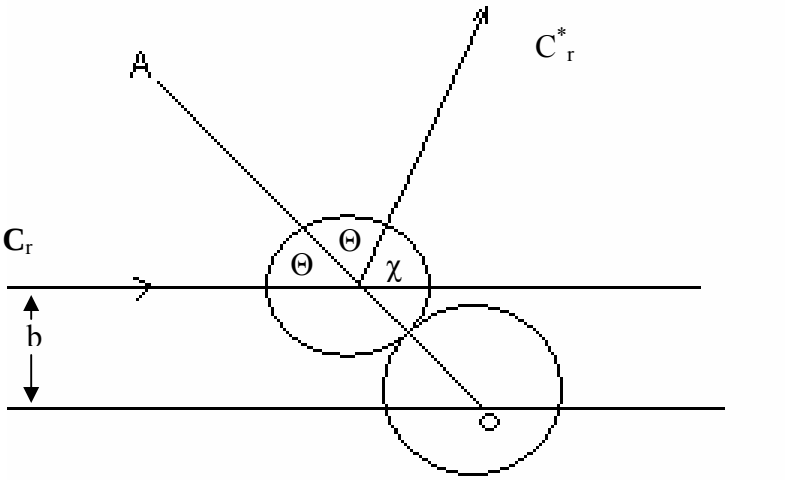

Figure 6.7. Collision Geometry

From Figure 6.7 the deflection angle χ is given by

$$\chi = \pi - 2\Theta \tag{6-12}$$

$$b = d\sin\Theta = d\cos(1/2\chi)$$

$$\chi = 2\cos^{-1}(b/d) \tag{6-13}$$

$$\cos\chi = 2(b/d)^2 - 1$$

d is the effective collision diameter . The *(b/d)* ^{2} is uniformly distributed between 0 and 1. This distribution is a random fraction itself:

$$\cos\ \chi\ =\ 2R_f\ -1 \tag{6-14}$$

where R_f is a uniformly distributed random fraction.

From the illustration of Figure 6.6, three post-collision components of the relative velocity are given by

$$
\begin{aligned}
u_r^* &= c_r \cos\chi \\
v_r^* &= c_r \sin\chi \cos\varepsilon \\
w_r^* &= c_r \sin\chi \sin\varepsilon
\end{aligned}
\tag{6-15}
$$

Once the components of relative velocity are available, equation (6-7) can be used to determine the post – collision velocities.

The temperature is calculated by:

$$
\frac{2}{3}kT = \frac{1}{2}m\left(\overline{u^2} + \overline{v^2} + \overline{w^2} - u_0^2 - v_0^2 - w_0^2\right) \tag{6-16}
$$

where ; u_o , v_o , w_o are the stream velocity and

u, v, w are the velocity

The velocity of a molecule relative to the stream velocity is called the thermal velocity. Temperature is basically defined based on that thermal velocity.

6.10 PROBLEM DESCRIPTION

The resistive heating holder modeled previously was incorporated into a simplified vacuum chamber as shown in Figures 6.8 & 6.9 for the purposes of performing gas from analysis with DSMC. It is the intent of these simulations to determine the molecular distribution within the chamber and to calculate the impingement rate on the sample. These parameters are critical to performing in-situ measurements where sensitive chemical reactions are desired.

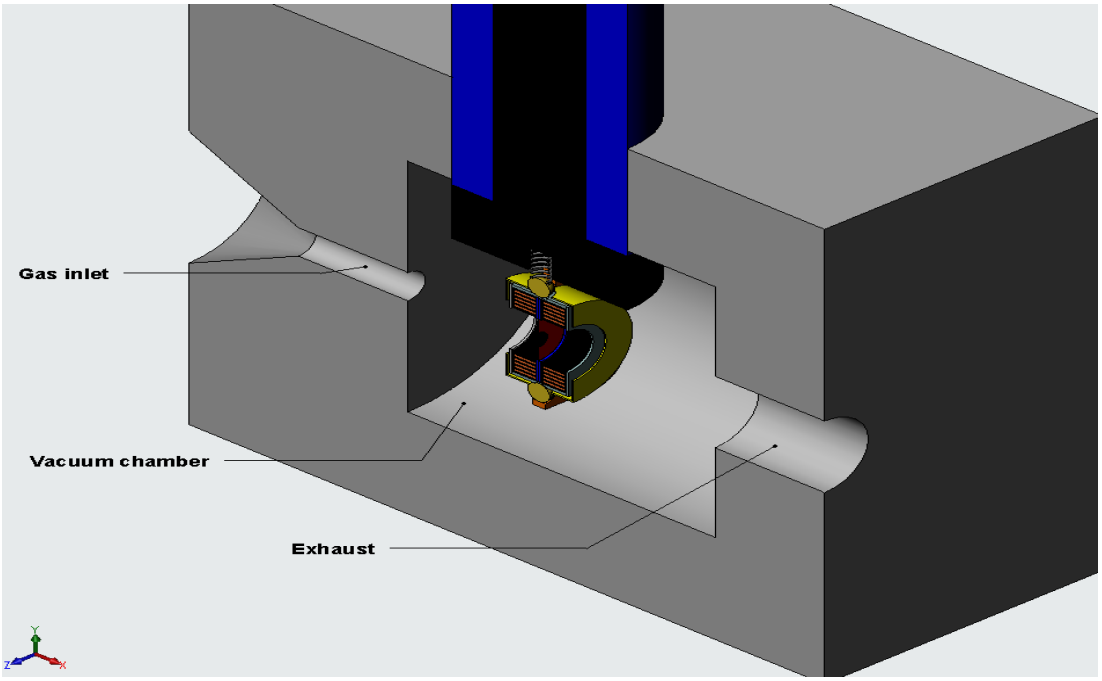

Figure 6.8. Section view of the proposed solid Model

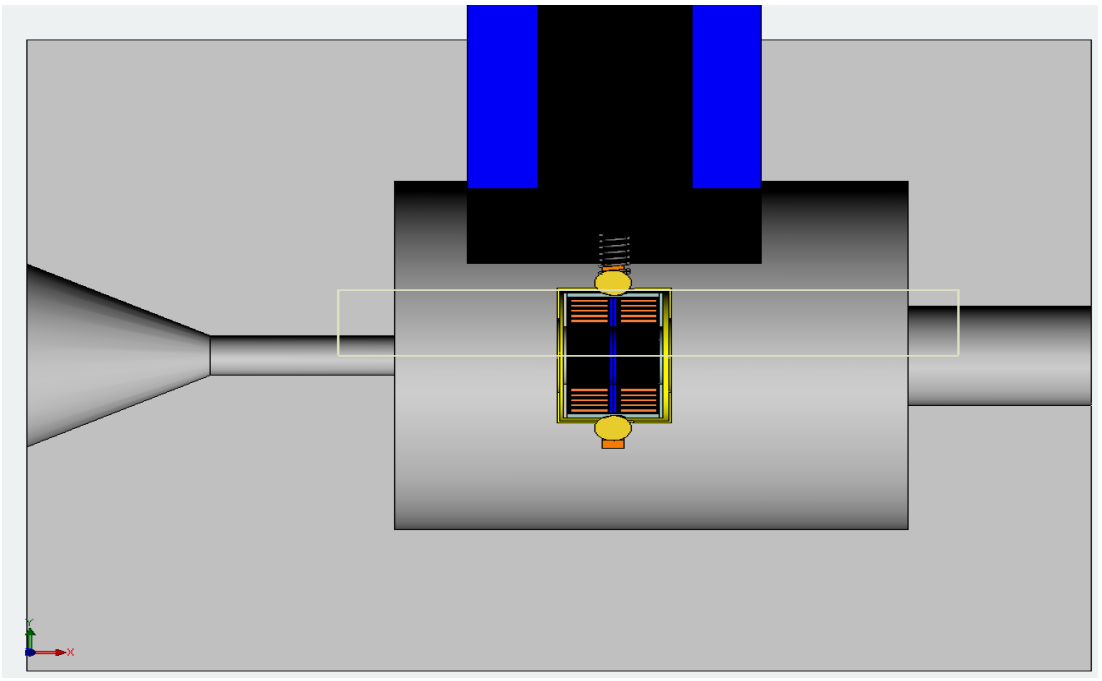

Figure 6.9. Solid Model

Based on the model shown in Figure 6.9, we consider rarefied subsonic gas flows in the chamber of 14 X 14 mm as shown in Figure 6.10. To shorten the calculation time, symmetry was used. The full computational domain includes four regions including a convergent duct, inlet, vacuum chamber and an exhaust region of the pump.

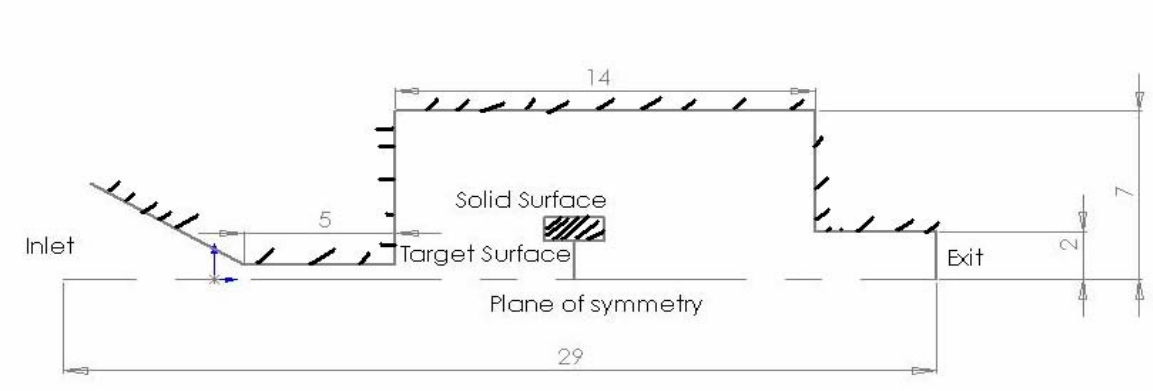

Figure 6.10. Flow Domain

Inside the chamber there is a specimen with a dimension of 3mm. The diameter for gas supply was chosen to be .6 mm. This simplified geometry was chosen to approximate our proposed design for the heating holder and chamber while injecting one or more gases into the volume surrounding the specimen. Simulations were run using 2D models. Molecules come in from the left side (inlet) and go out through the right side (outlet) where there is an assumed turbo vacuum pump. Since there is some shielding on the sample due to mounting, a solid surface was added to the model to simulate the effect of mounting on flow distributions.

6.10.1 Boundary Conditions

The flow fields were computed for specified values of the mass flow rate at the inlet, and vacuum pressure at the outlet. Simulations were carried out over a wide range of mass flow rates (.5 sccm to 60 sccm). A convergent duct was added upstream to allow flow to develop to the desired mass flow rate. An isothermal ~300 K boundary condition was used for the walls. All boundaries were set to diffuse surfaces. The inlet mass flow rate was calculated from the computed density and stream velocity of the molecules.

$$\dot{m} = \rho AU \tag{6-17}$$

Computations were carried out for hydrogen molecules. The molecular mass of a single H_2 molecules is assumed to be 3.3E-26 kg with a radius equal to 2.33000 A^o. Results of density, velocity, and mean free path were obtained for a relatively wide range of mass flow rate.

6.10.2 DSMC Computational Parameters

In DSMC, the computational time step must be less than the mean collision time. Another condition that must be satisfied during a DSMC procedure is that the smallest dimensions of the computational cells must not be greater than one-third of the mean-free path. The time step was chosen to be .03μs which is much less than one-third of the typical particle mean collision time. The initial guess of time step was based on using an approximated formula for the mean collision frequency which is given by

$$\nu = \bar{V} / \lambda \tag{6-18}$$

and V is mean thermal velocity given by

$$145\sqrt{\frac{T}{M}} \tag{6-19}$$

where M is the molar mass of H2

At 300 K and p~ 0.76 Torr, the mean collision time for a molecular is on the order of .1μs. Since DSMC methods become exact at very small size cells and very small time steps, .03 μs was chosen. The flow domain was divided into 4200 cells. Since the mean free path increases in the direction of the flow, the cell size increases in the direction of the flow. The dimension of the cells was chosen to be much less than the mean free path. At this time step, the typical molecular displacement in each direction is thus less than one third of the cell size. Every cell is subdivided into two sub-cells in each direction. The subcell is introduced to cause all collisions to occur between particles in neighboring cells.

6.10.3 Initial Conditions

Initially, we assumed the pressure inside the chamber to be of on the order of .76x 10^{-6} Torr and the temperature to be 300 K. At that pressure, the number density, which is the total number of molecules divided by unit volume, is computed by the ideal gas equation $p = nkT$ where k is Boltzman's constant, 3.3x10^{-23} J/K. Stationary particles per cell are set at random positions. When the simulation starts, the gas particles are accelerated and eventually the variation of the number of simulated particles in the flow field is small enough (within .01%), to assume the flow has reached the steady state condition. Since we used an approximated formula, Kn will range between .2-4, and a ''variable hard sphere'' (VHS) model was used to account for the collisions. The VHS model has been widely used in both slip flow and transition flow simulation.

6.11 DSMC RESULTS

An iteration of the entry conditions to the reservoir was used to give a realistic entry flow at the desired mass flow rate. Once we achieved the desired flow rate, we used the initial results to verify that the DSMC procedure requirements were satisfied. Two parameters were checked, the number of simulated particle in each cell and the ratio of time step to the mean collision time. Accurate DSMC simulations require at least 20 particles per cell. Throughout all of our simulations, the number of simulated particles per cell ranged between 50 and100. Figure 6.11 shows the contour of the ratio of the time step to the local mean free path. Good DSMC procedure requires this ratio to be below 1/3. These requirements were checked for every simulation. On the order of 40,000 iterations were performed to reach a steady-state of H_2 flow, after which data was sampled for approximately 10,000 iterations. The total time for this process depended on the level of the density number. For the five cases studied, it ranged between 80 minutes to 3 hours on a (3.2GHz Pentium 4, 2 GB of RAM) machine.

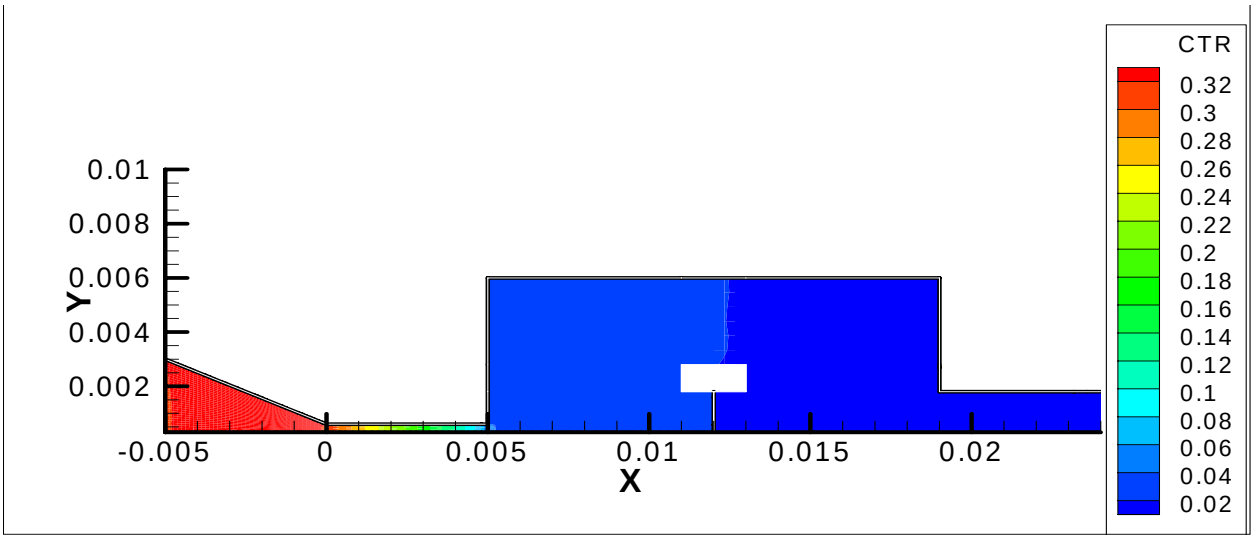

Figure 6.11. The Ratio between Time Steps to the Local Mean Collision Time

Table 6-1 lists the summary of the results obtained in the DSMC simulations. Five values of mass flow rate were investigated. Results obtained from DSMC shows that the impingement rate is proportional to the mass flow rate. The side that faces the inlet of the target surface was only considered to compute this rate.

Table 6-1 Summary of the results

Case No	Mass flow Rate (sccm)	Inlet Pressure (pa)	Impingement rate (Molecules/sec)	Outlet pressure (Pa)
1	.43	27.7	4.267×10^{14}	.612
2	1.383	51.51	6.01×10^{14}	.88
3	24	210	2.51×10^{15}	1.67
4	43	271	3.93×10^{15}	2.95
5	92.935	378.1	5.02×10^{15}	3.591

Figure 6.12 shows the molecular distribution inside the chamber. From Figure 6.12, it is shown that there is a significant difference between the two faces (note the difference in density number between two faces). Figure 6.14 illustrate the temperature distribution in the flow domain. One notable trend is the difference in temperature between the left and the right side of the target surface. Figure 6.12 demonstrates the inaccuracy of the typical assumption that states

molecules inside a vacuum chamber have a uniform homogenous distribution. Figure 6.13 shows the stream velocity (U) contours.

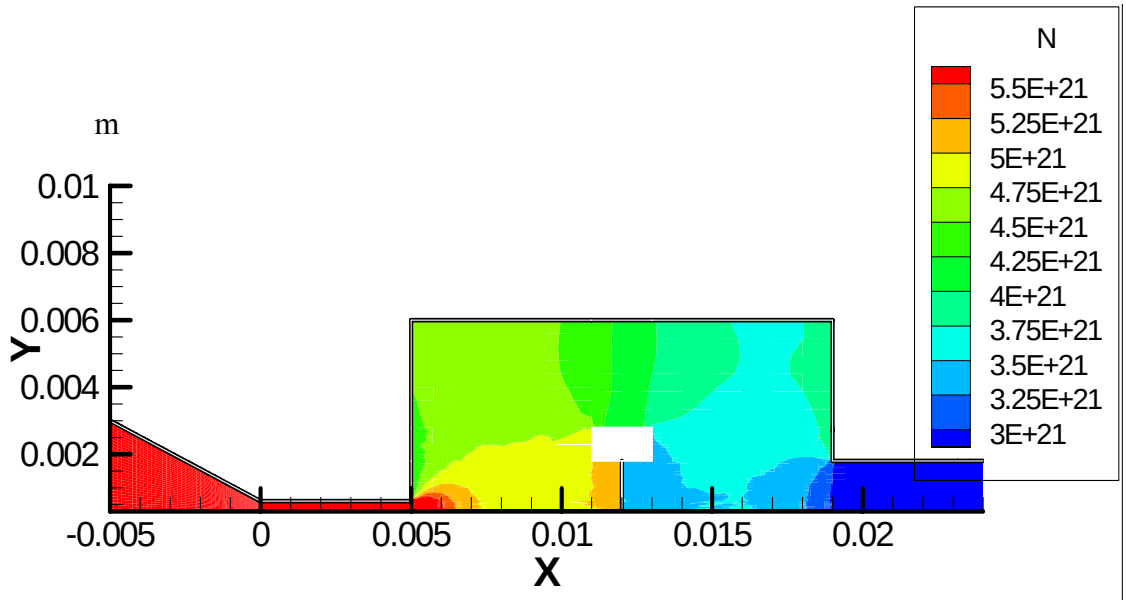

Figure 6.12. Molecular Distribution

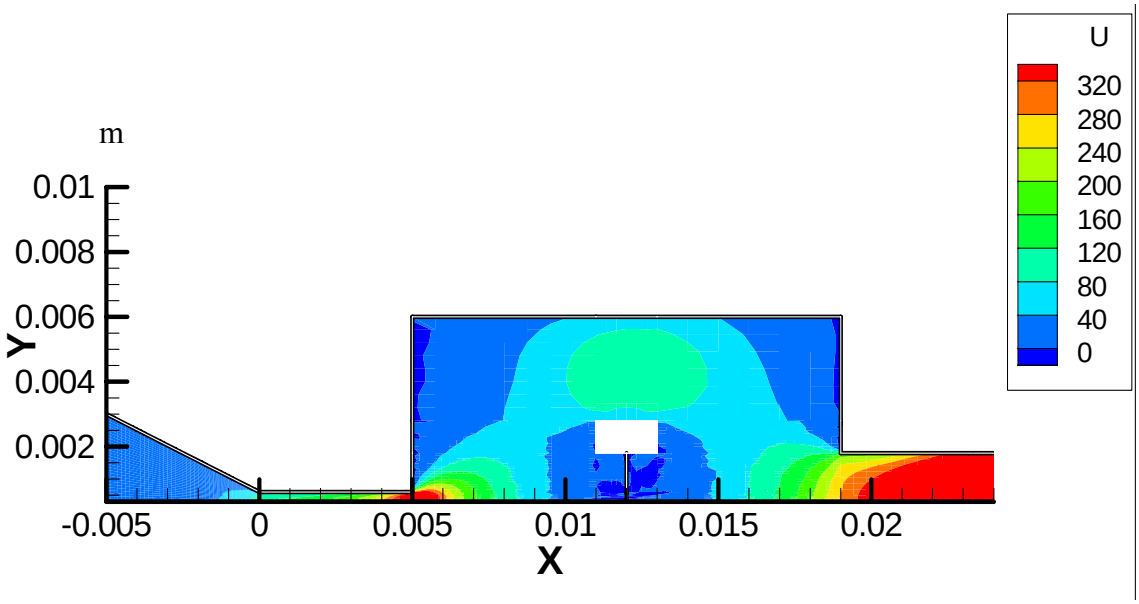

Figure 6.13. Stream Velocity Contour for 92.935 sccm

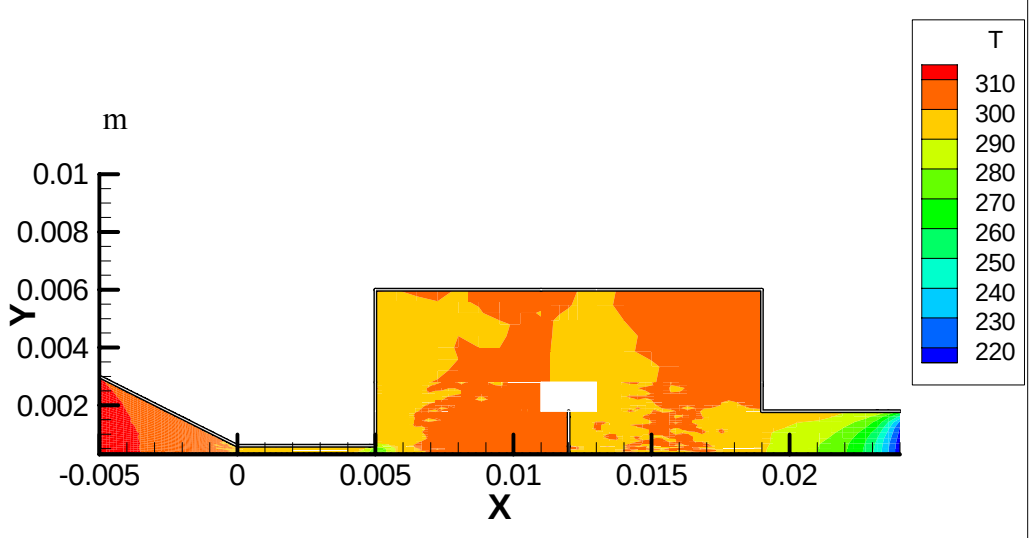

Figure 6.14. Temperature Contour

Figure 6.15 shows the computed local Knudsen Number (Kn) for the five values of mass flow rate. We chose the sample dimension to be the characteristic dimension for the flow. The Knudsen number (Kn) inside the chamber ranges between 0.4 and 3. The flow at this number is classified as slip flow (.2< Kn <1) and transition flow (1< Kn <10). In Figure 6.15, it is demonstrated that the computed values of Kn increases in the direction of the flow. Physical interpretation of Figure 6.15 illustrates that the local values of Kn is inversely proportional to the local pressure and that the pressure decreases in the direction of the flow. It should also be noted that the profiles of computed local Knudsen numbers have similar trends. This expected behavior correlates well with the classical flow regime classification. The computed Kn is inversely proportional to the density number. The density number is proportional to the mass flow rate for a given physical space. This explains the decrease in Kn profiles with the increase in the mass flow rate.

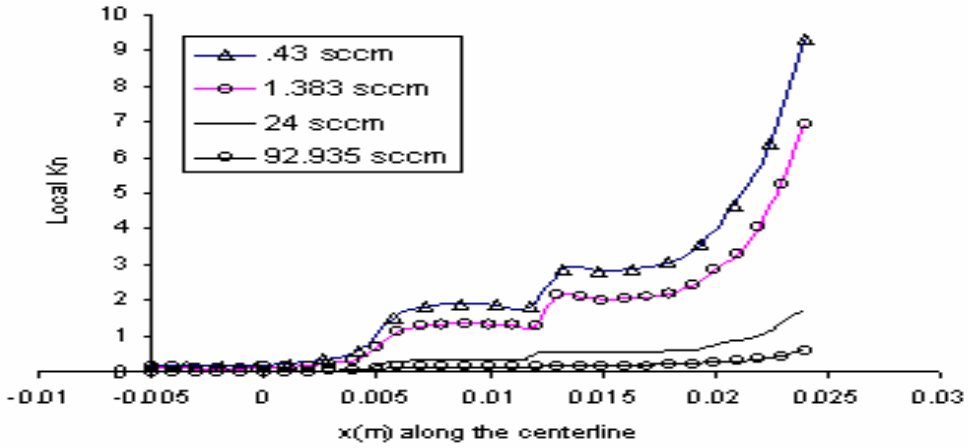

Figure 6.15. Computed Local Knudsen Number (Kn)

Figure 6.16 shows the mean free path along the plane of symmetry in the direction of the flow for four cases. All cases show similar trends for the mean free path. The local mean free path increases in the direction of the flow due to the reduced density. As mentioned previously, the Kn is the ratio between the mean free path and the characteristic dimension. This explains the similar trends shown by Figure 6.15 and 6.16.

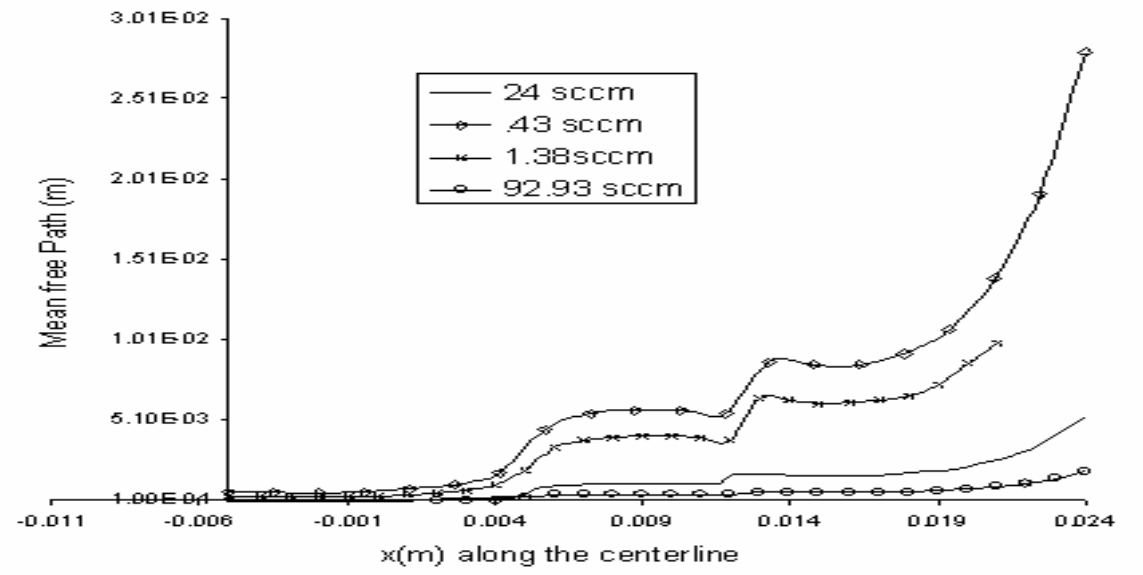

Figure 6.16. Mean Free Path

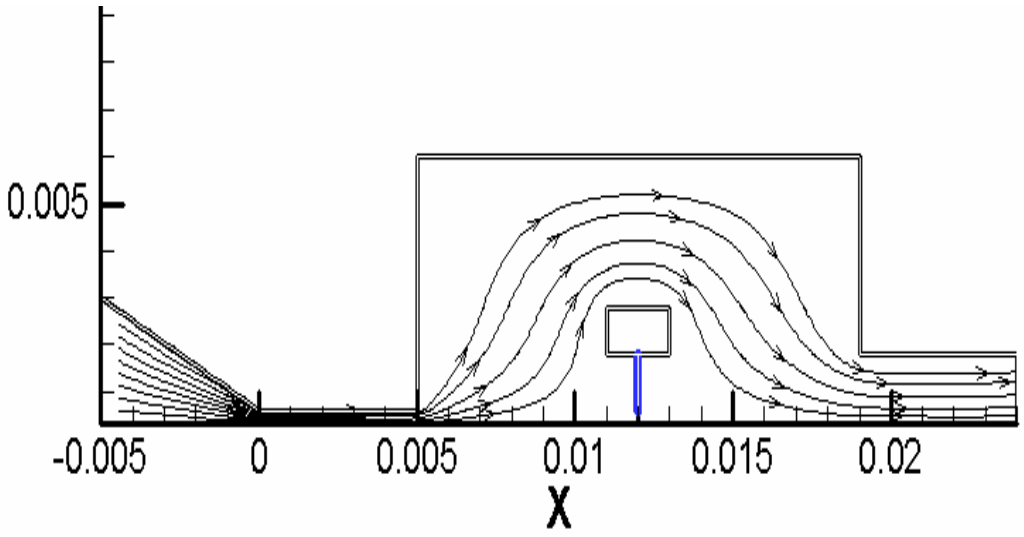

Figure 6.17. Streamlines for Case # 2

Figure 6.17 shows the streamlines. No vortices were formed. This is due to the low density in the flow field. If the flow was near continuum (high density flow), there will be vortices formed near the sample location and at flow domain corners.

6.12 DISCUSSION

DSMC was successfully used to investigate the flow characteristics inside a medium vacuum chamber (pressure between .1 to 100 Pa) that is designed for TEM analysis. Manufactures and researchers have built E- Cell TEM based on the assumption that the flow inside a chamber under a relatively medium vacuum has uniform molecular distributions. They also used approximated formulas to calculate quantities related to the dynamic processes. Using DSMC methods, we have demonstrated in this chapter that these assumptions are invalid if accurate reaction experiments are needed. This study also shows that carrying rarified gas dynamics analysis can be used to optimize the E –Cell TEM holder design. More especially, DSMC analysis should be used to design TEM holder and chamber units that require specific gas distribution and impingement rates. Previous and commercial E- Cell holders have been built to be used only with high voltage electron microscopes (HVEMs). The higher electron energies were useful due to their higher penetration power and allowed for higher effective mass thickness due to a high gas pressure and window materials. However, using HVEMs may lead to destruction of the intrinsic structure of materials due to radiation damage (electrons displacing atoms from their equilibrium sites). The present TEM in-situ holder and chamber technology have been designed with minimum working pressure to reduce the effective thickness of the sample. Having this minimum working pressure has three advantages: 1) it allows an electron beam at low or medium voltage electron beam to penetrate the sample due to reducing in the effective sample thickness; 2) it allows very thin membranes to be used, which also reduce the affective sample thickness and increase the life-time for such a membrane; 3) Third, at relatively low pressure there is less leakage to the microscope column, which serves to reduce the corrosion of the electron gun. For 3-D information, the assumption that the two sides of the

sample experience identical environments is generally not accurate. Results obtained by using DSMC show that the two sides operate at different temperatures due to the gas flow and experience different molecular distributions. We believe this knowledge of the molecular distributions will further our understanding of the reaction mechanisms and offers valuable insight into the chemical reaction processes and ways to optimize holder design.

7.0 CONCLUSION

The objectives of this dissertation were to develop novel TEM specimen holder technology that enables in-situ experiments to be performed at high temperatures and in diverse environmental conditions. The specific contributions of this dissertation include the following significant improvements over existing holder technology: the ability to obtain atomic resolution by overcoming the physical restrictions of small pole piece gaps, the ability to move from 2-D to 3-D experiments and analysis, and the ability to move from static to dynamic experimentation.

Utilizing advanced numerical techniques, two different improved holder designs were developed for performing in-situ experiments at specimen temperatures that span ambient to 2000 K. To obtain the new holder designs, rigorous theoretical analysis, current holder design evaluation, and experimental observations were performed. The new in-situ environmental holders were specially designed to obtain information about solid –gas reactions that is not presently available. The successful development of these holders will allow TEM applications to attain a new level of material analysis through highly advanced dynamic process observations. To the best of our knowledge, this dissertation includes the first comprehensive scientific approach for developing in- situ TEM holders. As a result, our proposed designs have been numerically shown to substantially outperform the specimen holder current available on the open market.

Reviewing the literature, little or no analysis has been performed on how environmental effects influence the stability of TEM. For this reason, this dissertation provides the literature with rich information about the limitations and sensitivity of TEM applications to environmental disturbances. It also provides a comprehensive study of air pressure and temperature fluctuations on the stability of TEM imagining techniques and gives practical solutions for increasing the

capability of TEM technology, particularly for in-situ analysis. Such knowledge will help educate TEM developers and researcher on the current experimental limitations of TEM technology and the way these limitations can be overcome.

By performing 'FEM' dynamic and thermal analyses of existing TEM holder technology, this dissertation also provides a comprehensive review of the current state of holder technology. With this knowledge, accurate and comprehensive development guidelines for both custom applications (researcher) and commercial production were formulated. Based on the analysis of the current holder design, an optimization approach has been presented that will help over come present technical and manufacturing issues related to holder design and fabrications. This includes the development of guidelines for selecting TEM holder materials and geometries that will substantially outperform existing specimen holders.

In existing holder technology, the temperature difference between the sample and resistive heating coils is on the order of 500 ^{o}C. This larger temperature difference is the reason for the short life of the heater coils. Utilizing the finite element method, design optimization was carried out to reduce the temperature difference between the heater coils and the sample. By focusing on radiation factors, successful design modifications were made to improve the current holder so that the temperature difference between the heater coils and the sample were on the order of 350 ^{o}C. It was found that delivering heat through radiation was an efficient mechanism in TEM experiments. This knowledge was used to develop completely new heating technology in TEM holders.

Based on the knowledge gained in analyzing the existing holders, two novel in-situ heating tomography holders were developed. The first technology utilized a conduction heat transfer mechanism instead of a radiation mechanism. It was found that the sample temperature in the new design operated only 30 degrees lower than the heater temperature and the overall depth was 3 mm. The depth will obtain significant higher resolution than the current holders and will substantially lengthen the heater life as the coils temperature were on the order of 1800 ^{o}C. The mass of the specimen furnace was also reduced to ensure rapid response to changes in heater current and minimum wattage usage. The rate of increase of specimen temperature can be better

controlled in the new design to a maximum of 3600°C per minute. In addition, the new technology was designed to minimize thermal drift and heat loss from the furnace to the specimen tip through specialized ceramic furnace supports. Numerical analysis showed that the new holder technology maintained the temperature of the specimen part that mates with the stage very close to ambient (temperature stages). Such a design is important as it eliminates the need for circulating coolant that will introduce vibrations. Through use of additional shielding the new design allowed the heated temperature to be localized in a small area and protected and increased the life of the other TEM components.

The second new design utilized innovative heating technology that incorporated a localized laser diode for heating a specimen to 2000 K. This technology has never been previously incorporated in TEM applications. A primary benefit of utilizing a laser heating system is that it will overcome the restrictions associated with the small pole piece gap so that tomography can be performed. In the holder design, the new overall depth was 1.2 mm. With such a holder, 3-D information is obtainable for experiments performed at elevated temperatures; something which is not possible at the present time. In the proposed design, the sample thermal stresses were minimized by carefully optimizing the sample support that allows symmetric temperature distribution. Based on the FEM analyses performed, the laser diode specimen holder significantly outperformed existing technology with the respect to thermal stability, dynamic stability, and stress placed on the sample.

To complete the design of TEM holders (in-situ E- Cell TEM holder), analyses were performed using DSMC. DSMC was used to investigate the flow characteristics inside a medium vacuum chamber that will house the new holders. To the best of our knowledge, our holders will be the first to successfully utilize DSMC for optimizing their design. The DSMC allowed optimization studies to be performed for reducing the effective sample thickness. For decades, E-Cell TEM was only possible for high voltage electron microscope and the DSMC shows that our new designs will allow analysis at medium voltage. It should be noted, however, that HVEM's may lead to destruction of the intrinsic structure of materials due to radiation damage. Since manufactures and researchers have built E- Cell TEM based on the approximated assumptions, the present work indicates that these assumptions should not be used if precision

experimental work is needed with respect to impingement rates and gas volume. Since DSMC was used to design a system at minimum pressure, the life-time of the membrane used in TEM will be increased. This also will reduce the amount of gas leakage to the microscope column which ultimately reduces electron gun corrosion. Finally, the DSMC analysis found that for 3-D experiments, the assumption that the two sides of the sample experience identical environments is not accurate. The results indicated that the two sides operate at different temperatures due to the gas flow and experience different molecular distributions. We believe this knowledge of the molecular distributions will further our understanding of the reaction mechanisms and offer valuable insight into optimizing chemical reaction processes.

Clearly, the design and analysis performed in this dissertation is on the cutting-edge of TEM holder technology. Though the numerical analyses performed, it has been shown that specimen holders can be designed and constructed to perform in-situ experiments in diverse environments. The analysis has also indicated that the two proposed new holder technologies will outperform anything existing in the marketplace, most of which were designed using trail and error rath. It is our belief that when incorporated into a specimen holder, the technology presented in this dissertation will drastically improve the state-of-the-art in TEM experimentations.

BIBLIOGRAPHY

1. J. Adler & S.N. Pagakis, Reducing image distortions due to temperature-related microscope stage drift.

2. Ann. Rev. Fluid Mech. 1978. MONTE CARLO SIMULATION OF GAS FLOWS G. A. Bird

3. Hakan Erturk Ofodike A. Ezekoye John R. Howell The Application of an Inverse Formulation in the Design of Boundary Conditions for Transient Radiating Enclosures

4. Design of a Low-Cost, In-Situ, Non-Contact, Temperature Sensor for Variable-Emissivity Surfaces in CIGS Deposition I.L. Eisgruber, D. Fisher.

5. L.A.Woods, An Introduction to the Kinetic Theory of Gases and Magnetoplasmas, Oxford University Press, 1993.

6. Boude C. Moore, Gas Flux Patterns in Cylindrical Vacuum systems.

7. G. Lewin, Gas flow in vacuum systems with local temperature variations for the molecular flow range

8. Frank P. Introduction to Heat Transfer, fourth edition.

9. G. A. Bird 1994, Molecular Gas Dynamics and the Direct Simulation of Gas Flows

10. Foundation of Vacuum Science and Technology

11. Bechwith, Marangon, Mechanical Measurements, fifth edition

12. ANSYS Release 8.1, Documentation Preview

13. Basil T. Wong, Nano-Scale Machining Via Electron Beam and Laser Processing

14. A.S. Edelstein, R.C. Cammarata, "Nanomaterials: Synthesis, Properties and applications", Institute of Physics Publications, 1996

15. Navrotsky, "Materials and Nanotechnology", MRS bulletin, Feb. 2003

16. C. Kisielowski, B. Kabius, et al., Report from 3rd TEAM Workshop, San Antonio, TX, 2003

17. R. Sharma, K. Weiss, et al., "Gas Reaction Chamber for Gas-Solid Interaction Studies by High Resolution Transmission Electron Microscopy", Proceedings of the Microscopy Society of America 52nd meeting, 1994

18. E. Boyes, "Controlled Environment (ECELL) HREM", Microscopy and Microanalysis, Vol 3, supp 2 proceedings, 1997

19. S.B. Newcomb, C.S. Baxter and E.G. Bithell, "The Preparation of Cross-Section TEM Specimens", Proceedings of the 9th European Conference on Electron Microscopy, Volume 1, Pages 43-48, 1988.

20. G. Thomas and M.J. Goringe, "Transmission Electron Microscopy of Materials," John Wiley and Sons, 1979.

21. R.D Schoone and E.A. Fischione, "Automatic Unit for Thinning Transmission Electron Microscopy Specimen of Metals," The Review of Scientific Instruments, Vol. 37, No. 10, 1351-1353, October 1966

22. Fischione, Kelly, Dalley, Holzman and Dawson-Elli, "Advances in Ultrasonic Disk Cutting and Precision Dimpling," Materials Research Society, Volume 245, December, 1991.

23. P.B Hirsch, A. Howie, R.B. Nicholson, D.W. Pashley and M.J. Whelan, "Electron Microscopy of Thin Crystals", The Butterworth Group, 1965

24. P.B. P.J. Goodhew, "Practical Methods in Electron Microscopy - Thin Foil Preparation for Electron Microscopy", Elsevier Science Publications, 1985

25. Uhlig Heumann and Zweck, "Development of a specimen holder for in-situ generation of pure in-plane magnetic fields in a transmission electron microscope", Ultramicroscopy, 94 (2003), 193-196.

26. Wall and Dahmen, "An in-situ nanoindentation specimen holder for a high voltage transmission electron microscope" Microscopy research and technique 42 (1998), 248-254.

27. Twitchett, Dunin-Borkowski, and Midgley, " Quantitative electron holography of biased semiconductor devices" Physical Review Letters, 88(2002), 23

28. D.B. Williams, C.B. Carter, "Transmission Electron Microscopy", Plenum Press, NY, 1996

29. P.A. Midgley, M. Weyland, et al., "3-D Analysis of Nanomaterials using Electron Tomography", Proceedings Micro and Microanalysis, Cambridge University Press, 2003

30. S.J. Pennycook, A.R. Lupini et al., "Sub-Angstrom Resolution through Aberration – Corrected STEM", Microscopy and Microanalysis 9(Suppl 2), 2003

31. Jane P.Chang, John C. Arnold, Kinetic study of low energy argon ion-enhanced plasma etching of polsilicon with atomic/ molecular chlorine, 1997

32. Jane P.Chang, John C. Arnold, Kinetic study of low energy argon ion-enhanced plasma etching of polsilicon with atomic/ molecular chlorine, 1997

33. P.J Matsuo, B.E.E Kastenmeir, Silicon etching in NF3/O2 remote microwave plasmas, American Vacuum Society

34. David A. Muller a, John Grazul, Optimizing the environment for sub-.2 nm scanning transmission electron microscope, 2001

35. Humphreys, F.J. & Hatherly, M. *Recrystallization and Related Annealing Phenomena*. Pergamon, Oxford, 1995

36. www.matweb.com

37. Renu Sharma. Design and Applications of Environmental Cell Transmission Electron Microscope for In Situ Observations of Gas–Solid Reactions. Microsc. Microanal. 7, 494–506, 2001

38. Sharma R, Weiss K, McKelvy M, Glaunsinger W (1994) Gas reaction chamber for gas–solid interaction studies by high resolution transmission electron microscopy. Proceedings of the 52nd Annual Meeting of the Microscopy Society of America, pp 494–495

39. Butler P, Hale K (1981a) In situ studies of gas–solid reactions. In: *Practical Methods in Electron Microscopy, Vol 9*. Amsterdam: North Holland, pp 239–308

40. Boyes ED, Gai PL, Hanna LG (1996) Controlled environment (ECELL) TEM for dynamic in situ reaction studies with HREM

41. Baker RTK, Harris PS (1972) Controlled atmosphere electron microscopy. *J Sci Instrument* 5:793–797

42. Heide HG (1962) Electron microscopic observation of specimen under controlled gas pressure. *J Cell Biol* 13:147–157

43. Butler P, Hale K (1981b) Wet cell microscopy. In: *Practical Methods in Electron Microscopy, Vol 9*. Amsterdam: North Holland, pp 309–355

44. Baker RTK, Chludzinski JJ (1980) Filamentous carbon growth on nickel–iron surfaces—effect of various oxide additives. *J Catal* 64: 464–478

45. Baker RTK, Chludzinski JJ, Lund CRF (1987) Further studies of the formation of filamentous carbon from the interaction of supported iron particles with acetylene. *Carbon* 25:295–303

46. Pratibha L. Gai Direct Probing of Gas Molecule-Solid Catalyst Interactions on the Atomic Scale. Advanced material , volume 10, issue 15, (P 259-1263)

47. Muntz E P 1989 .Rarefied Gas Dynamics. *Ann. Rev. Fluid Mech.* **21 P**387–417

48. Cheng HK. 1992. Perspective on Hypersonic Viscous and Nonequilibrium Flow Research, USCAE 151, August, 1992, Dept. Aero. Engine, Univ. Southern Calif., Los Angeles.

49. Bird GA. 1986b. Direct simulation of gas at the molecular level. First World Congr. Comput. Mech., Austin, TX